AD-A063 591 ARMY MILITARY PERSONNEL CENTER ALEXANDRIA VA F/G 17/7
A FEASIBILITY STUDY OF AN ALTERNATIVE POWER AND CONTROL SYSTEM --ETC(U)
DEC 78 M N RICHARD

UNCLASSIFIED NL

1 OF 2
AD A063591

LEVEL II

T-676

A FEASIBILITY STUDY OF AN ALTERNATIVE POWER AND CONTROL SYSTEM FOR A HIGH PRECISION GYRO

by

Marc Normand Richard

December 1978

Master of Science Thesis
Massachusetts Institute of Technology

The Charles Stark Draper Laboratory, Inc.
Cambridge, Massachusetts 02139

SECURITY CLASSIFICATION OF THIS PAGE *(When Data Entered)*

REPORT DOCUMENTATION PAGE		READ INSTRUCTIONS BEFORE COMPLETING FORM
1. REPORT NUMBER	2. GOVT ACCESSION NO.	3. RECIPIENT'S CATALOG NUMBER
4. TITLE *(and Subtitle)* A FEASIBILITY STUDY OF AN ALTERNATIVE POWER AND CONTROL SYSTEM FOR A HIGH PRECISION GYRO		5. TYPE OF REPORT & PERIOD COVERED Thesis for Masters Deg. 6. PERFORMING ORG. REPORT NUMBER
7. AUTHOR(s) Marc Normand Richard		8. CONTRACT OR GRANT NUMBER(s)
9. PERFORMING ORGANIZATION NAME AND ADDRESS Student, HQDA, MILPERCEN (DAPC-OPP-E), 200 Stovall Street, Alexandria, VA 22332		10. PROGRAM ELEMENT, PROJECT, TASK AREA & WORK UNIT NUMBERS
11. CONTROLLING OFFICE NAME AND ADDRESS HQDA, MILPERCEN, ATTN: DAPC-OPP-E, 200 Stovall Street, Alexandria, VA 22332		12. REPORT DATE December 1978 13. NUMBER OF PAGES 162
14. MONITORING AGENCY NAME & ADDRESS*(if different from Controlling Office)*		15. SECURITY CLASS. *(of this report)* Unclassified 15a. DECLASSIFICATION/DOWNGRADING SCHEDULE

16. DISTRIBUTION STATEMENT *(of this Report)*

Approved for public release: distribution unlimited

17. DISTRIBUTION STATEMENT *(of the abstract entered in Block 20, if different from Report)*

Approved for public release; distribution unlimited

18. SUPPLEMENTARY NOTES

Document is a thesis submitted to the Massachusetts Institute of Technology in partial fulfillment of the requirements for the degree of Master of Science. It was performed at the Charles Stark Draper Laboratory, Inc.

19. KEY WORDS *(Continue on reverse side if necessary and identify by block number)*

Permanent Magnet Gyro Wheel

Phase Lock Loop Speed Control

High Precision Gyros

20. ABSTRACT *(Continue on reverse side if necessary and identify by block number)*

A new gyro wheel drive system composed of an induction motor on the same shaft as, and in electical series with, a permanent magnet motor has veen designed, analyzed, implemented, and tested.

Its open loop operating characteristics have been determined for both a voltage source and current source power stage.

DD FORM 1 JAN 73 1473 EDITION OF 1 NOV 65 IS OBSOLETE

SECURITY CLASSIFICATION OF THIS PAGE *(When Dati*

20. The system is too unreliable in the open loop mode for high precision gyro applications.

A closed loop control scheme that relies upon the sensed back EMF of the PM motor has been developed to commutate the two motor system. Its steady state and transient response characteristics have been documented.

It has been shown that the entire system employing the two motors and closed loop control algorithm can start the gyro, accelerate it up to synchronous speed, and maintain synchronous lock much more effectively and efficiently than previously used hysteresis synchronous motor systems.

Also, it has been demonstrated that the same system can power the gyro through a rotary transformer interface with little degradation in system performance. The transformers would replace the flex leads that are present in existing systems. This would further improve upon the performance of the inertial navigation platform.

(6) A FEASIBILITY STUDY OF AN ALTERNATIVE POWER AND CONTROL SYSTEM FOR A HIGH PRECISION GYRO.

(10) Marc Normand Richard, 2LT
HQDA, MILPERCEN (DAPC-OPP-E)
200 Stovall Street
Alexandria, VA 22332

(11) Dec 78

(9) Final Report, December 1978

(12) 164p.

Approved for public release: distribution unlimited

A thesis submitted to the Massachusetts Institute of Technology, Cambridge, Massachusetts, in partial fulfillment of the requirements for the degree of Master of Science

A FEASIBILITY STUDY OF AN ALTERNATIVE POWER AND CONTROL SYSTEM FOR A HIGH PRECISION GYRO

by

MARC NORMAND RICHARD

B.S., Worcester Polytechnic Institute (1977)

SUBMITTED IN PARTIAL FULFILLMENT
OF THE REQUIREMENTS FOR THE
DEGREE OF

MASTER OF SCIENCE

at the

MASSACHUSETTS INSTITUTE OF TECHNOLOGY

December, 1978

Signature of Author Marc N. Richard
Department of Electrical Engineering
and Computer Science, November 10, 1978

Approved by _____
Technical Supervisor, CSDL

Certified by _____
Thesis Supervisor

Accepted by _____
Chairman, Departmental Graduate Committee

A FEASIBILITY STUDY OF AN ALTERNATIVE POWER AND CONTROL SYSTEM FOR A HIGH PRECISION GYRO

by

MARC NORMAND RICHARD

Submitted to the Department of Electrical Engineering and Computer Science on November 10, 1978, in partial fulfillment of the requirements for the Degree of Master of Science.

ABSTRACT

A new gyro wheel drive system composed of an induction motor on the same shaft as, and in electrical series with, a permanent magnet motor has been designed, analyzed, implemented, and tested.

Its open loop operating characteristics have been determined for both a voltage source and current source power stage. The system is too unreliable in the open loop mode for high precision gyro applications.

A closed loop control scheme that relies upon the sensed back EMF of the PM motor has been developed to commutate the two motor system. Its steady state and transient response characteristics have been documented.

It has been shown that the entire system employing the two motors and closed loop control algorithm can start the gyro, accelerate it up to synchronous speed, and maintain synchronous lock much more effectively and efficiently than previously used hysteresis synchronous motor systems.

Also, it has been demonstrated that the same system can power the gyro through a rotary transformer interface with little degradation in system performance. The transformers would replace the flex leads that are present in existing systems. This would further improve upon the performance of the inertial navigation platform.

Thesis Supervisor: John G. Kassakian
Associate Professor of
Electrical Engineering

Acknowledgement

I would like to thank my advisor Associate Professor John G. Kassakian for his interest, enthusiasm, and counsel in overseeing this project. Also, I would like to express my thanks to my company supervisor Donald Fulton whose keen insight and guidance helped me overcome obstacles countless times; to William Curtiss, the head of group 15G, who first proposed the project to me; to my friends Barry Blancha and Gail Bonda for their help and moral support; to Beverly Giarrusso for somehow managing to read my handwriting and type both first and second drafts of this paper; and finally to the 15G staff for their overall help and encouragement.

This report was prepared at the Charles Stark Draper Laboratory, Inc. under independent research and development project number 18765.

Publication of this report does not constitute approval by the Draper Laboratory of the findings or conclusions contained herein. It is published for the exchange and stimulation of ideas.

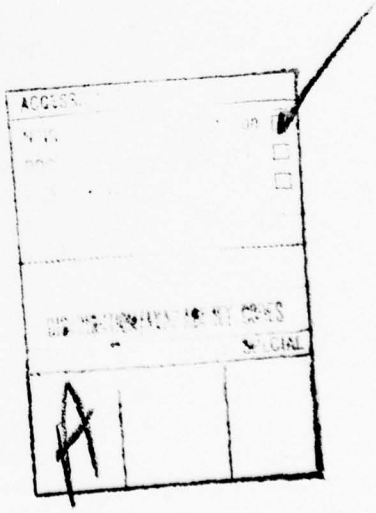

TABLE OF CONTENTS

Chapter Page

LIST OF FIGURES

Chapter I

Introduction

1.1 Overview

For many applications in guidance, certain directional references are required which serve as the basis for obtaining navigational data. These references must be maintained with little error despite various interferences. To date, the most suitable device for obtaining these references is the gyroscope.

A gyroscope is an inertial sensing device, i.e. if no outside forces act upon it, it maintains its orientation with respect to inertial space (the stars) indefinitely. The physics and design of this device have been more than adequately covered in a variety of texts[1,2,3]. However, to form a basis for the remainder of this paper, a short summary of its operation is included here.

A simplified vector model permits quantitative analysis of the device while maintaining the simplicity of its geometric properties.[1] The governing equation describing the forced response of the gyro to an applied torque can be developed with reference to Figure 1. It is

$$W_i \times H_s = T \qquad 1.1$$

where W_i is the angular velocity of precession of the gyro's angular momentum vector with respect to inertial space; H_s is the spin angular momentum of the gyro: and T is the applied torque.

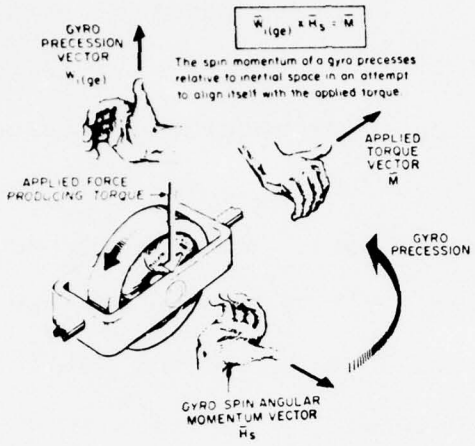

FIGURE 1: Simplified Gyro Torque Equation[1]

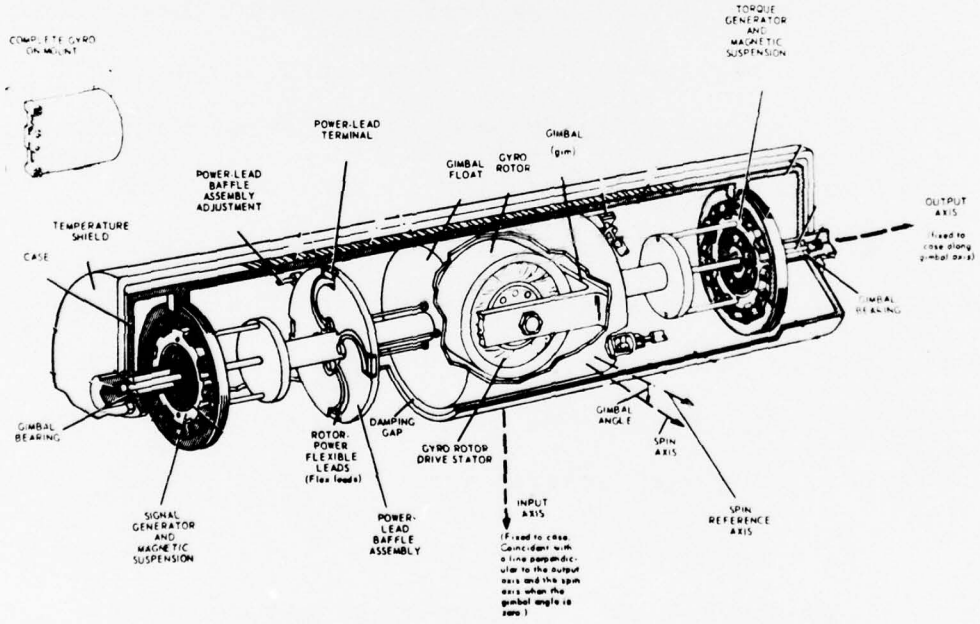

FIGURE 2: Single Degree of Freedom Gyroscope[1]

In effect, the spin angular momentum vector precesses with respect to inertial space in an attempt to align itself with the applied torque vector. Alternately, one can say that if the spin angular momentum vector is precessing with respect to inertial space, it produces torque in the direction shown.

In order that the measure of this torque be as error free as possible, there are three basic requirements for the gyro wheel related directly to the defining equation. They are:

1. The angular momentum, H_S, should be as high and as constant as possible.
2. The mass and dimensional instabilities of the gyro wheel with respect to time, temperature, and acceleration must be small.
3. A high degree of dynamic balance must be maintained.

The gyroscope functions in one of two modes. In the displacement mode the gyro wheel is suspended so that essentially no force can act upon it. It is then instrumented to measure the angular displacement, relative to the spin angular momentum vector of the gyro, of the vehicle carrying the gyroscope. In the second mode, the force mode, the gyro is constrained to follow the

motions of the vehicle and it is instrumented to measure the torque or force required to keep the gyro's axis aligned with a vehicle axis.

A single degree of freedom gyroscope which has no gimbals other than that of the gyro element itself can be operated in either the forcing or displacement mode. In some forcing mode applications a gyro may be used to precess an inertial platform at a constant rate by a known torque about the gyro output axis. The purpose of this project was to investigate a novel drive system for this gyro.

A general view of a single degree of freedom gyroscope is shown in Figure 2. As can be seen in this design, there is a gyro wheel inside a float which is suspended in a fluid and has freedom of limited motion about one axis. The motor to power the wheel is inside the float and power is provided through very thin flexible connections called flex leads. There is an angular displacement detector signal generator on one end of the device and a nulling torque generator on the other end.

1.2 History

The primary concern of gyroscope designers is the elimination of torque uncertainty about the output axis of the gyro. This uncertainty causes an unpredictable

gyro drift, which is a failure to maintain the inertial reference direction, and therefore an error is introduced into the calculation of the position or acceleration of the vehicle using the system. The technological history of the gyro, therefore, has been a never ending search for better support and drive materials to reduce friction at all rotating points, minimize mass shifting or deformations, and increase the speed and efficiency of the drive motors.

Early gyros were supported by ball bearings about the output axis. Subsequently, the gyro element was floated in a liquid and the ball bearing replaced by a jeweled bearing. The fluid filled an annular gap a few thousandths of a centimeter wide between the gyro element and its surrounding case. The jewel was later replaced by a passive magnetic field suspension. This device keeps the gyro element centered in its case, supports the residual weight not compensated for by the flotation, and is virtually frictionless.

New bearings for restraining the rotor from shifting along its spin axis produced a significant improvement in gyro performance since a shift in position of anything inside the gyro element produces an unacceptable torque when the device is acted upon by gravity or acceleration.

Gas bearings are currently used in high performance gyros. Although at start a much higher torque is required, the bearings have no running friction and they keep the rotor shaft centered with much tighter tolerances than the old bearings.

After assembly, a gyroscope is tested for its drift characteristics. Any drifts that are constant with time can be compensated. However, random effects can only be minimized by good design, manufacture and servicing. It is these random effects that limit the accuracy of the gyroscope and it is because of these problems and the limitations of conventional gyros that designers have tried new and exotic techniques. Different support structures for gyros have been investigated including cryogenic and electrostatic techniques[1] as well as an active magnetic suspension[4]. Other forms of angular momentum have been studied including the vibration of fluids and atomic particles[1]. Even the difference in the propagation times of oppositely directed beams of light have been used (ring laser gyro)[1].

At the present most of these methods are still experimental or applicable only to specialized situations. The most widely used and most reliable system in use today is still the conventional system explained in the preceding pages. This thesis investigates one

of the novel options that have been suggested for improving the conventional gyro wheel drive system in order to evaluate its feasibility for future gyro designs.

1.3 Gyro Drive System-Conventional Design

The function of the spin axis drive motor is to drive the gyro wheel at a constant speed and require the least power necessary to perform satisfactorily under load. The gyro has no productive work output and therefore the motor has only to supply enough torque to overcome windage and bearing friction at synchronous speed and starting friction at standstill. Depending upon the nature of the gas bearings used, the torque required at start can be up to three times greater than that required at the synchronous speed.

The drive methods used in the past have included air drives, hysteresis synchronous motors, and induction motors. The air drive system is used only for non-precision situations. Induction motors are used where efficiency of the drive system is required and a 1 to 3% variation in gyro wheel speed can be tolerated. Until recently, precision instruments required hysteresis synchronous motors driven by fixed frequency supplies.

The hysteresis motor is a self-starting synchronous ac motor whose starting torque is generated as a result of magnetic hysteresis energy losses in the rotor, the losses being induced by a rotating magnetizing field which is produced by the stator windings. At synchronous speed the rotor and stator magnetic fields are rotating at the same speed and therefore rotor losses go to zero. Synchronous operation is maintained by the fact that the rotor, at synchronism, supports a residual magnetic field.

The principal advantage of the hysteresis motor over other synchronous machines is its ability to accelerate a load inertia of any magnitude up to synchronous speed providing the torque required does not exceed the hysteresis torque.

The motor itself is mechanically simple. The rotor consists of only a ring of steel with no wires, slots, leads, slip rings or brushes required. It is rugged and rigid. It can be driven from a fixed frequency, fixed amplitude supply and will run at synchronous speed using only an open loop control scheme.

The motor has several disadvantages when compared with others. It has a relatively poor efficiency on the order of 30%. The residual magnetic field in the rotor is reformed every time the wheel is restarted. This means the rotor magnetic field strength is a function of the magnetic history of the stator flux and rotor position. Transients in the excitation source will also change the field. This variation in field strength requires that the stator current change to maintain the torque constant in order to keep the wheel at synchronous speed. This change in current causes a change in the heat dissipation in the motor which creates a thermal error. Also, a change in current in the power leads changes their mechanical properties[5,6]. These effects combine to produce a drift causing error torque about the gyro's output axis.

At synchronous speed the gyro wheel-hysteresis motor combination has very little damping. If a transient torque pulse is applied to the shaft, an extremely underdamped response results. The rotor hunts about its synchronous velocity (or angle) for several seconds. During this hunting, there is an instantaneous difference between shaft and sync speed which introduces another error into the calculations.

1.4 Case-to-Float Power Transfer - Conventional Design

The motor driving the gyro wheel must receive power from outside the float. This transfer of power must be accomplished with a minimum of disturbing torque applied to the free axis of the float, i.e. no torques that vary with time, displacement, or acceleration.

The power transfer medium must produce a minimum of bias and elastic restraining torque. Its torque variation must have a low sensitivity to current, voltage, or power changes. Furthermore, there must be low sensitivity to temperature changes and no hysteresis in its rotational response.

For the past twenty years, the most widely employed method of power transfer has been the flex lead. These extremely pliant leads are formed in a semicircular arc between the float and the case (see Figure 2). One end is fixed on the float and the other to a baffle plate. By rotating the baffle plate, static flex-lead torque can be adjusted to yield zero residual torque at null. However, rotation of the baffle plate or float with respect to the case changes the stress of the flex leads which cannot always be predicted.

Despite great advances in the materials technology of the leads, metallurgical hysteresis and relaxation

effects may occur in the wires. This changes the gyro's center of mass which changes the drift rate. Also, since the leads pass through the flotation fluid, the current in them must be limited to protect overheating of the liquid which could cause bubbles. If the leads overheat too much, they could possibly burn out. Another effect noticed is that the leads magnetically attract each other. If the current changes, the attraction varies and hence the torque changes[5].

1.5 Principal Requirements for the High Performance Gyro Drive System

In any system utilizing a high performance gyroscope, there are usually specific performance requirements as well as size and weight limitations. Since this project was a feasibility study, however, it was concerned with evaluating the operation of a new gyro wheel drive system in principle only, without a specific use in mind. Therefore, the constraints used were merely guidelines that give the general order of magnitude of the requirements of virtually all high performance gyroscope systems.

The motors used in high performance systems deliver between 2 and 15 watts of power at synchronous speed while producing an output torque between 12,000 and 100,000 dyne-centimeters. In present systems the motors run at speeds up to 45,000 revolutions per min-

ute; however, for this project gas bearings were unavailable, and therefore, speeds of 6,000 to 12,000 rpm were used. To simulate the gas bearing effect at start, the motors were required to start with a load torque higher than that which they drove at synchronous speeds.

Other requirements for the high performance drive system are:

Thermal stability: Very stable, low power into float for a constant load over entire run time.

Torque: Very stable, low torque about the free axis of the gyro. It should be predictable.

Center of mass and mechanical reliability: System is to be operated continuously for extended periods of time.

Heating of float: No unnecessary wires or electronics should be on float. If electronics are required, the premium is on simplicity and efficiency.

With these requirements in mind, several different designs have been considered utilizing a variety of drive motors and power transfer techniques. The alternatives are described in the following sections.

1.6 Methods of Power Transfer

The principal requirement for the power transfer medium is that it must supply the correct power and control signals to the motor on the float while allowing free rotation of the float about its output axis without introducing significant error torques. A problem that arises in choosing the medium is the small size of the float. This severely restricts the size of capacitors or transformers that could be used which limits the magnitude of the currents that can be supplied. This situation is compounded by the fact that at start, the motors must supply three times their running torque which means a large current is required.

The following paragraphs document the various methods considered.

1.6.1 Flex Leads

Their advantages and drawbacks have already been discussed. Their redeeming qualities are simplicity, long life, and the fact that their operating characteristics have been well documented through twenty years of use.

1.6.2 Electrostatic Power Transfer - Rotary Capacitors

One plate of the capacitor is on the float, the

other on the case. The parameter limiting the usefulness of this technique is the size of the float. The maximum practical value of capacitance per phase is 270 pf.

Due to this limitation as well as the breakdown voltage of the damping gap fluid, power transfer through the capacitors must be accomplished by superimposing the motor drive frequency signal on a radio frequency carrier. This necessitates the use of a demodulation circuit on the float. The problem then is to make the conversion efficiently without adding too much weight to the float.

After much consideration and literature searching, the simplest method found to date was suggested by Musoff[7] who used an extremely simple active demodulator on the float. The system worked well when applied to a hysteresis motor. However, its efficiency was only 51% and 10% of the power transferred was actually dissipated in the damping gap fluid. There is also a question as to the long term electrical and mechanical reliability of the demodulator circuit on the float. Since the float is encased in a fluid and carefully balanced, it is desirable that servicing of it almost never be required.

The chief advantage of this system over others is the fact that the attractive force between the plates can be made extremely low by using a high enough carrier frequency.

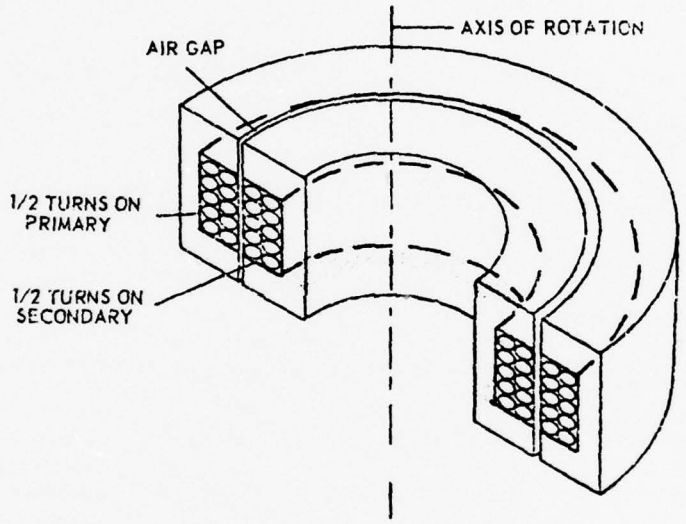

Figure 3: Air Gap Rotary Transformer[9]

1.6.3 Magnetic Power Transfer - Air Gap Rotary Transformer

A rotary transformer (see Figure 3) consists of coils wound on circular ferrite cores. The primary and secondary are concentric and separated by an air gap. Several may be placed adjacent to each other axially within the unit or radially at one position on the rotor[9].

Its advantages are:

1. It is practically frictionless.
2. There is no wear in high level power circuits.
3. It is reliable in high gravity or vibrational environments.
4. It is exceedingly rugged.
5. It has a long operating life.

Its disadvantages are:

1. The air gap is the limiting factor for power transfer.
2. There is a slight variation in amplitude with rotation due to eccentricities in the finished rings.
3. Its efficiency is not as high as flex leads.
4. The finished instrument is larger.
5. There is an error torque introduced due to the inhomogeneity of the core material.
6. There is an attractive force between the two cores across the damping gap.

This device has already been used in at least one prototype gyroscope system[8]. Many of its problems can be circumvented.

1.6.4 Magnetic Power Transfer - Hollow Core Rotary Transformer

This device is similar to the air gap transformer except that instead of an air gap separating two cores the primary and secondary coils are enclosed in a single hollow ferrite core. The primary is secured to the core while the secondary is suspended in the hollow and is free to rotate with respect to the primary about 2°. It is supported by connections to the float at perhaps two openings in the core.

This transformer has many of the advantages of the air gap type. However, the problem of magnetic attraction of the cores is reduced and the device has a higher efficiency. Its limitations are systems oriented. It has less freedom of rotation. It is much more difficult to make and service. Once installed on the float it makes for poor heat transfer. Finally, it has undocumented problems with regards to error torques caused by coil attractions and attractions between coils and the ferrite core.

1.7 Candidate Motors

1.7.1 Hysteresis Synchronous Motor

By virtue of its many desirable properties it must be included in any comparison. However, as has already been discussed, it has several severe disadvantages.

1.7.2 Permanent Magnet Motor

A permanent magnet motor is physically very similar to a hysteresis motor. It is only necessary to substitute for the hysteresis rotor one made of a hard permanent magnet, e.g. Alnico. Theoretically, if a PM motor could be brought near to synchronous speed it will lock onto the stator frequency. Then it could be run with a fixed frequency, fixed amplitude supply similar to a hysteresis motor supply.

The motor has several problems however. At synchronous speed, the system is extremely underdamped and hunts excessively if disturbed. This hunting can be so severe that it can throw the motor out of synchronous lock. If this occurs, the average torque of the motor will go almost to zero and either an auxiliary motor will be required to get the system back up to sync or the supply frequency will have to be reduced in an attempt to catch the rotor again. Also, since a PM motor has no hysteresis torque, it must either have an auxiliary starter motor or be started with a variable low frequency signal which rotary transformers could not handle.

Several schemes have been devised or suggested in order to overcome these problems. D. Fulton[6] has de-

veloped a closed loop control system for commutating the PM motor and operating it at a fixed synchronous speed by sensing rotor position using the motor back EMF. Efficiencies of 93% have been obtained. Starting of the motor is accomplished by a frequency ramping technique which would have difficulties at low frequencies in a transformer coupled situation.

1.7.3 Induction Motor

An induction motor is rugged, reliable, and can start using ac excitation. However, its start current, with a fixed amplitude voltage excitation, is excessive (4 to 5 times its run current), its efficiency at run speed is not as good as a PM motor (80 to 90%), it has thermal dissipation on the rotor, and it requires some form of closed loop control system to keep it running at a specified frequency. This closed loop control requires that some form of speed or position sensing device be on the same shaft as the rotor.

The design of this motor for gyro applications using a simple, fixed voltage excitation requires a major compromise. To obtain the high starting torque required while keeping the input current low enough for the power interface, a high resistance rotor (either squirrel cage or wire wound) is required. However, this reduces the

motor's efficiency at run speeds which means there is greater heat dissipation in the float as well as higher supply currents. Larger induction motors overcome this problem in part by using deep bar squirrel cages (skin effect) or wire wound rotors with slip rings to vary rotor resistance. In gyro applications, the motor is not big enough for effective deep bars and slip rings are precluded since they wear out.

1.7.4 Series Combination PM Motor and Induction Motor

The most attractive configuration found to date is the series combination of an induction motor and PM motor run on the same shaft. Because the motors are in electrical series, the system requires no more power connections than the previous systems while it incorporates the individual advantages of both motors.

At run speed (synchronous operation) the PM motor will supply the entire torque requirement since an induction motor produces no torque when its rotor is rotating at a speed synchronized with the excitation frequency. This means there will be no current in the induction rotor cage and hence no rotor losses at syn-

chronous speeds. There will still be losses due to the induction motor stator winding resistance. Nevertheless, the overall system operating efficiency can be made to approach that of the very efficient permanent magnet motor. Also, since the current in the rotor goes to zero, the induction motor can be tailored to supply the required high starting torque with relatively low current at a fairly high frequency through the use of a high resistance rotor, without sacrificing synchronous speed efficiency.

Another factor in favor of this system is the possible increase in efficiency of the power supply. A PM motor has very little self inductance. As a result a switching supply is not compatible with it due to the large harmonics present unless a large inductance is also added which takes up considerable room. Hence a linear or quasi-linear[6] amplifier is required which is not as efficient as a switching supply. An induction motor on the other hand has a high self inductance. At synchronous speed this inductance, if it is large enough, can be used to filter the input to the motors thereby reducing the harmonics of a switching signal.

The series motor combination has properties similar to that of a motor which has the induction cage and permanent magnet combined in the same structure. This motor would take up less space and operate in a manner similar to the series system; however, the mechanical instabilities and fabrication problems associated with such a complex rotor may preclude its use in a high speed gyro system.

1.8 Summary and Problem Statement

The primary aim of the project was to investigate in depth the most promising of the options in order to evaluate its feasibility for future considerations. The scheme evaluated in this thesis is the series combination of a PM motor and induction motor powered and controlled through a transformer interface. The induction motor is used to start the system and the PM motor to run the wheel at synchronous speed.

The performance of the system was evaluated and compared to that of present configurations. Its ability to reliably start the gyro was determined. Its responses to various wheel and signal disturbances were documented to ascertain if it actually performed better than present systems. Its efficiency was calculated. From a system standpoint, its reliability was assessed. In short, the two motor system was evaluated to determine if its operational characteristics make it a feasible and perhaps desirable alternative to present gyro drives.

The major thrust of the project centered upon characterizing, controlling, and powering the two motor system. An induction motor of the appropriate size was obtained. It was tested for its torque, speed, and current characteristics. After the criteria for the optimum matching of the two motors was decided upon, a PM motor was built to meet these specifications.

The system was first analyzed and run open loop using both a voltage source and a current source supply. It was found that at synchronism the system was more damped than existing hysteresis synchronous motor gyro systems. Its performance at synchronism is therefore better than existing systems and it is more efficient; however, other problems exist that tend to make this system unfeasible.

The open loop characteristics of the system were predicted analytically and then tested experimentally. An analogy was made between the pull-in of this system and the locking of a phase locked loop . Good consistency between the predicted pull-in range and experimentally determined pull-in range was obtained. The response of the system to steps of torque and transients in wheel supply were also observed.

Since the open loop system had some serious problems, e.g. it had such a limited pull-in range that in practice it is not self-synchronizing, a closed loop scheme was developed to start and commutate the motors. The control system prevents inadvertent failure to obtain or maintain synchronous lock and reduces the hunting of the wheel when in synchronism.

The principal features of this part of the investigation were the design of a power stage and the closed loop control scheme. The power stage is a 2 phase current source employing a pulse ratio modulation scheme (see section 7.3). It is similar in principle of operation to a power stage used successfully at CSDL for several other projects.

The closed loop control system employs a variation of the algorithm developed by D. Fulton[6] that uses the PM motor's back EMF to sense the PM rotor position to continuously control the angle of the stator magnetic field. The amplitude of the stator field is controlled by a speed control loop within the system that compares the angle of the sensed back EMF to the phase of a clock. The induction motor, which is in electrical series with the PM motor and the transformer interface, does degrade the PM motor back EMF signal somewhat, but it is still sufficiently unambigious to allow successful commutation.

The entire system is started open loop at a reduced frequency (1/4 synchronous frequency) to obtain maximum torque out of the induction motor. When the rotor speed is about .1 to .25 that of the synchronous speed, the back EMF is sufficiently large to allow closed loop commutation. The system is then switched to the closed loop control circuit and is run up to synchronous speed.

The completed system minus the transformer interface was tested for its synchronous response to steps in torque applied to the shaft, phase transients in the clock signal specifying shaft speed, and run-up characteristics from a standing start. These characteristics were then compared to the presently used systems employing a hysteresis synchronous motor. Efficiency calculations were also performed which showed the superiority of the system over the present system.

After the closed loop system was shown to be viable, a transformer interface was added between the power stage and the motors to simulate the interface that would exist between the float and case of a gyro employing hollow core rotary transformers. Although detailed experiments were not performed on the modified system, it was shown that a nonambiguous back EMF signal could be obtained through the transformers. Furthermore, the

wheel was able to start and run synchronously with little change in its performance or efficiency (90% of original) from the direct drive configuration.

CHAPTER 2

Permanent Magnet Motor

The PM motor is the principle drive motor in the gyro wheel power system used in this project. As has already been stated, it is relatively unaffected by all the things that disturb the rotor poles of the hysteresis synchronous machine since its rotor is a hard permanent magnet. Physically it it is just as rugged and as simple as the hysteresis motor. Its one significant drawback is that it does not develop any significant net torque unless the stator magnetic field rotates at the same rate as the rotor field. There is no hysteresis torque.

This chapter presents the relevant permanent magnet motor torque and voltage equations that characterizes its operation.

2.1 PM Motor Torque

The hard permanent magnet in the rotor and the currents in the stator windings create magnetic fields in the air gap separating rotor from stator. Torque is produced by the interaction of these two fields as they attempt to align themselves. The torque is proportional to the peak value of the mmf waves and the sine of the electrical space phase angle between them.

The final form of the PM motor torque equation is derived in Appendix A. It is

$$T_{PM} = KI_a H_r \sin \theta \qquad 2.1$$

where K is a constant of proportionality, I_a is the stator current (1 phase), H_r is the strength of the permanent magnet and θ is the angle between the stator and rotor fields.

The PM motor torque is thus proportional to the stator current, the strength of the permanent magnet, and the sine of the phase angle between the 2 resultant fluxes.

2.2 Generated Back Voltage

As the rotor of the PM motor rotates, the magnetic flux lines of the permanent magnet cut the coils of wire on the stator thus producing a back voltage at the motor terminals through generator action. The characteristics of this voltage can be derived with reference to Figure 4 which is a simplified model for one phase of the stator of a 2 pole machine.

The spinning magnet produces a sinusoidal space wave of flux density B at the stator surface such that

$$B = B_{peak} \cos \Psi \qquad 2.2a$$

where Ψ is in electrical degrees and

$$B_{peak} = \mu_o H_{peak} \qquad 2.2b$$

where H_{peak} is the magnetic intensity of the permanent magnet.

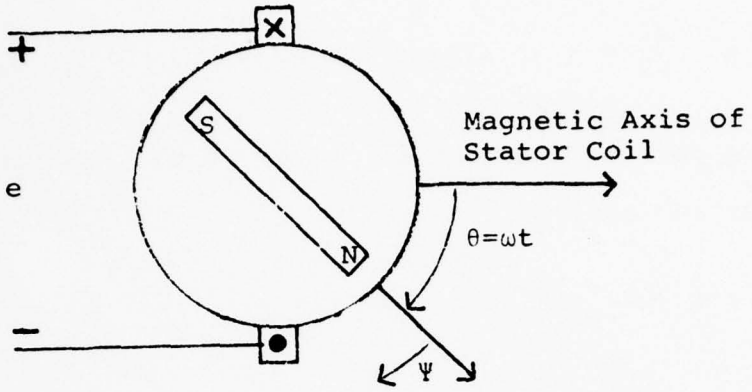

FIGURE 4: Simplified Model for One Phase of A 2-Phase PM Motor

Assume the rotor is rotating at a constant angular velocity of ω electrical radians per second. When the rotor poles align with the stator coil magnetic axis, the flux linkage is $N\Phi$ where Φ is air gap flux per pole which is determined as follows:

$$\Phi = \int_{-\frac{\pi}{2}}^{\frac{\pi}{2}} B_{peak}\cos\theta \; \ell r \; d\theta = 2B_{peak}\ell r \qquad 2.3$$

where ℓ is the axial length and r is the radius of the stator at the air gap. For a P-pole machine this becomes

$$\Phi = \frac{2}{P} 2B_{peak}\ell r \qquad 2.4$$

As the rotor turns, the flux linkage varies as the cosine of the angle θ between the magnetic axes of the stator coil and rotor bar. Therefore, the flux linkage becomes,

$$\lambda = N\Phi \cos \omega t \qquad 2.5$$

then

$$e = \frac{d\lambda}{dt} = - N\Phi \sin \omega t + N\frac{d\Phi}{dt}\cos \omega t. \qquad 2.6$$

Since the permanent magnet is "hard", Φ will not change with time and therefore

$$e = -\omega N\Phi \sin \omega t = -\omega N\Phi \sin \theta \qquad 2.7$$

2.3 Relation Between Rotor Position and Back Voltage

With reference to Figure 5 and section 2.2, the rotor flux as seen by the stator coil is

$$\Phi = \frac{2}{p} 2 \ell r B_{peak} \cos \Theta \qquad 2.8$$

The back voltage equation is

$$e = -\omega N \Phi \sin \Theta \qquad 2.9$$

As can be observed, the generated back voltage leads the rotor flux by 90°. If the stator current could be forced to be in phase with this back voltage then, since the stator flux is in phase with the stator currents, (section 2.1) the two mmf fields will be 90° apart and the maximum torque angle will automatically be maintained.

Chapter 3

Induction Motor

The induction motor is used to start the system and to provide the needed extra inductance to permit the use of a switching power stage. Since it is permanently coupled to the PM motor both electrically and mechanically, its operating characteristics (torque, terminal voltage, inertia, etc.) affect the operation of the entire gyro drive system even during synchronous operation. Therefore, it is necessary to be able to predict the motor's actions under those conditions that would occur during both the run-up and synchronous operation of the gyro system.

This chapter presents the torque and voltage equations that define the operating characteristics of the induction motor during both asynchronous (start) and synchronous operation.

3.1 Torque - Slip Curves for Induction Motor - Asynchronous Operation

The determination of the induction motor's torque output and back voltage is much more complex than for the PM motor since one has direct access only to the stator windings. The rotor, made up of short-circuited bars of conducting material, has a voltage induced in it by the action of the stator field, "cutting" across the bars. The volt-

age produces a current which, in turn, produces a rotor flux field which interacts with the rotating stator field to produce torque.

The gyro drive system has both an asynchronous and synchronous mode of operation. It is started asynchronously, i.e. a fixed frequency excitation is applied to the motor terminals and the system accelerates due to the torque developed by the induction motor. An approximate steady state analysis of the induction motor's torque output during this process can be performed with reference to Figure 5 which is a one phase equivalent circuit for the induction motor developed using d-q coordinates.[10]

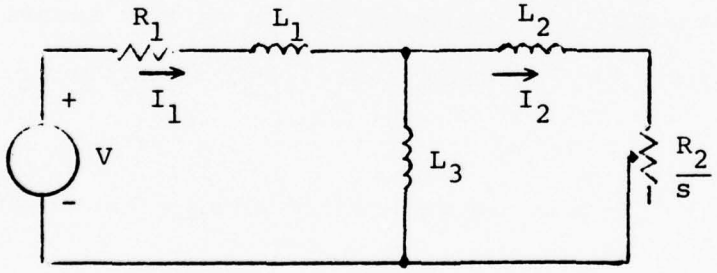

FIGURE 5: Induction Motor Equivalent Circuit

In this circuit the core loss resistance is neglected. The circuit parameters, referred to the stator, are:

V - rms input voltage per phase

I_1 - total rms input current per phase

I_2 - total rms rotor current per phase (as seen from the stator)

R_1 - stator winding resistance per phase

R_2 - rotor cage resistance per phase (as seen from the stator)

L_1 - stator winding leakage inductance

L_2 - rotor cage leakage inductance (as seen from the stator)

L_3 - magnetizing inductance

Other parameters of importance are:

ω_{in} - input excitation frequency

ω_s - synchronous angular velocity of stator field

$$\omega_s = \frac{1}{4}\,\omega_{in} \text{ for an 8 pole machine}$$

ω_o - actual rotor speed

s - the slip of the rotor with respect to stator field rotation.

$$S = \frac{\omega_s - \omega_o}{\omega_s}$$

The zero slip speed of the rotor (synchronous speed) is

$$\omega_{os} = \frac{1}{4}\,\omega_s \qquad 4.1$$

The internal electromagnetic torque is,

$$T = \frac{1}{\omega_s} q_1 I_2^2 \frac{R_2}{s} \text{ newton - meters} \qquad 3.1$$

for a 2-pole machine. The torque thus produced by an induction motor is seen to be proportional to the square of the rotor current and inversely proportional to the slip frequency.

If the power source to the motor were a voltage source then, by simple circuit analysis (solving for I_2 as a function of input) the equation relating torque output to the input voltage is

$$T_V = \frac{\frac{P}{2} q_1 R_2 V^2 (\omega_{in} L_3)^2}{s\omega_s [(\frac{R_1 R_2}{s} - \omega_{in}^2 L_1 (L_2+L_3) - \omega_{in}^2 L_2 L_3)^2 + \omega_{in}^2 (R_1 (L_2+L_3) + \frac{R_2 (L_1+L_3))^2}{s}]} \qquad 3.2$$

where P is the number of poles in the device.

If the power stage were a current source, as is the case in the present system, then the torque equation would be

$$T_I = \frac{\frac{P}{2} q_1 R_2 I_1^2 (\omega_{in} L_3)^2}{s\omega_s [\omega_{in}^2 (L_2+L_3)^2 + (\frac{R_2}{s})^2]} \qquad 3.3$$

The following page contains plots of torque versus rotor slip calculated from the motor circuit parameters of the small 8 pole induction motor used in this project (see Appendix B). The point where the two graphs intersect is the point where the reflected voltage at the motor terminals and the current into the motor are the same for both methods of motor drive.

The two torque equations show that the developed torque is inversely proportional to rotor slip frequency and proportional either to the square of the input voltage or current. Hence, if the excitation frequency is reduced or the current or voltage increased, one can obtain a higher starting torque. In fact, if the excitation frequency is reduced enough, the maximum torque point of the curves can occur at s=1, i.e. at start (see Appendix C).

The effective rotor resistance R_2 also plays a role in the location of the peak torque point. By increasing R_2 the maximum torque point moves towards the left on the graphs which also tends to increase the starting torque.

3.2 Induction Motor Torque During Synchronous Operation

Theoretically, if an induction motor could be run perfectly at its synchronous speed there would be no torque

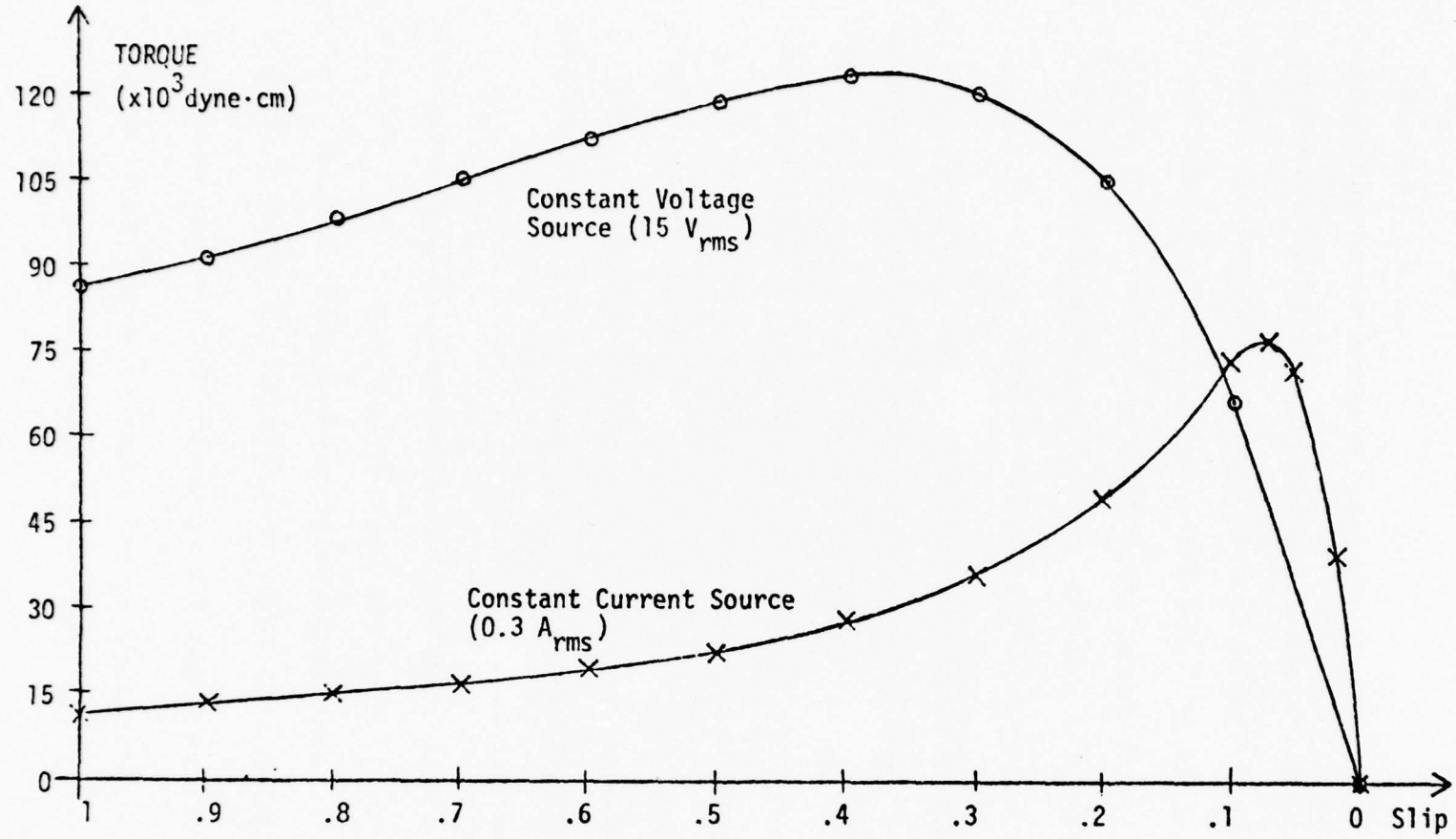

FIGURE 6: Torque versus Slip for 8-Pole Induction Motor

produced. However, in the PM and Induction motor combination system (run open or closed loop), although the shaft is said to be rotating synchronously there is some rotor disturbance whenever a torque transient is applied. The time average effect of this motion reduces to zero but instantaneously the rotor can be rotating at a speed different from synchronous speed.

As shown in section 3.1, whenever an induction rotor cage is rotating at a nonsynchronous speed, a torque will be developed. When the system perturbates around sync this torque does not act as a restoring torque but as a damping term. With a constant voltage excitation this effect can be explained by the fact that the current into the motor can change and thus the excess rotor energy is transmitted to the voltage supply.

A constant current source, however, appears as an open circuit to the motor and, therefore, it would be expected that there would be little damping. The reasons explaining why this is not the case are presented in section 3.2.2 using the alternate induction motor model presented in section 3.2.1.

3.2.1 Alternate Induction Motor Model

This model for the induction motor gives a much clearer picture of the motor's torque characteristic when it is operating at or near synchronous speed (around the slip = 0 point). At synchronism, the motor can develop no torque as was previously explained. However, with the ever present rotor perturbations that exist, the rotor will instantaneously be rotating at a speed different from the synchronous velocity. During this asynchronous operation, the stator field induces a voltage in the rotor which causes a current to flow which in turn creates a rotor flux that interacts with the original stator flux according to the equation

$$T_{ind} = K \phi_s \phi_R \sin \Theta \qquad 3.4$$

where ϕ_s and ϕ_R are the stator and rotor fluxes respectively and Θ is the space phase angle between them.

The simplified model that will be used to explain this mechanism was first proposed by D. Fulton[11]. Figure 7 is a schematic for the model which can be considered one phase of a multiphase 2 pole motor.

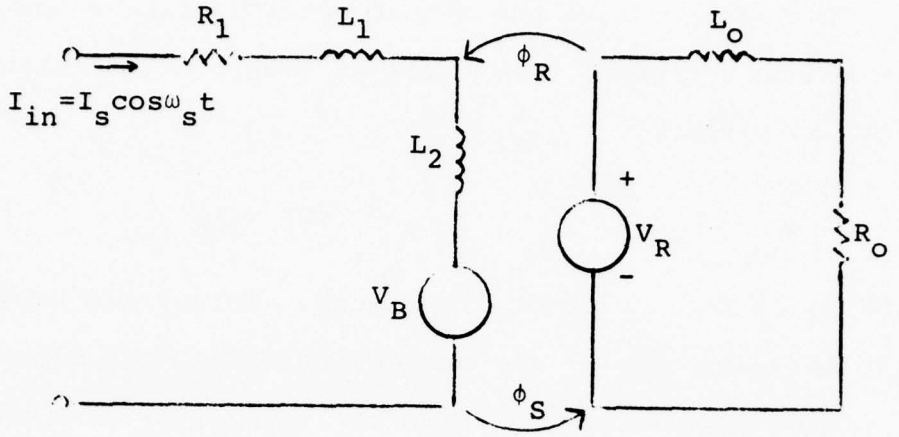

FIGURE 7: Alternate Model For Induction Machine

The circuit parameters are:

R_1 stator winding resistance

L_1 stator winding leakage inductance

L_2 effective stator-rotor mutual inductance as seen from stator

$L_2 = \frac{N_1^2}{R}$ where N_1 is the number of turns per phase on stator and R is the air gap reluctance

L_o rotor magnetizing and leakage inductance

R_o rotor resistance

The current into the stator winding creates the stator flux in the air gap. This field as seen from the stationary stator is given by

$$\phi_{\substack{s \\ at \\ stator}} = \frac{N_1 I_{in}}{R} = \frac{N_1 I_s}{R} \cos \omega_s t \qquad 3.5$$

where ω_s is the excitation frequency. This field rotates about the periphery of the air gap as for the PM motor. The rotor cage is turning and therefore the stator flux that it encounters does not have the same frequency as the flux referenced to the stator. The stator flux as seen by the rotor is

$$\phi_{\substack{s \\ at\ rotor}} = \frac{N_1 I_s}{R} \cos (\omega_s - \omega_r)t \qquad 3.6$$

where ω_r is the rotor rotational speed.

This flux induces a voltage in the rotor V_R given by

$$V_R = N_2 \frac{d\phi_s}{dt} \qquad 3.7$$

$$= \frac{-N_1 N_2 (\omega_s - \omega_r) I_s}{R} \sin (\omega_s - \omega_r)t \qquad 3.8$$

where N_2 is the effective turns per phase of the rotor cage. This generated voltage produces a rotor current I_R such that

$$I_R = \frac{V_R}{R_o + j(\omega_s - \omega_r)L_o} \cdot \qquad 3.9$$

If the slip is small, then $R_o >> (\omega_s - \omega_r) L_o$ and therefore

$$I_R = \frac{V_R}{R_o} = - \frac{N_1 N_2 (\omega_s - \omega_r) I_s}{R_o \; R} \sin(\omega_s - \omega_r)t. \qquad 3.10$$

This current produces a flux

$$\phi_{\substack{R \\ \text{at rotor}}} = \frac{N_2 I_R}{R} = - \frac{N_1 N_2^2 (\omega_s - \omega_r) I_s}{R_o \; R^2} \sin(\omega_s - \omega_r)t \qquad 3.11$$

Referring this back to the stator one obtains

$$\phi_{\substack{R \\ \text{at stator}}} = - \frac{N_1 N_2^2 (\omega_s - \omega_r) I_s}{R_o R^2} \sin \omega_s t \qquad 3.12$$

This is the flux that interacts with ϕ_s to produce the electromagnetic torque of the motor.

As can be observed, the phase angle between the two flux waves for small slips is approximately 90° and hence

$$T = K \; (\phi_{\substack{s \\ \text{at stator}}}) \; (\phi_{\substack{r \\ \text{at stator}}})$$

$$= K \; \frac{N_1^2 N_2^2 \; I_s^2 (\omega_s - \omega_r)}{R_o \; R^3} \qquad 3.13$$

If $\omega_s > \omega_r$ the rotor is rotating slower then the stator field. A positive torque results implying motor action. Conversely, if $\omega_s < \omega_r$ the rotor is rotating faster than the stator field and generator action results.

3.2.2 Damping Effect of Induction Motor With Constant Current Source

When the two motor system is running at synchronous speed it will exhibit some rotor perturbation i.e. the phase angle between the shaft and the rotating stator field will have a small time varying component about some fixed dc value. When this phase difference is increasing, the shaft is instantaneously going faster than the stator field and conversely when the angle is decreasing it is going slower than the field.

The angular displacement of the shaft will therefore have the following relation,

$$\Theta_{\text{shaft}} = \omega_s t + \Theta_1(t) \qquad 3.14$$

where ω_s is the synchronous angular velocity and $\Theta_1(t)$ is the time varying hunting term.

The perturbation hunting frequency was found experimentally to be very small (0 to 4 Hz). Hence the low slip approximation made in section 3.2.1 is valid. The stator flux is still

$$\Phi_{\substack{s \\ \text{at stator}}} = \frac{N_1 I_s}{R} \cos \omega_s t \qquad 3.15$$

However, the rotor now sees a stator flux of,

$$\Phi_{\substack{s \\ \text{at rotor}}} = \frac{N_1 I_s}{R} \cos(\omega_s t - (\omega_s t + \Theta_1(t))) \qquad 3.16$$

$$= \frac{N_1 I_s}{R} \cos(-\Theta_1(t))$$

This induces a voltage given by

$$V_R = N_2 \frac{d\Phi_s}{dt} = [-\frac{N_1 N_2 I_s}{R} \sin(-\theta_1(t))] \cdot \frac{d(-\theta_1(t))}{dt} \qquad 3.17$$

The current that flows then creates a rotor flux given by

$$\Phi_{\substack{R \\ \text{at rotor}}} = \frac{N_2 I_R}{R} = [\frac{-N_1 N_2^2 I_s}{R_o R^2} \sin[-\theta_1(t)]] \cdot \frac{d(-\theta_1(t))}{dt} \qquad 3.18$$

Referring this back to the stator one obtains,

$$\Phi_{\substack{R \\ \text{at stator}}} = [\frac{-N_1 N_2^2 I_S}{R_o R^2} \sin(\theta_s t)] \cdot \frac{d(-\theta_1(t))}{dt} \qquad 3.19$$

Then, by an argument similar to that given in section 3.2.1 the torque thus produced is given by

$$T = K \; (\Phi_{\substack{s \\ \text{at stator}}})(\Phi_{\substack{r \\ \text{at rotor}}})$$

$$= -K \frac{N_1^2 N_2^2 I_s^2}{R_o R^3} \frac{d\theta_1(t)}{dt} \qquad 3.2.6$$

The torque is proportional to the rate of change of the perturbation angle of the system about its desired synchronous angle $\omega_s t$. Therefore, this is a damping term and the induction motor will tend to attenuate any hunting in the 2 motor system when in synchronous operation.

3.3 Back Voltage At Induction Motor Terminals

When run open loop with a current source, the back voltage of the induction motor has little significance and could be ignored for all intents and purposes. However, in the closed loop system developed in this project, the induction motor voltage can be critical. The closed loop system relies on sensing an unambiguous PM motor back EMF for commutating the system. If the induction motor's EMF contaminates the PM voltage enough, no commutation will be possible and the system will not be able to maintain the required synchronous gyro speed.

The major problem in analytically determining the back voltage of the induction motor is the fact that the equations that model the system are coupled, nonlinear differential equations which are difficult to manipulate. In a steady state situation, the approximate model used in section 3.1 can be used. In a transient situation, such as during hunting, the following analysis can be used to obtain an approximate representation of the voltage.

Assuming a small slip caused by hunting during synchronous operation, the approximate model of section 3.2 can be extended to give a general idea of what the back EMF will look like with a constant current source.

The rotor flux at the stator is (refer to Figure 7)

$$\phi_{\substack{R \\ \text{at stator}}} = \frac{N_1 N_2^2 I_s}{R_o R^2} \sin(\omega_s t) \frac{d\theta_1(t)}{dt} \qquad 3.21$$

The voltage induced in the stator by this flux is

$$V_B = N_1 \frac{d\phi_{\substack{R \\ \text{at stator}}}}{dt}$$

$$= \frac{N_1^2 N_2^2 I_s}{R_o R^2} \left[\sin \omega_s t \frac{d^2\theta_1(t)}{dt} + \omega_s \frac{d\theta_1(t)}{dt} \cos \omega_s t\right] \qquad 3.22$$

In a steady state situation with

$$\frac{d\theta_1(t)}{dt} = \text{constant} = \omega_1 = \text{slip speed} \qquad 3.23$$

this reduces to

$$V_B = \frac{N_1^2 N_2^2 I_s}{R_o R^2} \omega_s \omega_1 \cos\omega_s t \qquad 3.24$$

As the slip increases a lag terms evolves from this since L_o becomes significant. In other words, the voltage reflected at the motor terminals, after eliminating the leakage and winding resistance terms, starts to lag the current.

For the transient hunting situation, the in-phase term will cause little problem in the closed loop control system. The problem arises from the quadrature term. This factor will contaminate the PM motor back voltage signal during transients in current or speed in

such a way so as to decrease the effectiveness of the control system. As a worst case, it could contaminate the back EMF signal of the PM motor to such an extent that the control system would be unable to run the motors properly. It might be possible to build a mechanism into the control system to account for this term; however, in the present case this was unnecessary since the term became negligibly small through the proper choice of motors.

Chapter 4

Description of Motor Requirements and Test Stand

4.1 Requirements for the Combination System

The specifications for the test stand were chosen to reflect the needs of the closed loop system. There were two principal requirements. First, the induction motor had to develop the necessary starting torque at a given excitation frequency and current. Second, the PM motor had to produce the needed running torque with a minimum amount of losses. These stipulations imply small winding resistance and low currents.

The closed loop system uses two modes of operation in order to meet the above performance requirements. At start, the excitation frequency is fixed at one-fourth the run frequency in order to obtain the required torque from the induction motor. Once the system has run up to approximately one quarter speed open loop, the system switches over to closed loop control and runs the system up to synchronous speed.

Figure 8 is a circuit model for the 2 motor series system during synchronous operation. As can be seen, each motor can be modelled as a series combination of a resistance, inductance, and a voltage source. The motor

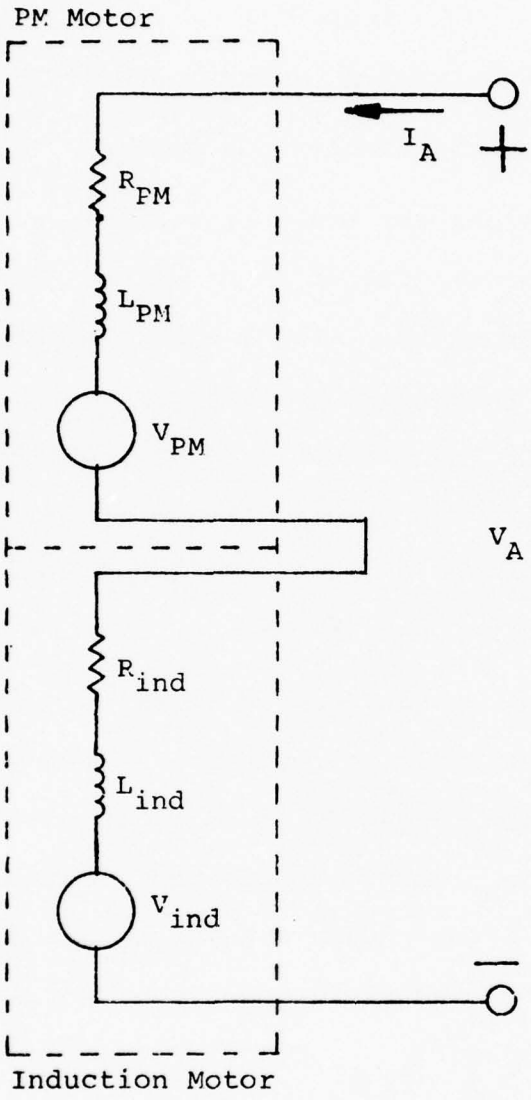

FIGURE 8: Circuit Model for Series Connection of PM and Induction Motors at Synchronous Speed

control algorithm relies upon sensing the back EMF of the PM motor for commutating and operating the system at synchronous speed. By knowing the motor terminal voltage (V_A), current (I_A), and circuit parameters (R_{ind}, R_{PM}, L_{ind}, L_{PM}), one can obtain the following,

$$V_{ind} + V_{PM} = V_A - I_A((R_{ind}+R_{PM}) + s\ (L_{ind}+L_{PM})). \quad 3.25$$

In order to introduce the least distortion into the PM voltage signal, it is desired that it be the dominant term of all the voltage drops in the motor. As far as the permanent magnet motor terms are concerned, this implies that the rotor (PM) flux be large relative to the stator flux. This requires that a strong permanent magnet be used on the rotor.

The generated back voltage of the induction motor is proportional to slip and to stator current (section 3.3). If one reduces the current, the back voltage is reduced. At synchronous speed, a minimum current results, for a given torque, whenever the PM rotor magnet is at maximum strength. This follows directly from the PM motor torque equation of section 2.1. It is probably possible to develop an algorithm that automatically accounts for this induction motor term; however, through the proper choice of motors, the voltage term became negligible and the algorithm was not needed.

For maximum efficiency, stator winding resistive losses should be kept to a minimum. This requires larger wire volume (not more or less turns, just a larger wire size) and low currents. A strong permanent magnet rotor will once again require the least current and hence provide for maximum efficiency.

A problem that arises in the operation of the system is that the induction motor requires approximately 3 times the synchronous current at start to overcome the starting friction and magnetic drag of the motors. The system must be so designed that this current does not destroy the PM stator coil or demagnetize the permanent magnet. This requirement implies a reasonable wire size and limits the number of turns on the stator of the PM motor.

The tradeoff, in summary, is as follows. To obtain the least distorted back emf one wants the strongest permanent magnet possible in the PM motor. For better efficiency (less resistive loss) and ability to survive high start currents, a larger wire volume is required. This increases motor size.

The induction motor chosen was a readily available 2-phase pump motor used in previous inertial navigation systems. Although slightly larger than necessary, it did have a high rotor resistance. This meant that the

maximum torque point occurred at a large slip (S = .35 for voltage source). Hence one could use a relatively high starting frequency, one-fourth the synchronous frequency, and still obtain a high torque even at rotor standstill. This high start frequency further reduced the restrictions on the interface rotary transformers which had to be large enough not to saturate at start.

After the circuit parameters and running characteristics of the induction motor were obtained (Appendix B), the PM motor characteristics were decided upon (Appendix A) to give the maximum torque per ampere and largest back emf within the restriction that the windings and permanent magnet be capable of surviving the high start currents.

The transformers, added later, had to be large enough so as not to saturate at the start frequency. This was the condition with the largest volt-time product. Concurrently, copper loss and core loss had to be kept low. The final design for these devices is shown in Appendix D.

4.2 Test Stand

The test stand contained three 2-phase motors whose shafts were connected together with universal lateral couplings (see Figure 9). Along with the PM and induction motors there was a 6 pole hysteresis synchronous motor.

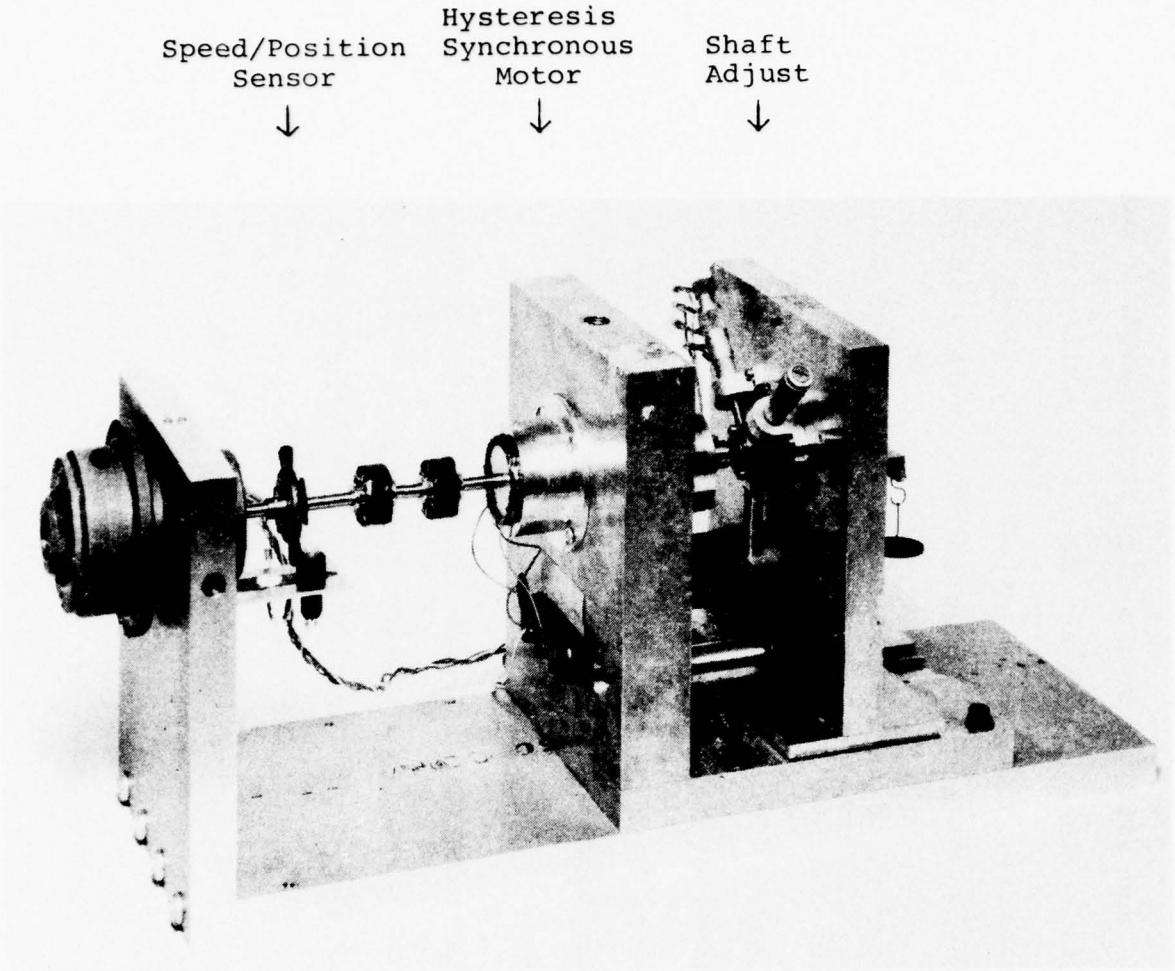

FIGURE 9a: Motor Test Stand

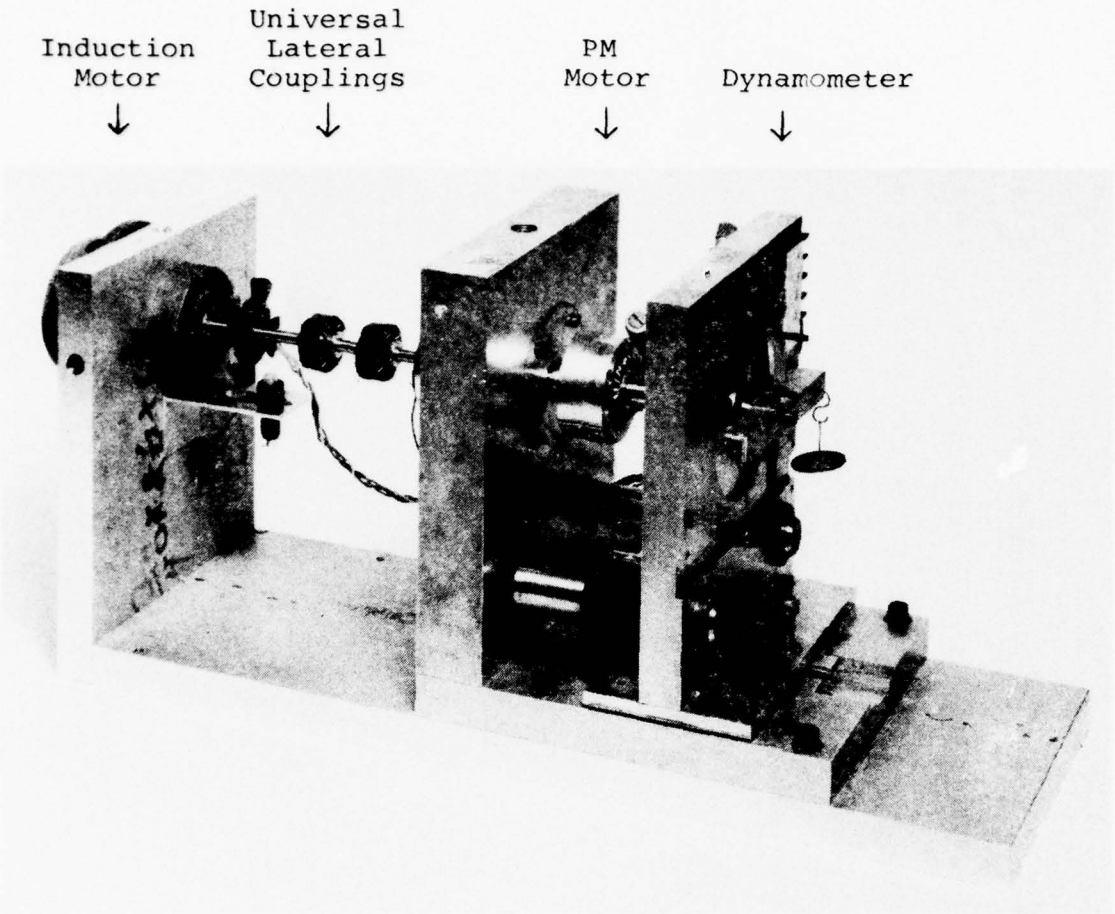

FIGURE 9b: Motor Test Stand

It was used for the initial tests on the other 2 motors as well as to introduce an extra load torque on the series motor system in order to test the system's response (see section 8).

The stand also had a dynamometer built into it. Both the PM stator and rotor were built on rotating shafts. Any torque supplied by the PM motor to the main shaft was reflected back to the stator. A balance arm was attached to the stator shaft to which gram weights could be added to determine the torque that the PM motor was producing.

Chapter 5

Open Loop Operation

Initially the system was analyzed and tested to determine if the series motor combination would have enough damping and pull-in torque to be able to be reliably run as a self-synchronizing open loop gyro system. Although the open loop scheme was found impractical for reasons to be given in section 5.2, several observations were made and a novel scheme for predicting pull-in frequencies for the PM motor was developed.

5.1 Phase Locked Loop Analogy for the Acquisition of Synchronism in the Two Motor System

The equations of motion that characterize the combination system as it attempts to acquire synchronous lock in an open loop, current controlled mode of operation are identical in form to those of a phase locked loop as it tries to lock onto an input signal within its pull-in range. Using PLL theory, therefore, it is possible to predict the pull-in range for the two motor system. This can give the designer a feel for how the induction and permanent magnet motors interact and gives evidence of the system's ability to acquire synchronous lock in an open loop mode.

The following discussion details the 2 motor system - PLL analogy.

5.1.1 Phase Locked Loop

A phase locked loop (PLL) is a frequency feedback system comprised of a phase comparator, low-pass filter, and an error amplifier in the forward path and a VCO in the feedback path (see Figure 10). Its operating characteristics are explained in detail in Appendix E.

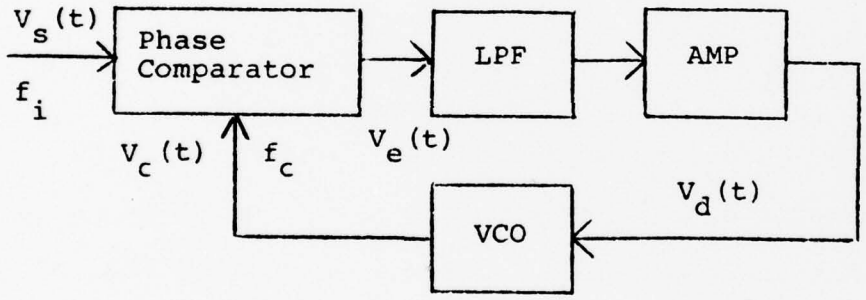

FIGURE 10: Phase Locked Loop Block Diagram

In essence, if f_i is sufficiently close to f_c, the free running frequency of the VCO, the difference component out of the phase comparator, V_e, will pass relatively unattenuated through the filter and eventually the VCO will synchronize or lock with the incoming signal. Once lock is acquired, there is only a finite phase difference

necessary to generate the required V_d. The system will lock whenever the input frequency falls within the capture range of the system.

5.1.2 Analogy

To make the analogy between the series combination of a PM and induction motor, run open loop with a current source, and the PLL the following approximations were made:

1) Only the fundamental component of current is considered significant.
2) The bearing and windage friction of the system combine to make the damping torque proportional to shaft speed, i.e.

$$T_{bearing} + T_{windage} = f_o \omega_{shaft} \qquad 5.1$$

3) The ratio between rotor speed and stator excitation frequency is such that the system is operating on the linear section of the torque/slip curve of the induction motor (see section 3.1).
4) The system utilizes a pair of 2 pole motors instead of the 8 pole devices actually used in experiments.

The rotor speed is analogous to the VCO frequency f_c. The stator field rotational speed has the same

significance as the input signal V_i to the PLL. The pulsating PM motor torque (when not in sync) is analogous to the error voltage V_e of the loop.

The free running frequency of the system is that rotational speed which would be maintained if the induction motor alone were driving the system. In other words,with just the induction motor engaged, the shaft speed will be less than the stator field rotational speed by an amount equal to that slip speed necessary to maintain the required torque level. Since with a current of sufficiently high magnitude (greater than .5 amp) the slip will be small (less than .05), the non-synchronous operation of the system will lie in the linear region of the induction motor's torque - slip curve for a constant current source (see Figure 11).

The following definitions are needed for the derivations:

ω_s: synchronous speed - same rotational speed as the stator field.

ω_o: rotational speed of system if it were powered by just the induction motor - free running frequency.

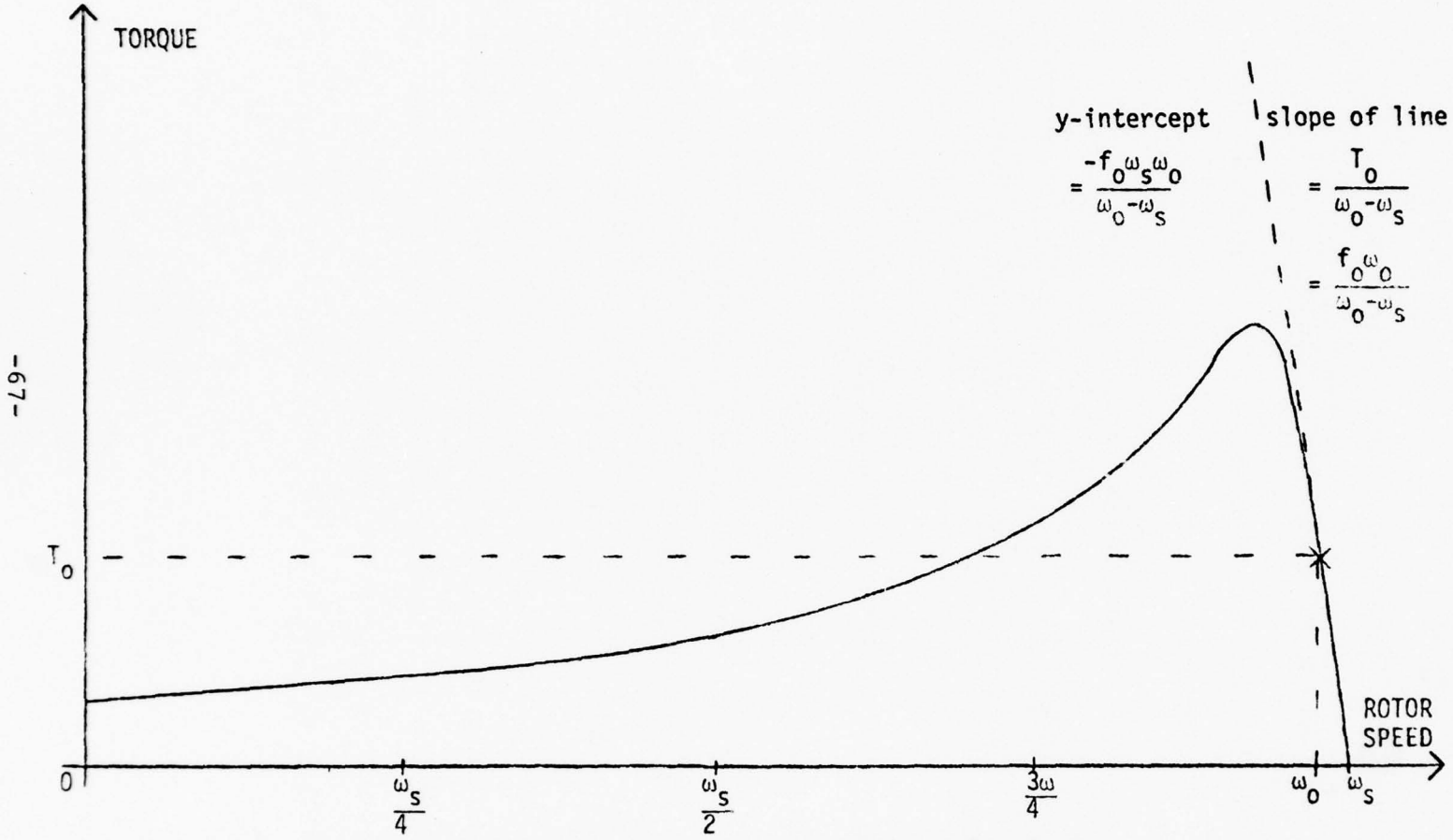

FIGURE 11: Operation of Induction Motor in Linear Torque-Slip Region

f_o: coefficient of damping friction.

J: moment of inertia of system.

K: torque constant for a 2 pole PM motor under balanced excitation, i.e.

$$T_{PM} = KI\sin\phi \qquad 5.2$$

where I is current per phase, ϕ is the angle between stator flux field and the rotor flux field.

T_{ind}: induction motor supplied torque.

T_{PM}: PM motor supplied torque.

The torque supplied by the induction motor when the shaft frequency is ω_o is

$$T_o = f_o\omega_o = \text{steady state torque} \qquad 5.3$$

Because operation is on the linear portion of the induction motor's torque-slip curve, (figure 11) as the rotor speeds up (with the same current and stator frequency) the torque is assumed to fall off linearly until at ω_s it is zero. Therefore, the equation for the induction motor torque becomes,

$$T_{ind} = \frac{f_o\omega_o}{\omega_o-\omega_s}\,\omega_{shaft} - \frac{f_o\omega_s\omega_o}{\omega_o-\omega_s}\,. \qquad 5.4$$

The torque equation for a 2 pole PM motor is

$$T_{PM} = KI\sin\phi \qquad 5.5$$

where $\phi = \int_0^t (\omega_s - \omega_{shaft})\, dt$ 5.6

The equation of motion for the entire system then becomes

$$T_{PM} = J\ddot{\Theta}_{shaft} + f_o \dot{\Theta}_{shaft} - T_{ind} \qquad 5.7$$

where Θ shaft is the angular displacement of the motor shaft from a fixed reference and $\dot{\Theta}_{shaft} = \omega_{shaft}$.

After substituting for T_{ind} and simplifying one obtains

$$T_{PM} + \frac{f_o\omega_s\omega_o}{\omega_o - \omega_s} = J\ddot{\Theta}_{shaft} + \left(\frac{f_o\omega_s}{\omega_s - \omega_o}\right)\dot{\Theta}_{shaft} \qquad 5.8$$

The induction motor's torque is thus seen to produce a "steady-state" torque, $\frac{f_o\omega_s\omega_o}{\omega_o - \omega_s}$, which contributes a steady-state or free running rotational frequency of

$$\omega_{ss} = \omega_o$$

Therefore, by superposition, the PM motor merely works around this rotational speed with an equation of motion given by

$$T_{PM} = J\ddot{\phi}_1 + \left(\frac{f_o\omega_s}{\omega_s - \omega_o}\right)\dot{\phi} \qquad 5.9$$

or $$KI\sin\phi = J\ddot{\phi} + \left(\frac{f_o\omega_s}{\omega_s - \omega_o}\right)\dot{\phi} \qquad 5.10$$

where $\phi = \int_0^t (\omega_s - \omega_{shaft})dt = \omega_s t - \int_0^t \omega_{shaft}\, dt$ 5.11

$= \psi_s - \psi_{shaft}$

where $\psi_s = \omega_s t$ and $\psi_{shaft} = \int_0^t \omega_{shaft}\, dt$.

This system can be written in operator notation as

$$T_{PM} = (Js^2 + (\frac{f_o \omega_s}{\omega_s - \omega_o})s)\phi \qquad 5.12$$

or

$$\phi = \frac{T_{PM}}{Js^2 + (\frac{f_o \omega_s}{\omega_s - \omega_o})s} \qquad 5.13$$

The system can be drawn in block diagram as follows:

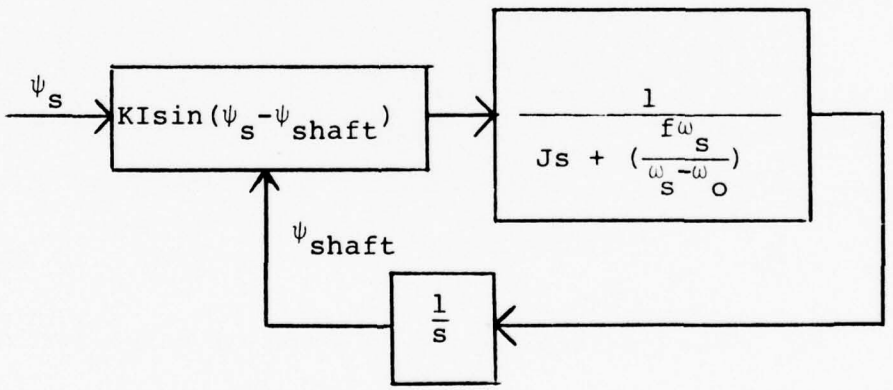

FIGURE 12: Block Diagram of Series Connection of PM and Induction Motors Run Open Loop

This diagram has the same configuration as a phase locked loop containing a simple first order lag type filter in the feedforward path. If ω_s and ω_o are close enough, the PM motor torque will become a slowly varying function of time. The torque beat note then would no longer be sinusoidal (see Appendix E). The waveform becomes an aperiodic cusp as can be seen in Figure 13a. Due to the asymmetry of the waveform there will be a finite dc component which will push the system toward ω_s and into synchronous operation.

Once in lock, $\omega_{shaft} \approx \omega_s$ and only a phase error will exist. Figure 13b shows the pull-in waveform for the motor. As can be seen, its waveform closely matches that of the PLL pull-in shown in Appendix E. Due to the narrow filter bandwidth, the response of the motor system is underdamped once synchronous lock has been achieved as can be observed from the figure.

5.1.3 Prediction and Measurement of Capture Range for Motor System

The two motor system - PLL analogy has a single low pass filter and an open loop pole at the origin. This means the feedback system is a 2nd order loop. The system block diagram can be redrawn in terms of filter time constants and loop gains as shown in Figure 14.

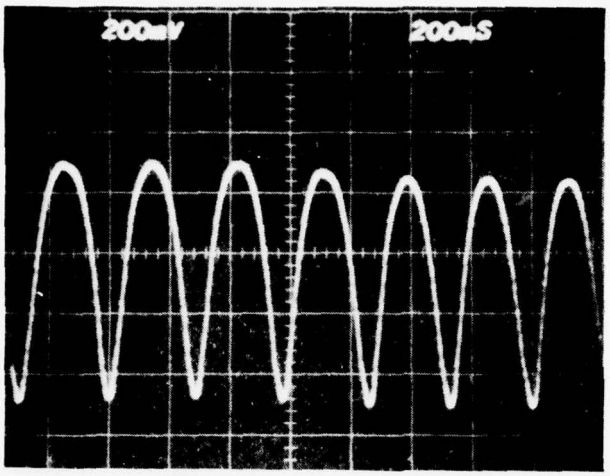

Vertical Scale
0.5 Hz/Div

← 60 Hz

a. Typical Aperiodic Cusp Waveform of Rotor Rotational Velocity Prior to Synchronous Lock

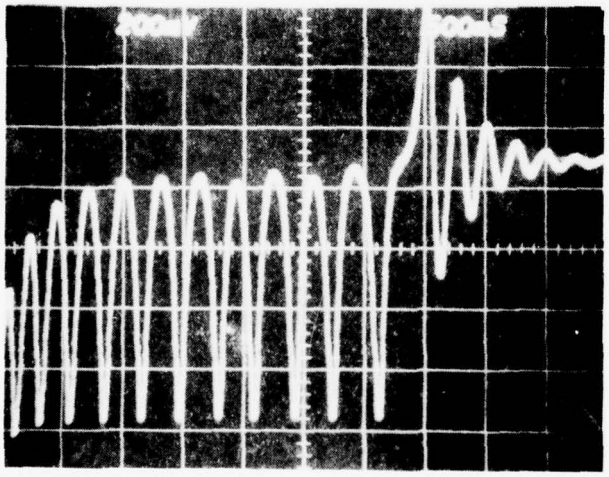

Vertical Scale
0.5 Hz/Div

← 52.5 Hz

b. Rotor Rotational Velocity During Synchronous Pull-In

FIGURE 13: Instantaneous Rotor Speed During Synchronous Lock Acquisition

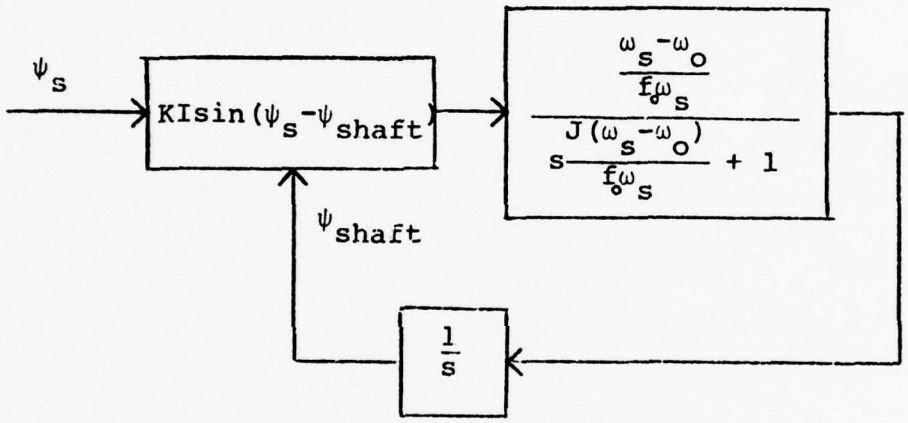

FIGURE 14: Block Diagram for PLL Analogy

The open loop gain K_v is given by

$$K_v = KI \frac{\omega_s - \omega_o}{f_o \omega_s} \qquad 5.14$$

and the filter time constant by

$$\tau = \frac{J(\omega_s - \omega_o)}{f_o \omega_s} \qquad 5.15$$

The capture range of a phase locked loop is difficult to predict analytically. Therefore, empirical formulas have been developed to obtain an approximate range. For the system shown above, with a first order lag LPF the capture range ω_c is given by [14]

$$\omega_c = (\omega_s - \omega_o)_{max} = \frac{\sqrt{K_v}}{\tau} = (\frac{KI}{J})^{1/2} \qquad 5.16$$

It predicts the largest free running slip frequency allowed for a given system at a given current.

The two motor combination used in this project contained 2-eight pole machines. Therefore, the analogy to a PLL breaks down somewhat since the phase detector gives a torque waveform that varies at 4 times the difference frequency instead of at the difference frequency. As a result the expected pull in range should be less. In

fact, since there is an integration in the loop one can make the assumption that the open loop gain is smaller by a factor of 4 over what it would be if the devices had only 2 poles. In other words, in the 2 pole systems

$$K_v = KI \frac{\omega_s - \omega_o}{f_o \omega_s} \qquad 5.17$$

In the 8 pole system this becomes

$$K_v = \frac{KI}{4} \frac{\omega_s - \omega_o}{f_o \omega_s} \qquad 5.18$$

Therefore the expected capture range then becomes

$$\omega_c = \left(\frac{KI}{4J}\right)^{1/2} = 1/2 \left(\frac{KI}{J}\right)^{1/2} \text{ rad/sec}$$

To test the prediction, the motor combination was run open loop using the power stage described in section 7. This current source power supply was run at several predetermined currents in order to measure several capture ranges.

Using the power stage, and a tachometer circuit for observation, for a given current the system frequency ω_s was increased until synchronous lock could no longer be obtained. Then this frequency was recorded along with the current and the rotor frequency when just the induction motor alone was run with this stator excitation. The PM

motor was still coupled on the same shaft but it was no longer connected in electrical series with the induction motor. The pull-in frequency or capture frequency was defined as the difference between the final synchronous frequency and the rotor frequency when just the induction motor was supplying the torque. This was then compared with the capture range predicted by the PLL analogy. In all cases a pull in time of up to 3 minutes was allowed.

The motor system's constants were found to be:

$J = 811.5$ gm-cm^2

$K = 270{,}000$ dyne-cm/ampere

$f_o = 87.5$ dyne-cm/rad/sec

The following result were obtained:

trial #	1	2	3	4
current (amperes)	.60	.58	.55	.50
rotor sync.freq. (Hz)	70.425	55.275	47.975	36.025
free running freq. (Hz)	69.05	53.95	46.675	34.775
capture range (Δf actual)(Hz)	1.375	1.325	1.3	1.25
capture range (Δf predicted(Hz)	1.13	1.11	1.08	1.03
Δf actual/Δf predicted	1.22	1.20	1.21	1.22

Table I

As can be seen,the values predicted miss the mark by 20%. This can be attributed to several causes. First, only the fundamental waveforms were considered while the power stage introduced several harmonics that might have interferred with the pull-in process. Second, the initial assumption that the open loop gain can merely be reduced by a factor of 4 when using 8-pole machines could be invalid. Third, the currents although nominally at the values given above could vary somewhat due to the finite loop gain in the power stage and therefore this also caused an error.

The consistency of the data, however, implies that the pull-in range of the two motor combination and perhaps other systems using a PM motor can be predicted accurately.

5.5 Results of Open Loop Tests

As demonstrated in the previous section, unless the current into the two motor system is excessively high, the motors will attain synchronous lock only for low excitation frequencies. Once the system is locked, the frequency can slowly be ramped up to the run frequency and the motors will follow it. However, if the frequency ramps up too fast, a transient occurs in excitation, or there is a torque transient on the shaft, the system will fall out of synchronism and the entire process will have to be repeated.

A second starting method that can be used to start the motors does not attempt to obtain synchronous operation before ramping the frequency. A low frequency start signal brings the system up to approximately 1/4 full speed using the steady torque from the induction motor. The frequency is then ramped up to 1.1 times the run frequency. The induction motor provides enough torque to enable the shaft to follow the ramp with only a small slip.

With the small slip the shaft is then rotating at a rate greater than the desired run speed. The excitation frequency is then stepped down to the run frequency. As the rotor slows down it gets "caught" by the new stator field and locks into synchronism. Once lock is attained the stator currents are reduced from the original .5 amperes down to about .25 amperes in order to obtain a higher efficiency.

Using either start algorithm it is possible to run the system up to synchronous speed. However, there are several inherent problems with open loop operation.

One of the major problems associated with a hysteresis synchronous motor gyro drive is its tendency to be extremely underdamped at synchronous speeds. In other words, if a torque transient or stator excitation transient occurs in the system, the shaft will oscillate about its expected rotational vector for a considerable amount of time. If one

time-averages this signal over a long enough period the error will reduce to zero. If instantaneous readings are required this is not possible.

An experiment was performed to document the 2 motor system's transient response to a torque step applied to the shaft. Both current and voltage source drives were used. The steady state rotational frequency of the shaft was 100 Hz. The steady state load torque was 50,000 dyne cm. The pulse of torque added an extra 11,500 dyne cm for approximately six seconds and then removed it. For this size step, the minimum open loop current drive to the motor was .26 amperes per phase. Anything less resulted in a loss of sync. When run with a voltage source, the minimum voltage was 25 Vrms.

The rotational displacement angle of the shaft can be modelled as

$$\Theta_{shaft}(t) = \omega_s t + \Theta_1(t)$$

where ω_s is the synchronous velocity and $\Theta_1(t)$ is the hunting angle. Therefore

$$\omega_{shaft} = \omega_s + \frac{d\Theta_1}{dt}$$

The pictures in Figure 15 are a plot of this instantaneous $\frac{d\theta_1}{dt}$ as the motors are subjected to the torque pulse. The traces indicate how far from sync speed the shaft rotational velocity actually is at that moment.

As can be observed, the voltage source drive provides slightly more damping than the current stage although the difference is negligible. This gives experimental verification for the analysis presented in section 3.2 that predicted the damping effect of the induction motor at synchronous speeds.

Although the hunting is reduced over that of a hysteresis synchronous system which is virtually undamped, it is still not acceptable for the intended applications. As will be shown in section 8, closed loop back EMF control reduces this hunting significantly and increases the efficiency of the system as well.

There are drawbacks to the open loop system other than the hunting. For maximum efficiency, it is desired that the PM motor be run at a torque angle of 90° (see section 2). In an open loop situation this is impossible since it leaves no torque margin for transients that inevitably will occur. Thus it must be run at less

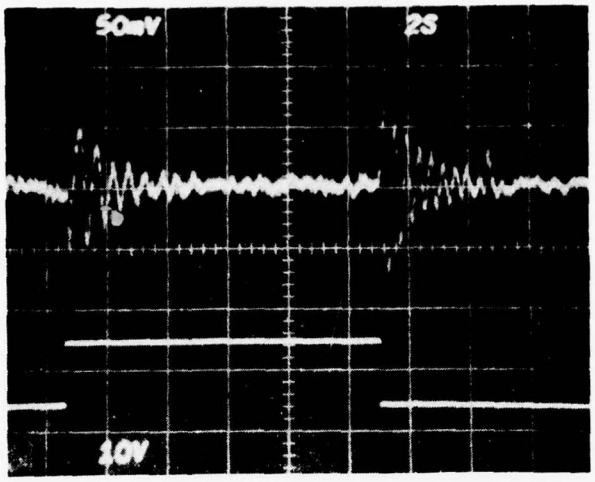

Vertical Scale
0.125 Hz/Div

Steady State Rotor
Frequency = 100 Hz

←

Torque Pulse
11,500 dyne·cm

Steady State Shaft
Torque
50,000 dyne·cm

a. Current Source Excitation (I= 0.26 A)

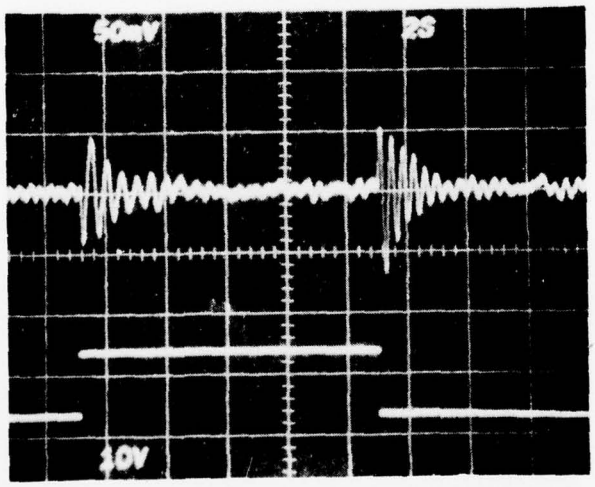

Vertical Scale
0.125 Hz/Div

Steady State Rotor
Frequency = 100 Hz

←

Torque Pulse
11, 500 dyne·cm

Steady State Shaft
Torque
50,000 dyne·cm

b. Voltage Source Excitation (V= 30 V_{rms})

FIGURE 15: Rotor Hunting In the Open Loop System When Disturbed by A Torque Pulse Applied To Shaft

than 90° which means there is a greater current required and consequently more resistive losses. The efficiency is reduced considerably depending upon how much of a safety margin is desired.

As has been stated, if the current used is 0.26 A, a torque step of 11500 dyne - cm can be tolerated. Any greater torque has a good probability of knocking the system out of synchronous lock. A transient in the stator excitation frequency will do the same. Once out of synchronism this system must be reset and restarted. Therefore, some sensor is required that can determine if and when sync is lost. It must then recycle the control system.

The hunting, low efficiency, requirement for a loss of synchronism sensor, inability to hold sync and run-up difficulties all contribute to making the open loop scheme unreliable. It is for these reasons that the decision was made to implement the closed loop back EMF control scheme that become the principal objective of this project.

Chapter 6

Theory of Closed Loop Operation

The basic restriction for the control scheme of the series motor system is that it must be able to operate the motors through either the standard four flex lead interface or through the optional rotary transformers. A shaft position transducer such as a Hall - effect device placed on the float cannot be used since it would require more connections.

It is possible, technically, to place all the control electronics or a control multiplexer on the float. However, engineering problems associated with thermal effects, packaging, and circuit stability preclude this.

6.1 Control Scheme

The technique used for commutating the two motor system was originally developed by D. Fulton.[6] His system was designed for just a single permanent magnet motor powered through flex leads. Nevertheless the principle remains the same for the series system. If the back EMF of the PM motor can be sensed, then as was shown in section 2.2, it would provide all the unambiguous information that is needed for commutating and controlling the speed of the motors.

As previously derived, the back EMF of each winding is a sinewave proportional to the rate of change of the flux linked by that winding. It leads the flux by 90°. For maximum efficiency, the permanent magnet motor is run at a 90° torque angle. This means one must inject current into each stator winding in such a way that it is 90° away from the PM rotor flux. Combining this requirement with the characteristics of the back voltage gives the control algorithm first suggested by Fulton:[6]

> Sense back EMF of a PM motor winding and force the current in that winding to be in phase with the back EMF. In this way the motor is commutated at a 90° torque angle.

6.2 Sensing PM Motor Back EMF

If the motors are run synchronously, as they would be in closed loop mode, the induction motor can be approximated as a resistance and inductance in series with a small noise term. The PM motor can likewise be approximated as a resistor and inductor in series with a voltage source, the generated back EMF.

Figure 16 shows the technique used to determine the PM back EMF even while the system is excited. The voltage reflected at the motor terminals is very nearly equal to the sum of the impedance drops and the back EMF. The im-

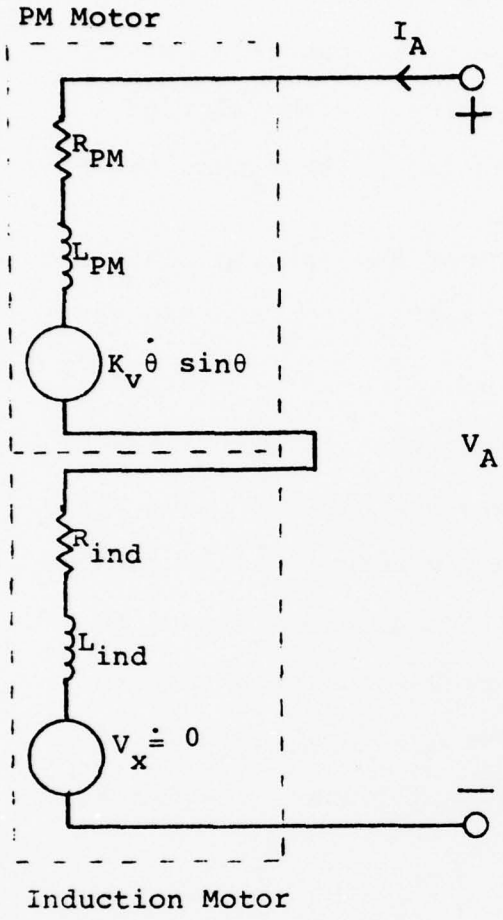

$R = R_{PM} + R_{ind}$

$L = L_{PM} + L_{ind}$

Motor Input Equation

$V_A = (Ls + R) I_A + K_v\dot{\theta}\sin\theta$

Integrated Back EMF

$K_v \cos\theta = \frac{1}{s}[V_A - (Ls+R) I_A)]$

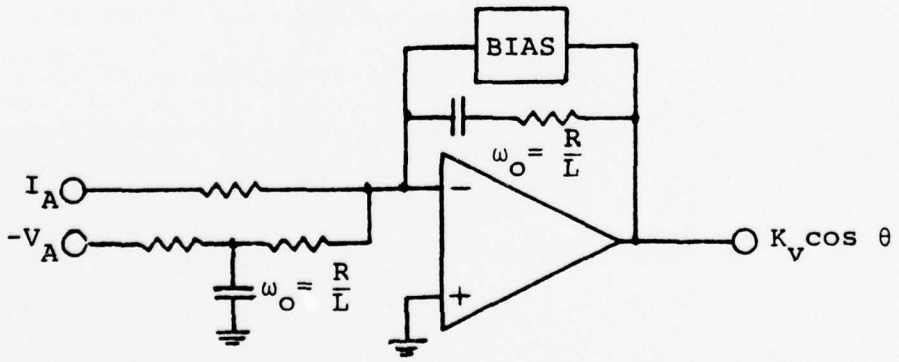

FIGURE 16: Technique for Recovering and Integrating the Back EMF of PM Motor

pedances can be reasonably well modelled for both motors. The induction motor does have some cross coupling between phases which introduce some distortion. With balanced supplies, however, this distortion can be kept negligible.

By sensing the terminal current and voltage and performing the indicated scaling and subtraction one can thus obtain the back EMF signal.

The system also employs an integrator. This stage performs several useful functions. The back EMF is a sine wave proportional in amplitude to the rotational frequency. The gain of an integrator is inversely proportional to frequency. The output of the sensing circuit is thus a sine wave with a constant amplitude over a wide range of speeds. The integrator also acts as a filter to attenuate any high frequency noise.

At gyro speeds of 24,000 to 45,000 rpm the back voltage is at least an order of magnitude greater than the impedance drops and induction motor interference. Thus, the control scheme is very compatible and works well with the combination motor system. Also, with the strong permanant magnets available today as well as the capability of running the PM motor at a 90° torque angle, the motor currents can be kept low (approximately 200 ma/phase for a torque requirement of 50,000 dyne-cm). This gives a marked improvement in gyro efficiency over hysteresis synchronous motor systems and the open loop series motor system.

6.3 Description of Entire Control System

Figure 17 is a block diagram of the entire control system. Note that the system senses the EMF in both phases. It then integrates these signals and uses the resultant sine waves as the main component driving the motor supplies.

The phase A and B currents are

$$I_A = I_o \cos \Theta\ (t)$$

$$I_B = I_o \sin \Theta\ (t)$$

where I_o is determined by the system and Θ (t) is simply the instantaneous angle of the input signal.

The recovered back EMF's, with 90° commutation, are

$$V_A = K_v \dot{\Theta} \cos \Theta$$

$$V_B = - K_v \dot{\Theta} \sin \Theta$$

where K_v is the back EMF proportionality constant. These signals are then integrated to give constant amplitude sine waves. However, phase A is negated while phase B is not. The integrator outputs are

$$V_1 = - K_2 \int V_A dt = - K_v K_2 \sin \Theta$$

$$V_2 = K_2 \int V_B dt = K_v K_2 \cos \Theta$$

where K_2 is simply a gain term.

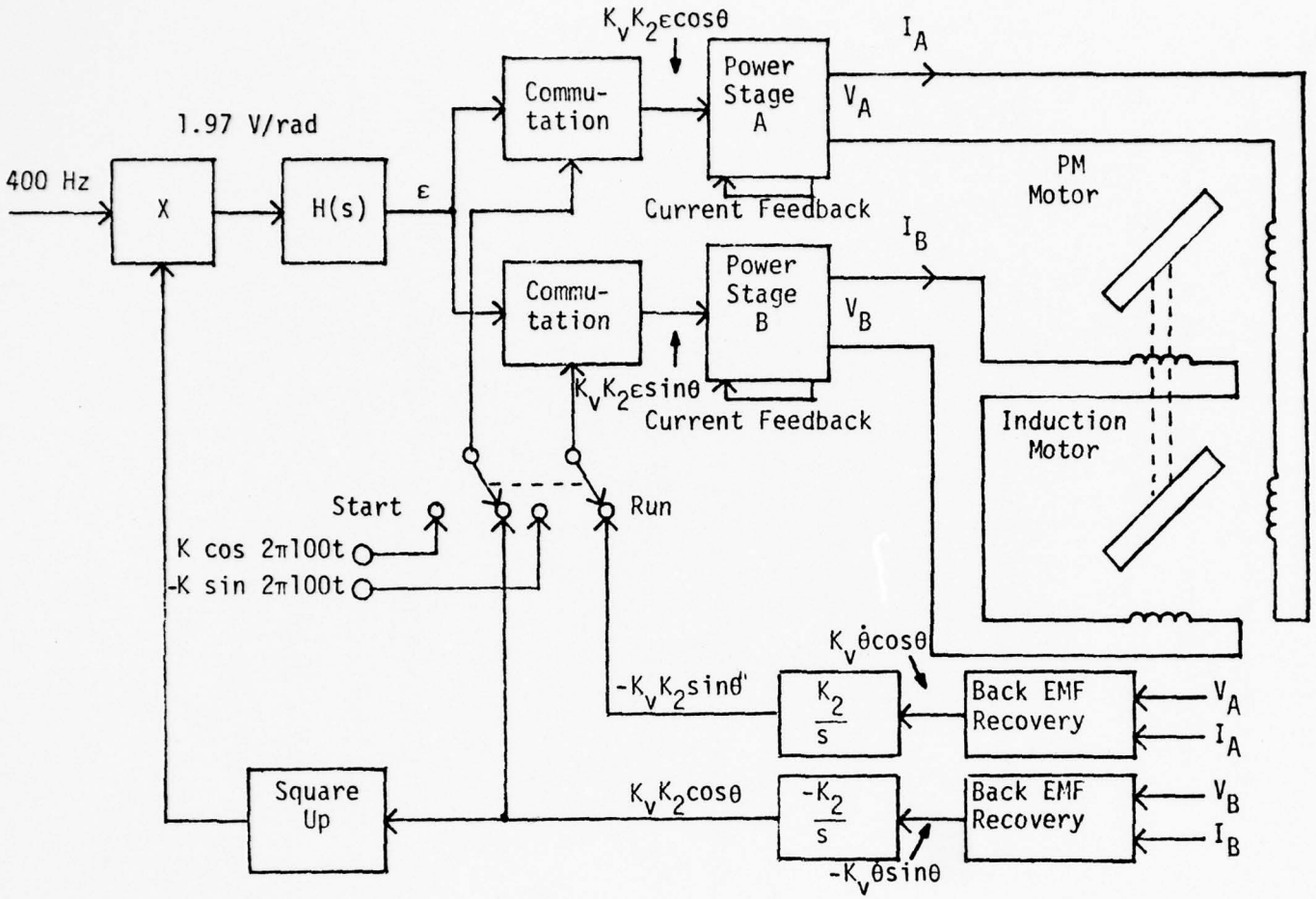

FIGURE 17: Control System for Two Motor Gyro Drive System

These constant amplitude signals form the basic signal driving the power stages. V_1 drives stage B and V_2 stage A. Commutation is performed by scaling these currents with a weighting function. The magnitude of the input currents to the motor is controlled by the speed control error ε. This error component is generated by squaring up one of the back EMF signals and phase locking it to the system clock.

H(s) is a compensation network which insures stability and a well-damped response to disturbances to the system.

There is also an open loop start circuit provided. At start two quadrature signals at 1/4 sync frequency are provided as the basic current drive signals. These are multiplied by the maximum error signal since the system is out of sync. This weighted signal then provides the desired maximum current (approximately 500 ma) to the induction motor which enables it to overcome starting friction and magnetic drag. Once the system is up to about 15 to 20% of its sync frequency, the back EMF signal is sufficiently dominant to enable the system to switch to closed loop control.

Chapter 7

Circuit Implementation

An objective of this thesis was to investigate the feasibility of the series motor configuration for gyro drive applications. In light of this goal, the electronic systems designed for the tests were perhaps more complex than those that would actually be used. Operational blocks which could have been combined were kept separate. For example, the back EMF recovery system and the following integration stage could probably have been built with one op amp.

This modularization and expansion permitted design flexibility. One could easily vary the characteristics of only one stage to see what effects this produced on the system response. Now that the concept has been verified, more compact and efficient systems could be devised.

7.1 Back EMF Recovery

A practical circuit for recovering one phase of the PM motor back EMF is shown in Figure 18. This circuit differentially senses the current into and the voltage at the motor terminals, scales them, performs the necessary subtraction, and then integrates the final signal.

The voltage is sensed directly from the motor terminal of the series motor system. The current is sensed indirectly by differentially sensing the voltage across two small resistors in series with the motors.

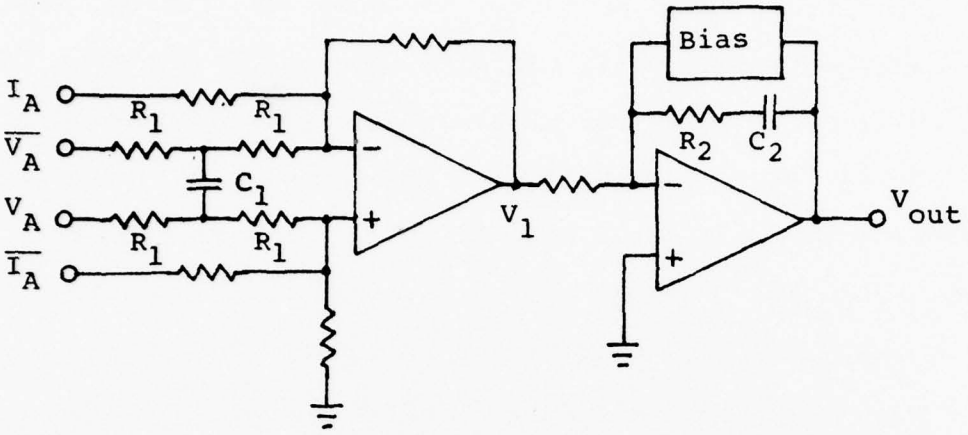

Transfer Function: $V_{out} = \frac{1}{s}[(V_A - \overline{V_A}) - (sL+R) \cdot (I_A - \overline{I_A})]$

$R = R_{PM} + R_{ind}$

$L = L_{PM} + L_{ind}$

$\omega_o = \frac{R}{L} = \frac{1}{R_1 C_1} = \frac{1}{R_2 C_2}$

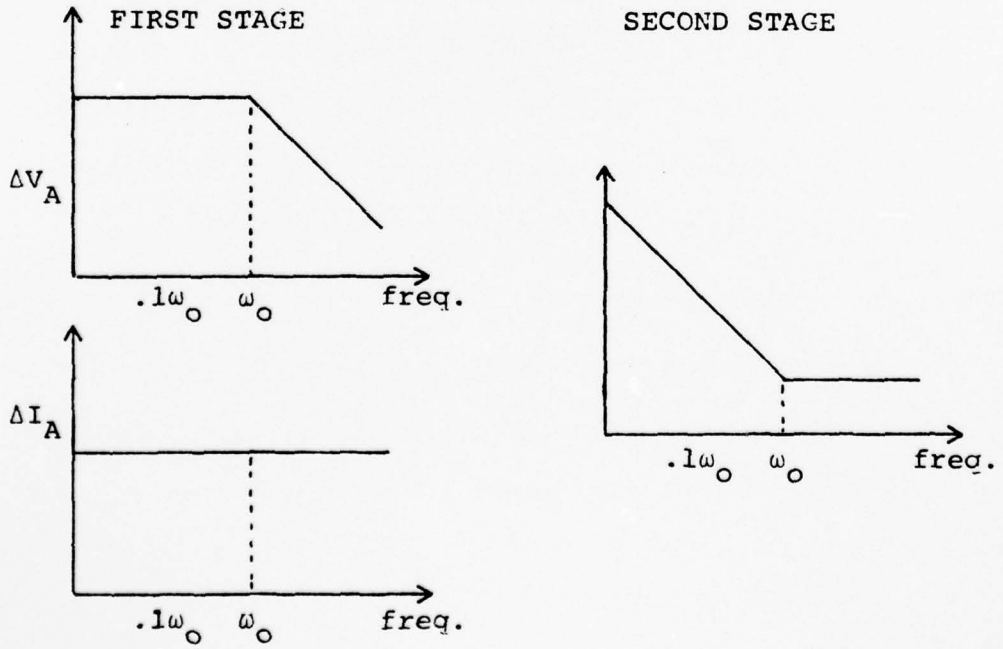

Bode Plots for the Individual Signal Paths

FIGURE 18: Practical Back EMF Sensing Circuit

The first stage primarily performs the sensing, scaling and subtraction while adding a gain term. The pole on the voltage inputs is set at the resistive/inductive (R/L) pole of the motor combination. The second stage performs a partial integration of both signals with a zero at the same R/L point. The cascade of the two stages therefore fully integrates the voltage and integrates the current only up to the R/L frequency. This is consistent with the integrated back EMF equation of Figure 16. The algorithm was performed in this manner to obviate the need to build a differentiator for the current term. The final output is of constant amplitude as the motor runs up to synchronism.

This circuit is a simplified version of the system actually implemented (Appendix C). Due to the high noise content of the switching power stages it was necessary to add several low pass filters to the network.

7.1.1 Design Considerations

Noise is the biggest factor in the design of this unit. The integrated back EMF's are the signals used as the fundamental drive components to the power stages. If these signals have phase jitter or amplitude oscillations, motor current noise will be produced. This not only varies the thermal input to the gyro but also, as was observed, if the noise is severe enough, synchronous lock can be lost.

AD-A063 591 ARMY MILITARY PERSONNEL CENTER ALEXANDRIA VA F/G 17/7
A FEASIBILITY STUDY OF AN ALTERNATIVE POWER AND CONTROL SYSTEM --ETC(U)
DEC 78 M N RICHARD

UNCLASSIFIED NL

2 OF 2
AD
A063591

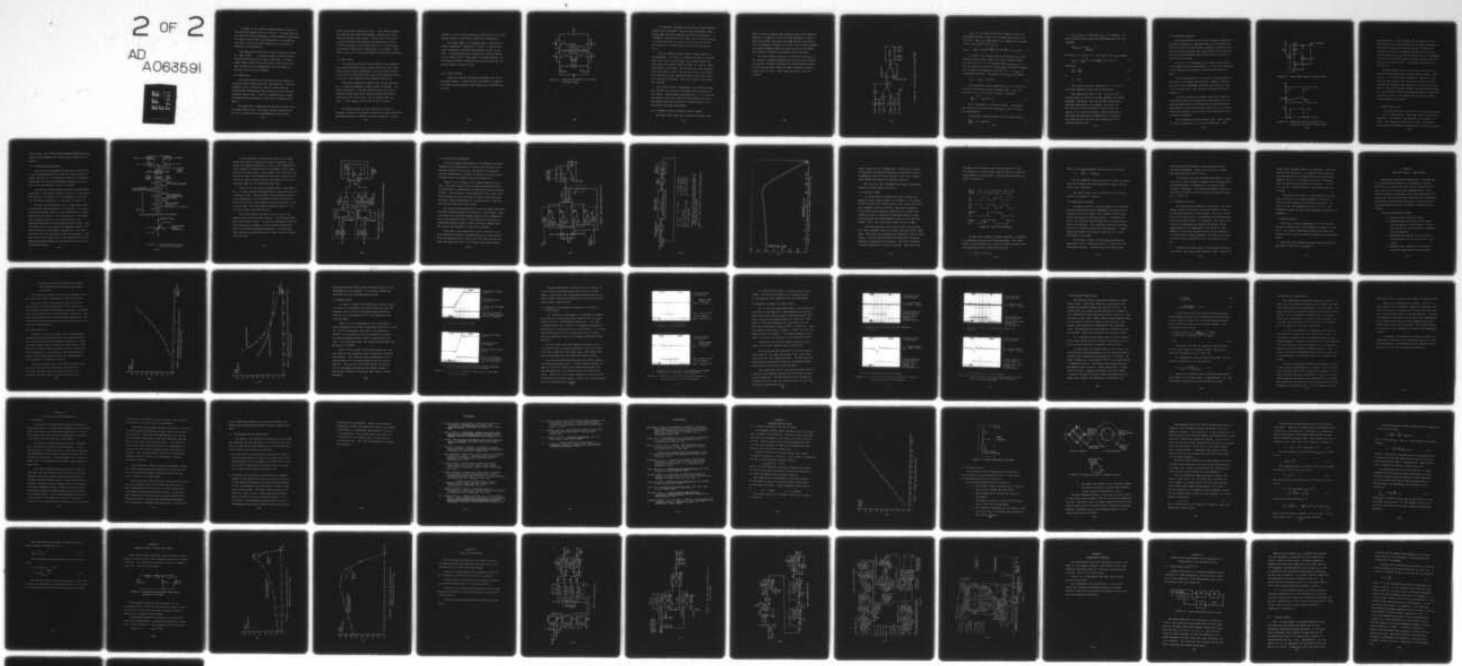

END
DATE
FILMED
3-79
DDC

As shown in the control scheme diagram of Figure 17, both back EMF signals must be recovered. Although one signal contains enough information to both commutate the motors and control their speed, the manufacture of a quadrature sine wave to drive the other phase would unnecessarily complicate the electronics.

This design will work with either a linear or switching power stage. A switching stage requires heavier filtering but the basic concept is the same. A quasi - linear supply would require much less filtering but this type of supply may be incompatible with the higher inductance of the two motor system.

7.2 Commutation

The stator field of the PM motor can be viewed as a rotating vector having direction and magnitude. The commutating circuit forces this vector to have a preset average phase displacement from the poles of the rotating permanent magnet rotor. This is accomplished by scaling the magnitude and frequency of the A and B phases of the motor.

The magnitude is controlled by the error signal from the speed control loop. The stator vector frequency (position) is controlled by the commutation signal coming

from the back EMF recovery circuits. Since these networks are tracking the rotor displacement, the PM rotor cannot vary the average torque angle. If the rotor is hit with a torque transient and retards, the commutation circuit retards the angle of the stator field in a similar manner. An average torque angle is maintained at all times. This angle is set at 90 electrical degrees for maximum efficiency.

7.3 Power Stage

The principal tradeoff in the design of the commutation system and power stage is motor efficiency and ripple torque versus circuit complexity. In the original design of the control electronics for a gyro wheel powered by just a PM motor, the tradeoff favored maximum simplicity.

The series combination system also favors simplicity but it gives the designer a wider choice of methods. The larger inductance of the new system permits the use of a switching power stage which improves system performance, increases circuit efficiency, and is simpler than the quasi - linear supply used in the original project.

The system chosen for this feasibility study is actually a variant of the power stage used to drive hysteresis synchronous motors in another inertial navigation system.

Instead of a pulse width modulation design with its limited dynamic range, a pulse ratio concept was implemented.

The power stage is a switching supply operating at a nominal (quiescent) frequency of 35 KHz. It uses pulse ratio modulation to deliver the required current to the load. It incorporates both voltage and current feedback and can operate over a wide range of voltage supplies. It also employs several different means for insuring that no overlap between switches occurs.

7.3.1 Basic Circuit

Figure 19 gives an operational schematic for one of the power stages. As can be seen, the system is actually an H switch with the motor load forming the horizontal bar of the H.

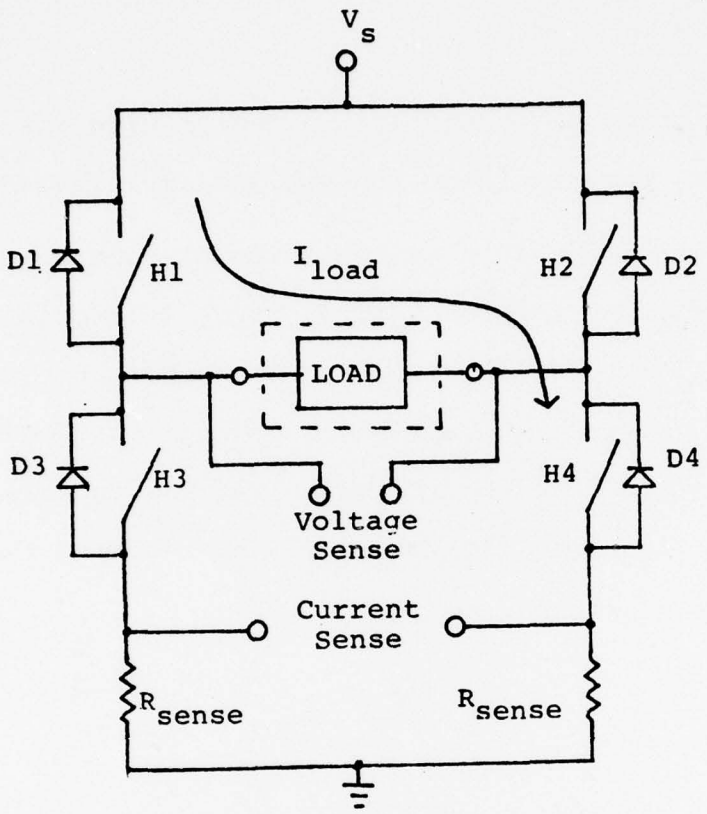

FIGURE 19: Simplified Diagram of One Phase of Power Stage

In operation, switches H1 and H4 are closed together and H2 and H3 likewise. The two pair of switches alternately open and close applying positive then negative (reversed) voltage across the load. For a positive current in the direction of the arrow in the Figure, H1 and H4 are closed for a longer time than H2 and H3 during one cycle.

With an inductive load, current cannot change instanteneously. If current is flowing as shown in the diagram, then when H1 and H4 open, the voltage across the load flips and forward biases D2 and D3 in order to maintain current continuity. The current will then exponentially die down. Even if H2 and H3 turn on, the current will continue to flow through D2 and D3 until the inductor's energy is depleted. Once this occurs, the current will reverse.

The actual circuit incorporates a time delay between the turn-off of one pair of switches and the turn-on of the others. This provides approximately a 5 to 6 μsec delay between transistor turn-off and transistor turn-on. The delay allows for the decay of stored charge in the previously saturated transistors.

7.3.2 Feedback Control Loop and Current Command

The power stage uses both voltage and current feed-

back in order to develop the required pulse ratio modulated waveform. Primarily a little voltage feedback is used to lower the current loop gain and stabilize the loop and to set the quiescent frequency of 35 KHz. The current feedback and current command inputs are used to vary the quiescent pulse widths to obtain the desired current waveform.

The basic control structure is pictured in Figure 20. The voltage is sensed differentially at the load terminals. The current is sensed indirectly by differentially measuring the voltage drop across two small resistors placed in series with the load. These resistors have a value of 1Ω each.

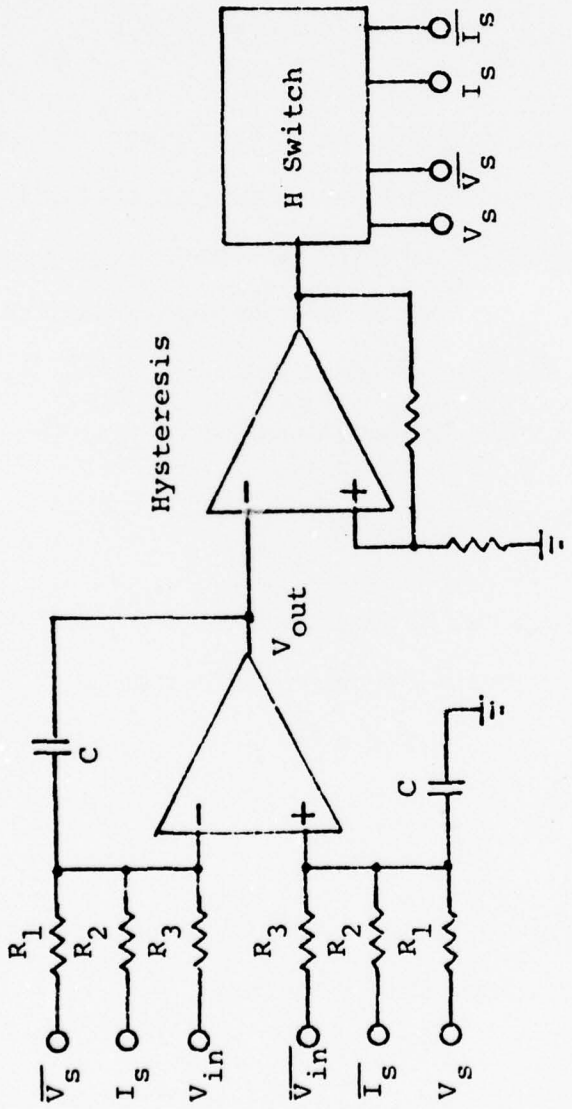

FIGURE 20: Control Structure for Power Stage

V_{out} is a triangular wave which ramps up until the hysteresis switch triggers. This reverses the polarity on the load. Then V_{out} ramps down to its symmetrical negative value. The equation for V_{out} is

$$V_{out} = -\left(\frac{1}{R_1C}\int(V_s-\bar{V}_s)dt+\frac{1}{R_2C}\int(\bar{I}-I)dt+\frac{1}{R_3C}\int(V_{in}-\bar{V}_{in})dt\right) \quad 7.1$$

As stated, the voltage sets the quiescent pulse frequency or pulse width. When the current command inputs are zero ($V_i-\bar{V}_i = 0$) it is desired that $I_{load\ average} = 0$. With an inductive load and a high enough switching frequency one can make the assumption that when $\Delta V_i = 0$, I_{load} is instantaneously zero. The equation for V_{out} then becomes

$$V_{out} = -\frac{1}{R_1C}\int(V_s-\bar{V}_s)dt \quad 7.2$$

The hysteresis on the comparator is $\pm$ 2.5 volts. With a desired square wave as the quiescent pulse, V_{out} will ramp from -2.5 to 2.5 in 1/2 a period. Therefore,

$$-\frac{1}{R_1C}\int_0^{T/2}(V_s-\bar{V}_s)dt = 5 \quad 7.3$$

With f quiescent = 35 Khz, T is known. By choosing the required V_s one can then determine R_1 and C to meet the requirements.

The desired transfer function of the power stage is

$$\frac{I_{out}}{\Delta V_{in}} = 0.1 \text{ amp/volt} \quad 7.4$$

If $V_{in}-\bar{V}_{in}$ is 1 volt then I_{out} = 0.1 amperes. In this situation one can make the approximations that over 1 period,

$$Vs_{average} = V_{out\ average} = 0$$

Therefore, if R sense = 1Ω, the equation for V_{out} becomes

$$V_{out} = -\frac{1}{R_3C}\int_0^T (1-0)dt+\frac{1}{R_2C}\int_0^T (.1-0)dt = 0 \qquad 7.5$$

Therefore,

$$\frac{1}{R_3C} = \frac{0.1}{R_2C} \qquad 7.6$$

or

$$R_3 = 10R_2 \qquad 7.7$$

With these relations, equations 7.3, 7.4 and 7.7, the final component values can be determined.

The system does have a flaw. Its loop gain is controlled by the ratio of voltage feedback to current feedback. Therefore, with the PM motor generating a back EMF proportional to frequency, the loop gain gets smaller as the rotational or excitation frequency of the system increases. This problem can be minimized by choosing the feedback ratio carefully. The speed control loop can then compensate for the remaining sensitivity.

7.3.3 Protection Devices

The final version of the circuit actually implemented is shown in Appendix C. Although there is no overload protection circuit as would exist in a design intended for an actual inertial platform, the circuit does incorporate several protection elements whose functions are not entirely obvious at first sight.

Figure 21 is a schematic of the lower right switch of the basic H switch configuration. It will be referenced in the following discussion of the protective measures used.

The first problem that can arise in the operation of the circuit is dynamic shoot-through. Assume a negative current is being commanded (negative with respect to the arrow in Figure 19). The relevant waveforms are drawn in Figure 22.

In this situation no current ever flows through Q1 since the current in the load never goes above zero. If, when the upper switch turns back on, the collector-base capacitance of Q1 and Q2 were not charged up, the transistors could actually turn-on due to the large voltage step at their collectors.

The protection circuit prevents this. When current is flowing through D3, $V_1 < 0$ by one diode drop. This

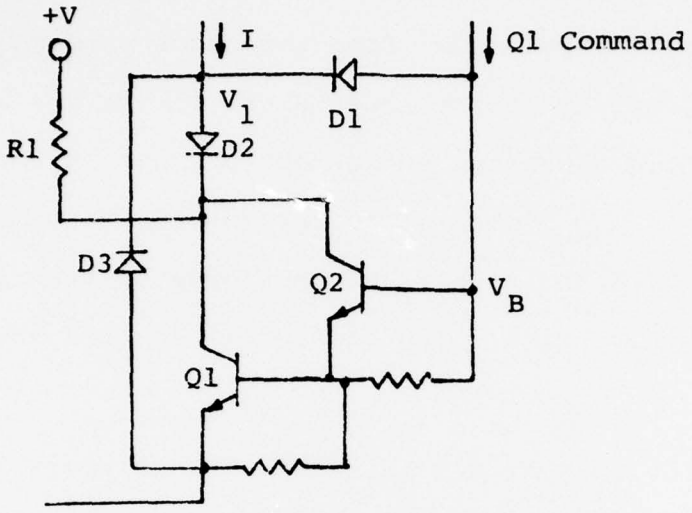

FIGURE 21: Lower Right Switch of Power Stage

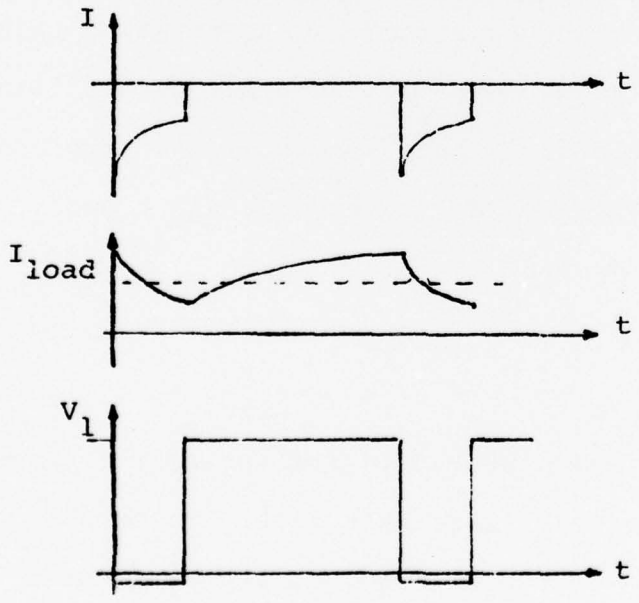

FIGURE 22: Waveforms Used In Description of Protection Devices of Power Stage

means that $V_B \simeq 0$ which disable the darlington pair by drawing the drive current away from the bases through D1. This allows current to flow through R_1 to charge the collector junction capacitances thereby preventing the shoot-through. If I_{load} does go to zero while the command to turn Q1 is still on, then V_1 becomes greater than zero and V_B is allowed to rise. The command is enabled and Q1 turns on.

Another problem that can arise when the circuit is operating concerns multiple reverse current paths. Whenever $I_1 < 0$, current flows through D3. However, if D2 were not also present then some current could also flow through the collector base junction of Q1 saturating this device. When the voltage reversed, the upper switch turns on, these devices could still have some stored charge and therefore turn-on. This would create virtually a dead short between V_s and ground.

7.4 Speed Control Loop

The speed loop was pictured in its entirely in Figure 17. It is a phase locked - loop that locks the squared up back EMF of one phase of the PM motor to the phase of a clock. The angular velocity of the rotor is thus controlled exactly through the control of the angular position

of the rotor. The control when properly compensated also insures a well-damped rotor response with little or no hunting.

7.4.1 Phase/Frequency Detector

The critical requirement of the motor control loop is that the phase detector be able to reliably achieve proper acquisition. It should not lock onto subharmonics and should also provide the maximum accelerating torque signal when the system is not at run speed.

The use of a phase/frequency detector accomplishes these goals. The design chosen is the same as the system developed by D. Fulton[6] to run the feasibility PM motor. Its principle of operation is presented in Figure 23.

The heart of the detector is a 3 stage shift right/left register whose center bit is monitored. One input clocks the register left at a rate proportional to rotor speed trying to place a 1 in the center bit. The other signal clocks right at a rate proportional to the commanded speed and fills the register with zeroes. When the gyro is at its run speed (the commended speed), the shift left-shift right clock frequencies are the same. The shift left and right operations then alternate. The duty cycle of the center bit is thus proportional to the phase difference between the clocks when the gyro is at synchronous speed.

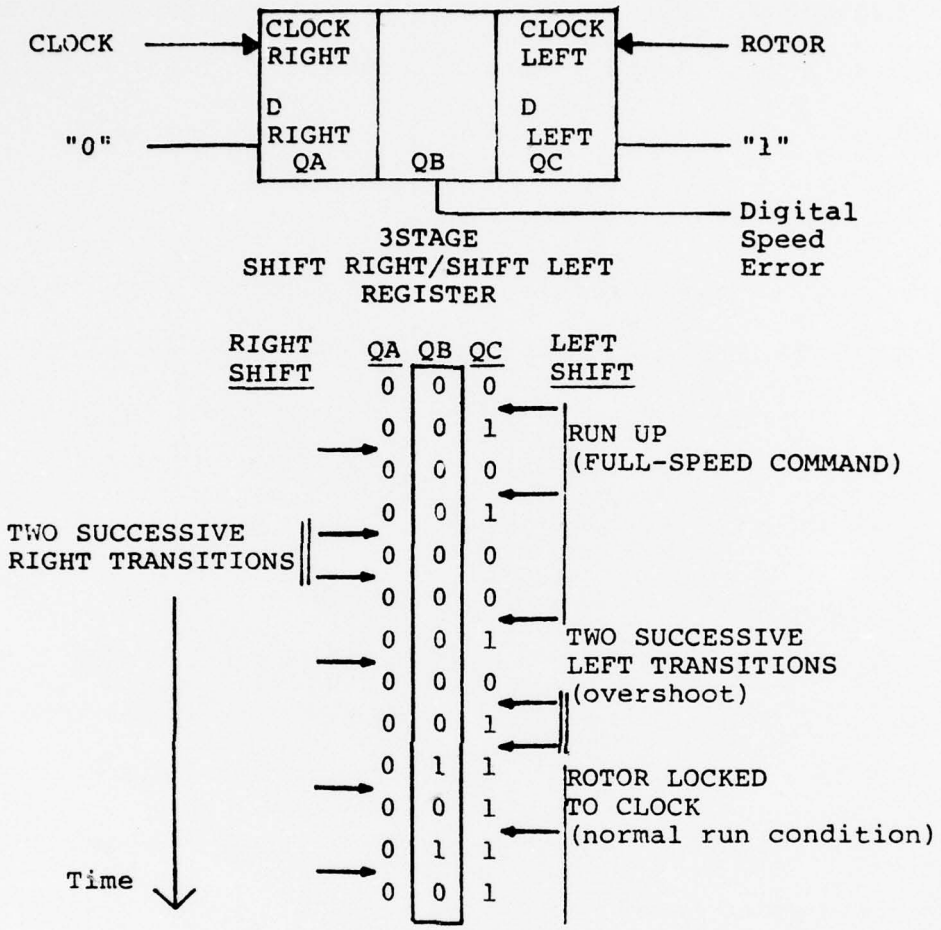

FIGURE 23: Phase/Frequency Detector-
Principle of Operation

If two successive clock pulses occur on any input, either the rotor is rotating too fast or too slow. The center bit becomes constant at a one or zero respectively and it remains constant until two successive clock inputs occur on the other input. This implies that there will always be at least one overshoot of the rotor velocity as it runs up to sync in order to knock the detector out of its frequency mode into its phase detector mode.

Figure 24 is the actual implementation of the detector. It uses a readily available shift right register with a parallel input. The two inputs are converted to pulses by the monostables. The monostable outputs are needed to form a joint clock which toggles the shift register on the trailing edge. The front edge determines whether a 1 or 0 will be loaded into the register.

While the motors are being run up to sync, it is possible that two pulses may overlap. A clock pulse could then conceivably be lost. It will not adversely affect the run-up except for perhaps an extra transient speed overshoot just before synchronous operation. During steady state operation the pulses are 180° apart and this problem will not occur.

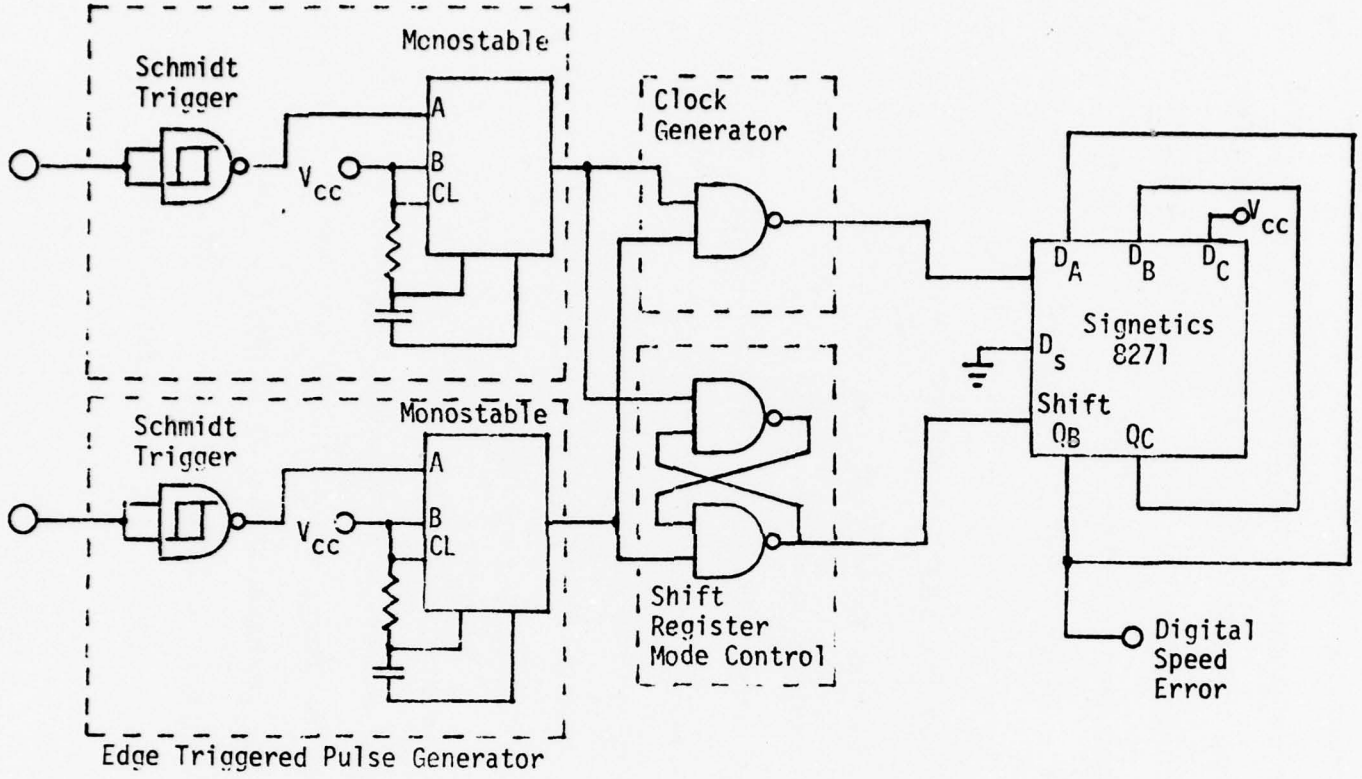

FIGURE 24: Implementation of Phase/Frequency Detector

7.4.2 Speed Loop Compensation

As far as speed loop stability is concerned, the motor dynamics can be modelled as virtually pure inertial since bearing friction is very low. The speed loop therefore requires compensation in order to achieve the proper phase and gain margin for stable closed loop operation.

Figure 25 is a diagram of the speed compensation circuit. The logic signal from the phase/frequency detector is converted to a symmetrical waveform using analog switches (DG191). This waveform is then applied to the op amp stage which filters out noise and adds a ripple cancelling term. The small signal compensation is provided by an α lead network at the front end of the op amp.

The linear block diagram for the entire system including the motor dynamics appears in Figure 26. This diagram, however does not include the damping effect around synchronism due to the induction motor. The response of the system is therefore slightly closer to being critically damped than the closed loop response in Figure 27 indicates.

Also shown in the speed lock circuit (Figure 25) is a bias resistor which sets the operating point of the system. With the operating point chosen such that the clock and the back EMF signals are 180° out of phase, the digital speed

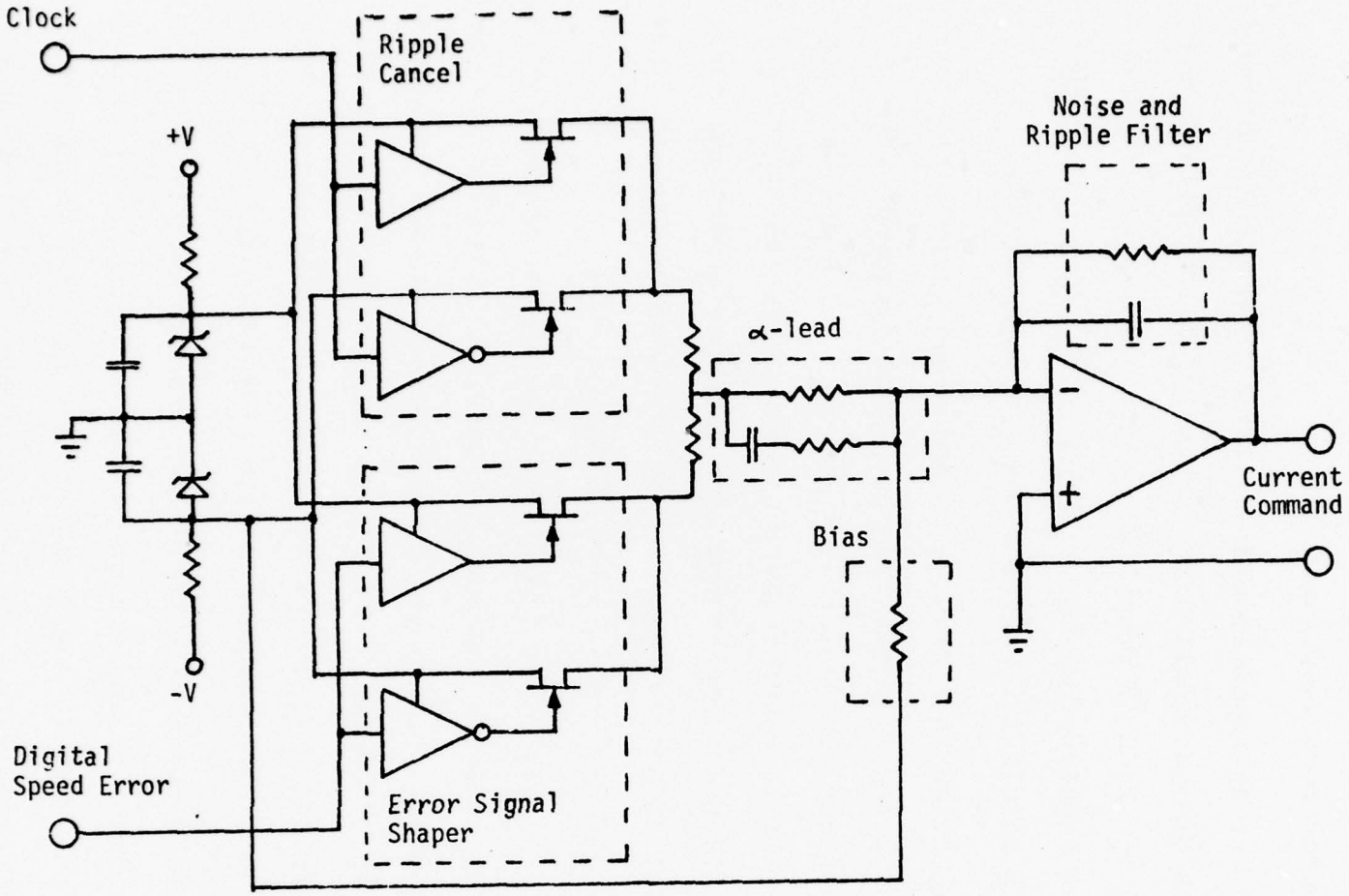

FIGURE 25: Speed Loop Compensation Circuit

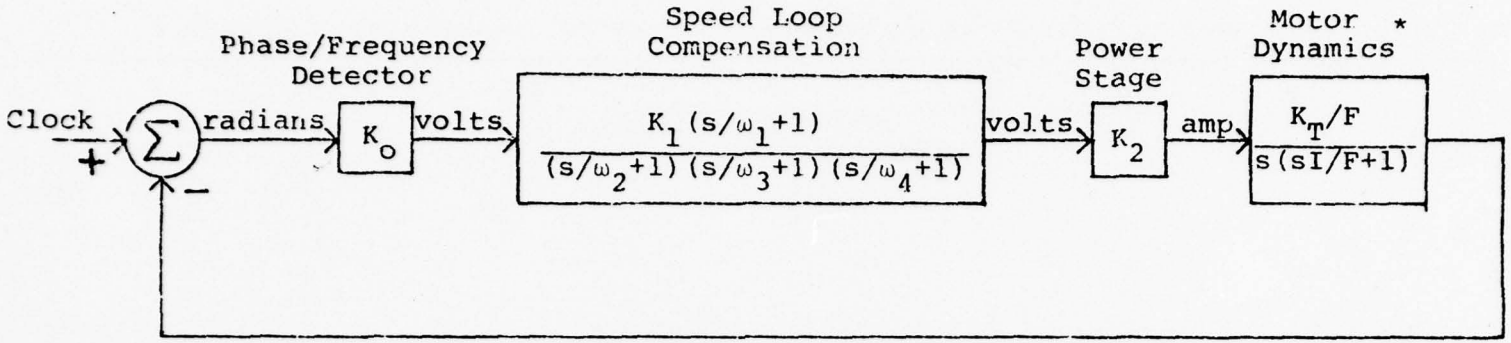

$K_o = 6.2/\pi = 1.97$ V/rad

$K_1 = 1.35$

$K_2 = 0.1$ amp/volt

$K_T/F = 3085.8$ sec/rad·amp

$F/I = 9.26$ rad/sec

$\omega_1 = 4.095$ rad/sec

$\omega_2 = 41.32$ rad/sec

$\omega_3 = 123.45$ rad/sec

$\omega_4 = 222.2$ rad/sec

* Motor dynamics do not include damping effect of induction motor during perturbations around the synchronous shaft speed

FIGURE 26: Speed Control Loop Linear Block Diagram

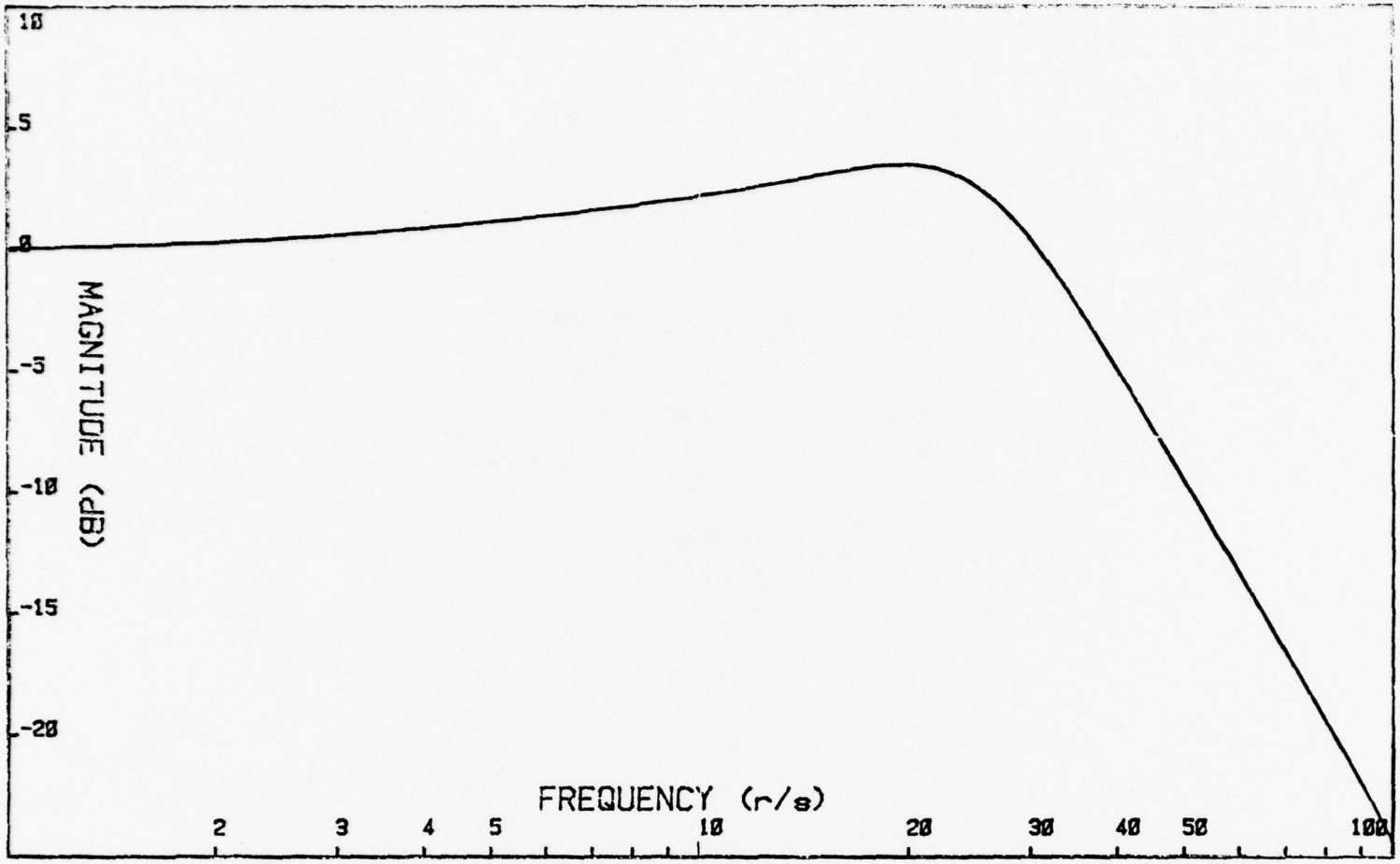

FIGURE 27: Calculated Closed Loop Response of Speed Control Loop

error signal will be a square wave. The large ac ripple of this wave can then be cancelled by subtracting from it a symmetric (about 0 volts) version of the clock signal. This reduces the amount of filtering required.

The circuitry that implements this ripple cancelling function is also shown in Figure 25.

7.5 Starting Circuit

It is desired for simplicity's sake to keep the number of input clock signals to a minimum. In an actual 45,000 rpm gyro drive system using 8 pole motors the clock sync frequency would be 3000 Hz. The start frequency, on the other hand, would be around 100 Hz to enable the induction motor to develop the required starting torque. This signal can be synthesized by counting down the sync signal. Only one input clock signal is then needed.

Since gas bearings were not available, the synchronous rotor frequency used on the test stand was 100 Hz (6000 rpm). The clock sync frequency was therefore a 400 Hz logic signal. For the 100 Hz starting waveform two sinusoidal signals in quadrature are required. The 400 Hz waveform is first divided by 2 using a flip-flop. Both the Q and

$\overline{Q}$ outputs of the flip-flop are then divided by 2 again. This results in 2-100 Hz logic signals with one signal 90° phase shifted from the other. The relevant waveforms are shown in Figure 28.

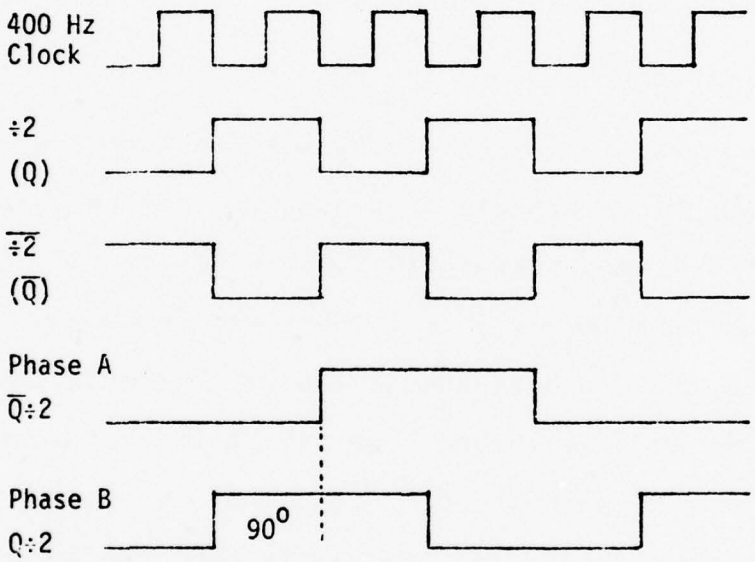

FIGURE 28: Start Circuit Waveforms

The two logic signals are then converted to symmetric $\pm V_p$ waveforms using a DG 191 analog switch. The fundamental of this waveform is a 100 Hz sinusoid in phase with the square wave with a peak value given by

$$V_1 = \frac{4}{\pi} V_p = 1.273\ V_p.$$

There is no second harmonic and the third is given by

$$V_3 = \frac{4V_p}{3\pi} = 0.4244\ V_p$$

The two symmetric square waves are filtered to attenuate the harmonics and then amplified to obtain the desired signal amplitude.

The actual start circuit utilized in this project appears in Appendix C Figure C1.

7.6 Speed/Position Sensor

In order to obtain a signal related to the back EMF position and frequency but independent of the electrical network in which the motors ran, a photo-detector speed sensor was placed on the motor shaft. In essence the device is a circular disc divided into 8 equal sections about the periphery. Four alternate sections were then cut out of the disc to let light pass through. A small light was placed on one side of the disc with a photo darlington on the other.

As the shaft rotates the darlington generates a square wave with a frequency equal to 4 times the rotor rotational velocity. For the eight pole motors used,

this frequency corresponds to the system electrical excitation frequency. Hence it can be set to reflect the flux position of the PM rotor.

To overcome the noise introduced by ambient light and to get a good squared up signal, the instantaneously generated waveform is compared to its average value through a comparator. The resulting signal is then converted to TTL logic levels for further processing (Appendix C, Figure C2).

7.7 Tachometer Circuit

The speed sensor produces a square wave. The tachometer circuit takes this signal and converts it into a dc level proportional to rotor speed. For every falling edge of the square wave, a monostable multivibrator with fixed pulse width output is triggered. The greater the number of triggerings per second, the greater the dc output level of the monostable. This signal is then added to a high pass filtered version of its complement to remove the ac ripple component. The resulting signal is then low pass filtered to give a low ripple dc output.

Because of the high gain in the transfer function, 2.5 Hz/volt, the final output stage is used to cancel any

steady state component that is not required. This prevents op amp saturation. For example, when observing the open hunting of the system around its synchronous speed of 100 Hz it is necessary to cancel the steady state dc term caused by the 100 Hz rotation. In this way only the transients which are the desired data are recorded.

The primary restriction on the system is the fact that it needs a high enough bandwidth to be able to respond to the fastest rotor transient expected. In light of this, the bandwidth was set at 15 Hz. The schematic diagram for the circuit appears in Figure C3 of Appendix C.

7.8 Complete System

The actual circuit implementation of the back EMF sensor and speed control loop appears in Appendix C, Figure 4. Its various operational blocks, previously described in this text, are labeled to show the interconnections.

The pulse ratio modulation power stage circuitry is depicted in Figure C5 of Appendix C.

Chapter 8

Back EMF Control - Test Results

The entire series motor combination - back EMF control structure was tested for its response to various transients, its ability to start and run the system up to sync, and for its steady state characteristics. Also, whenever possible, comparable tests were performed on the system with the induction motor replaced by its equivalent synchronous inductance and resistance in order to determine the induction motor's influence on synchronous operation.

The tests performed included:

1. Measuring motor starting torque.
2. Characterizing the run-up of the system from the moment of switch-over to closed loop control to the attainment of synchronous run frequency.
3. Recording the response of the system to step transients in the phase of the clock signal.
4. Recording the response of the system to pulses of torque applied to the shaft.

5. Observing the re-attainment of the back EMF signals when the signals are momentarily lost.

The results of these tests are also compared to the open loop series motor combination tested previously.

After the tests on the basic system verified its capabilities, the circuits parameters were adjusted to run the motors through a transformer interface. The hollow core rotary transformers were not readily available. Tape wound cores constructed of orthonal were substituted. The reconfigured system was then qualitatively tested for its operating characteristics.

8.1 System Starting

Figures 29 and 30 are graphs of the experimentally measured induction mtoor starting torque versus current and starting torque versus frequency respectively. Since the steady state running torque was approximately 50,000 dyne.cm, the desired start torque was about 3 times this or 150,000 dyne.cm. As implied by the graphs and verified by tests, the required current was approximately 0.52 amperes at a frequency of 100 Hz.

With this current level, the motors quickly came up to 25% run speed at which point the system was switched from open loop to back EMF control. The switching from open loop to closed loop control was

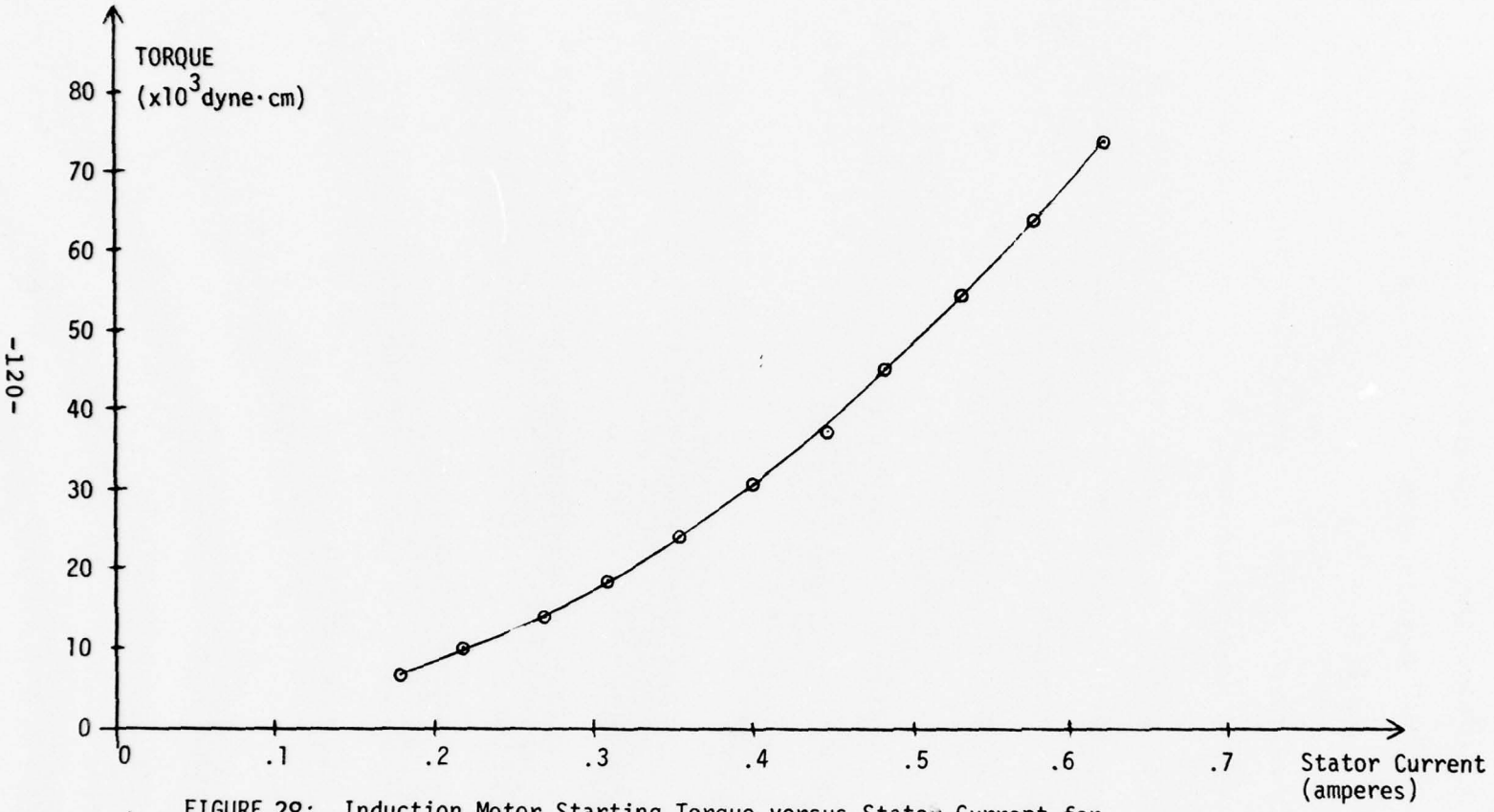

FIGURE 29: Induction Motor Starting Torque versus Stator Current for An Excitation Frequency of 100 Hz

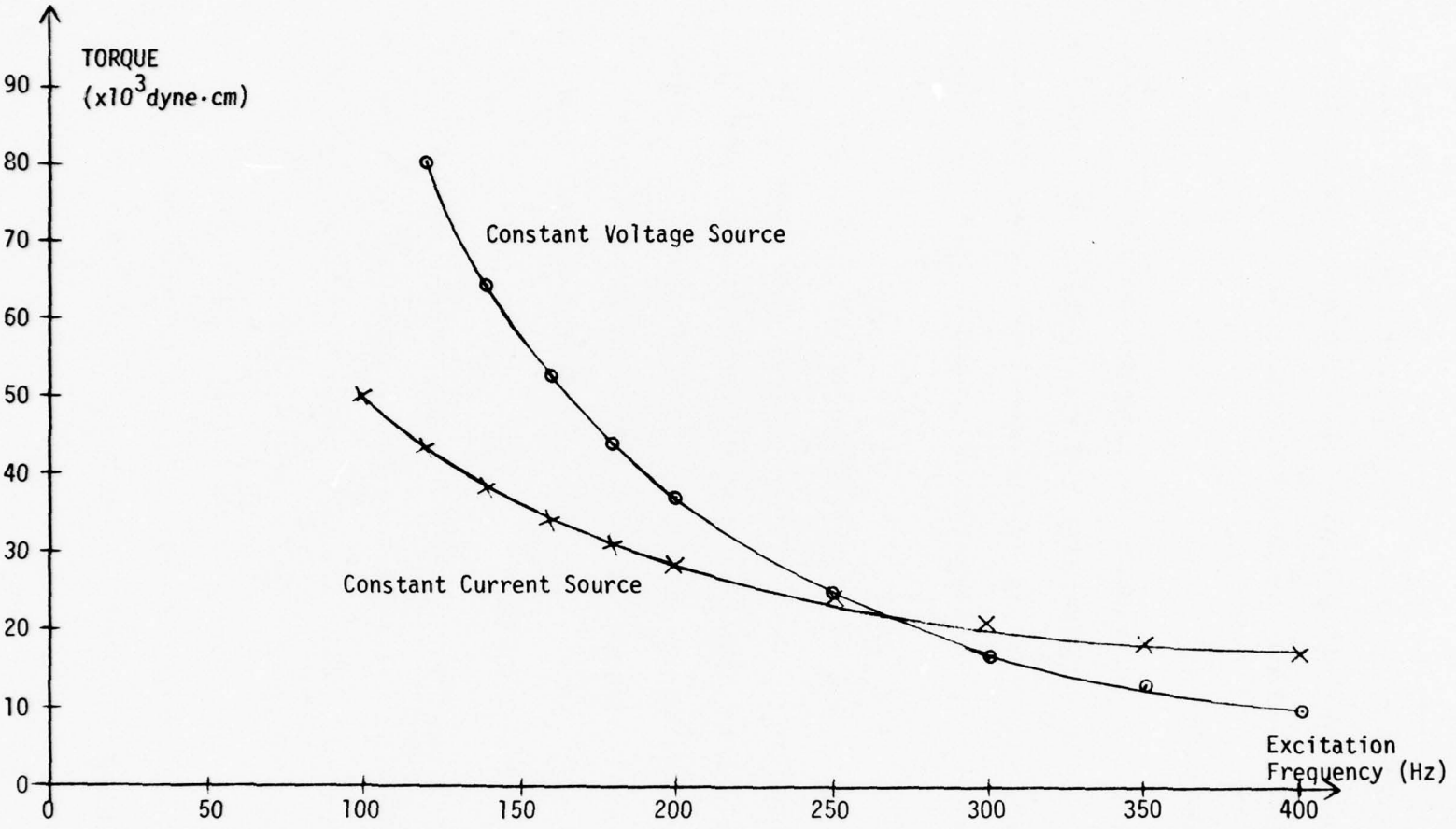

FIGURE 30: Induction Motor Starting Torque versus Frequency For A Constant Voltage ($15V_{rms}$) and Current ($0.3A_{rms}$) Supply

performed manually using several switches built into the breadboard for this purpose. In an actual system the switching would be performed automatically.

8.2 System Run-Up

In order to record the closed-loop synchronous pull-in as well as to determine the run-up time, the unit was observed, with the aid of the speed sensor/tachometer circuits, as it accelerated up to and locked onto synchronous speed.

Figure 31a is a photograph of the instantaneous rotor frequency as the motors accelerated from 90 Hz to 100 Hz. As can be observed, the pull-in, as explained in section 7.4, requires at least one overshoot to switch the phase/frequency detector into its phase detecting mode. Once into phase mode, the system rapidly damps the hunting of the shaft.

Figure 31b is a photo of the same run-up but with each phase of the induction motor replaced by a resistor and inductor. The induction motor contributes to the dynamic damping of the system whereas the R-L circuit does not. The run-up is obviously faster and the system is less damped as shown by the greater number of hunting oscillations of the motor shaft about the sync frequency.

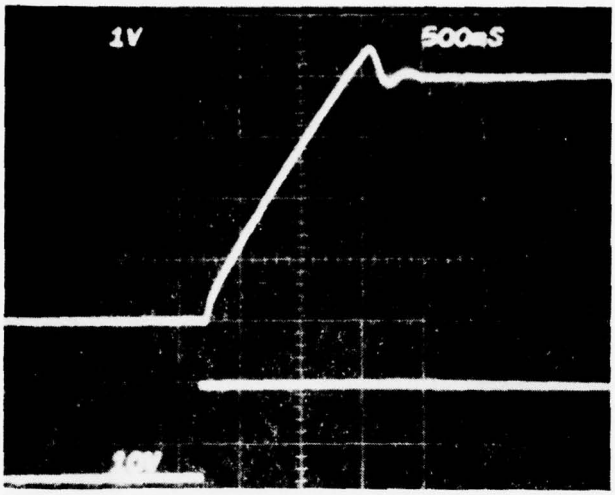

Final Rotor Speed
100 Hz

Vertical Scale
2.5 Hz/Div

Initial Rotor Speed
90 Hz

← 100 Hz Command
Motor Speed Control
← 90 Hz Command

a. Response of Entire System

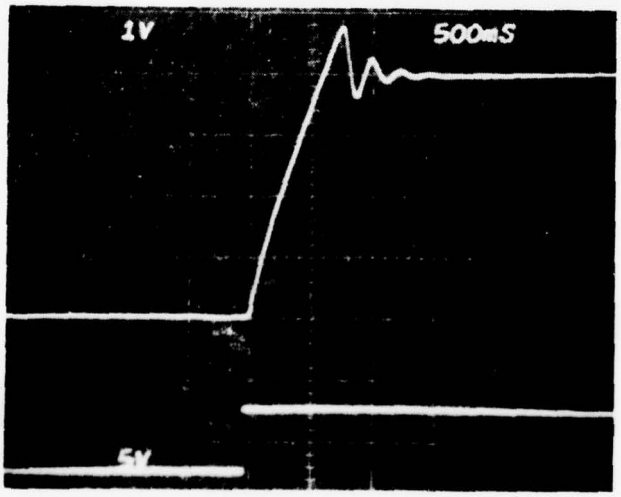

Final Rotor Speed
100 Hz

Vertical Scale
2.5 Hz/Div

Initial Rotor Speed
90 Hz

← 100 Hz Command
Motor Speed Control
← 90 Hz Command

b. Response of System With Induction Motor Replaced By Equivalent Resistance And Inductance

FIGURE 31: Run-Up and Synchronous Acquisition of Back EMF Controlled System

The back EMF system was able to run the motors up to sync from a starting velocity as low as 5% of sync speed. Synchronous lock was achieved and maintained for various shaft torque requirements up to the limits of the power stages' capabilities.

8.3 Response of the System to Transients in Phase of Clock Signal

In a radiation environment it is possible to temporarily lose the controlling clock signal or for the clock signal to have an instantaneous phase jump. If a jump of moderate size (90°) occurs in a hysteresis synchronous system there is hunting but sync is maintained. If a large jump knocks the gyro out of synchronous lock, the hysteresis synchronous motor will reacquire synchronism automatically.

In the 2 motor open loop system, which was run at a low current level for better efficiency, sync was usually lost after a moderate (90°) phase jump. The closed loop system maintained sync and exhibited little hunting.

The test performed entailed using two clock signals, one leading the other by 90°. Using a simple switch, the input to the motor controls was alternated between the two waveforms while the system response was being monitored. Figure 32a is the rotor response for the back EMF controlled series motor system. Figure 32b is the response with the induction motor removed.

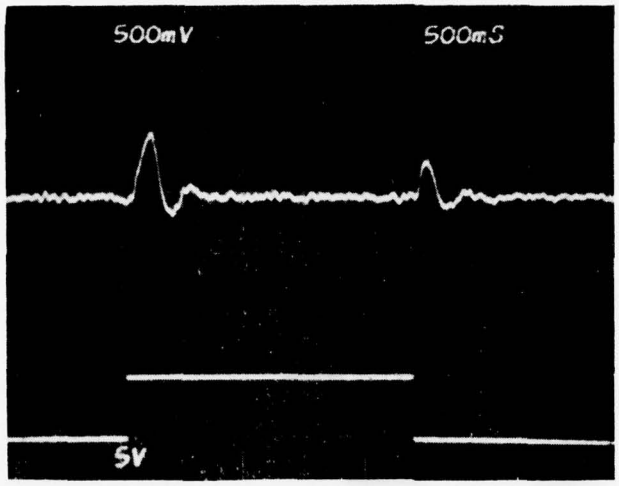

Vertical Scale
1.25 Hz/Div

Steady State
Rotor Freq.
← = 100 Hz

← 400 Hz @ 90°
Clock Command
← 400 Hz @ 0°

a. Response of Entire System

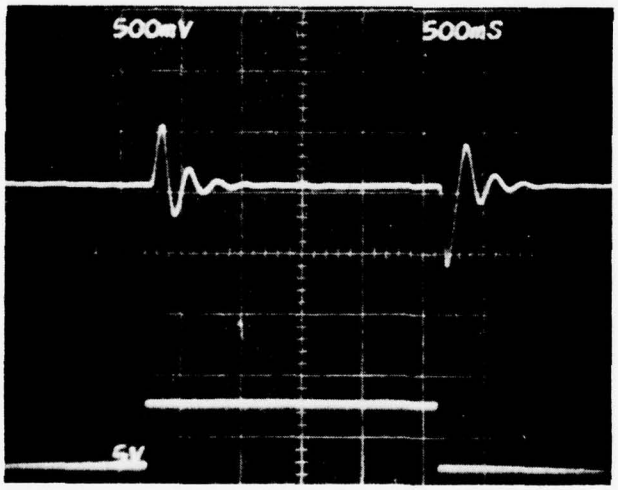

Vertical Scale
1.25 Hz/Div

Steady State
Rotor Freq.
← = 100 Hz

← 400 Hz @ 90°
Clock Command
← 400 Hz @ 0°

b. Response of System with Induction Motor Replaced by Equivalent Resistance and Inductance

FIGURE 32: Response of Back EMF Controlled System To A Phase Transient in the Clock Signal

It is obvious that there is little hunting in the system. The damping provided by the induction motor is also apparent when comparing the two photographs.

8.4 Response of System to Torque Pulses

As in the open loop system test, a torque pulse of 11500 dyne cm was applied to the synchronously rotating motor shaft using the hysteresis synchronous motor. The system transient response appears in Figure 33a. This photo has the same dimensions as those taken for the open loop torque pulse response shown in Figure 15. Note the dramatic reductions in hunting. Figure 33b is an expanded version of Figure a. The jitter apparent in the photo is a noise term inherent in the measuring circuit.

Figures 34a and b are the same situations as in Figure 33 with the induction motor removed once

The system was also subjected to a torque pulse of 35000 dyne cm. The open loop system fell out of sync every time with this large transient. The back EMF controlled system exhibited at most two overshoots before settling into synchronous operation again.

The closed loop system has therefore been shown to maintain a well damped response when subjected to large torque transients. The performance shows a marked improvement over the open loop system as well as over the hysteresis synchronous system.

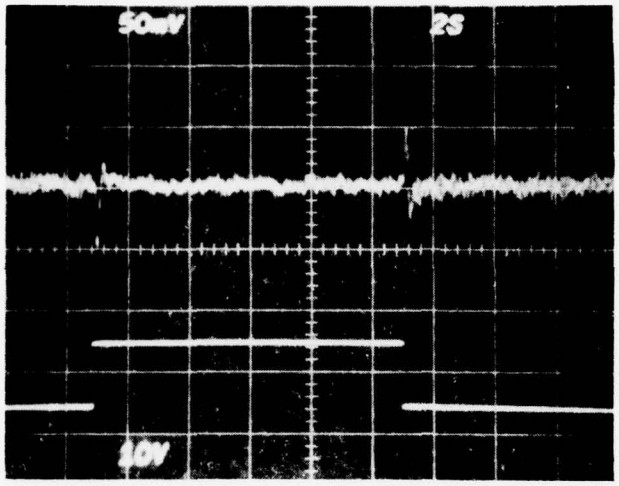

Vertical Scale
0.125 Hz/Div

← Steady State
Freq. = 100 Hz

Torque Pulse of
←11,500 dyne·cm

Steady State
←Torque of
50,000 dyne·cm

a. Same Time Scale As For Open Loop Response in Figure 15

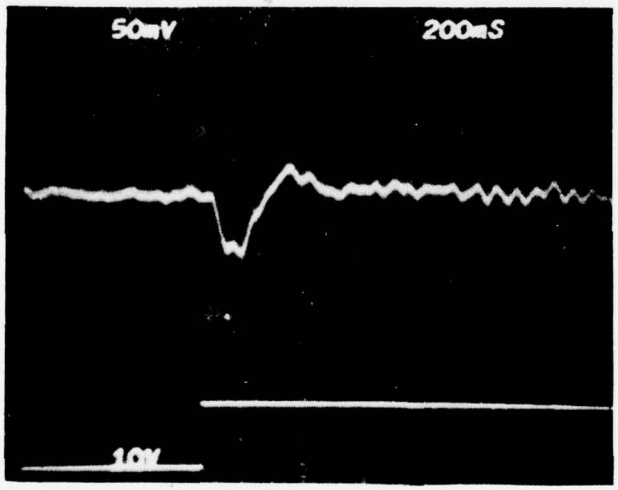

Vertical Scale
0.125 Hz/Div

Steady State
← Freq. = 100 Hz

Torque Pulse of
←11,500 dyne·cm

Steady State
←Torque of
50,000 dyne·cm

b. Time Expanded View Of The Response

FIGURE 33: Response of Closed Loop System To A Pulse In Torque Applied To The Motor Shaft

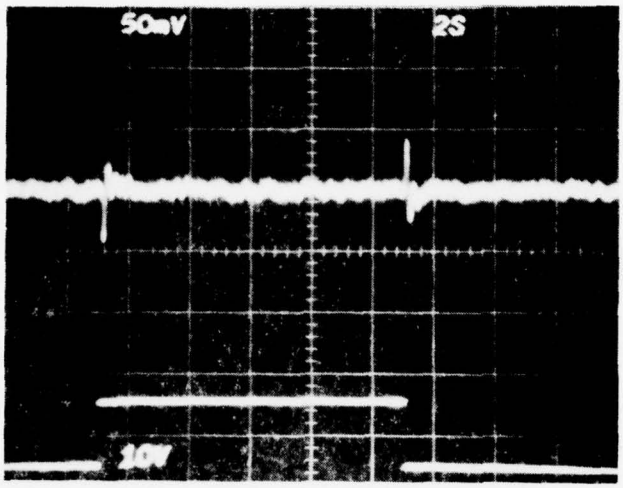

Vertical Scale
0.125 Hz/Div

← Steady State
Freq. = 100 Hz

Torque Pulse of
11,500 dyne·cm

Steady State Rotor
Torque of
50,000 dyne·cm

a. Same Time Scale As For Open Loop Response in Figure 15

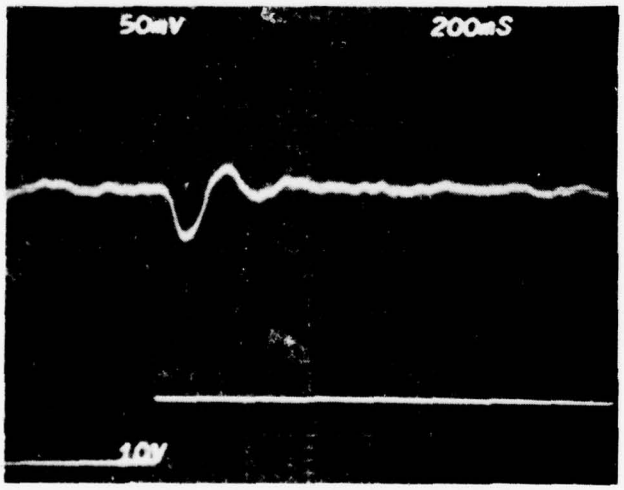

Vertical Scale
0.125 Hz/Div

← Steady State
Freq. = 100 Hz

Torque Pulse of
11,500 dyne·cm

Steady State Rotor
Torque of
50,000 dyne·cm

b. Time Expanded View of the Response

FIGURE 34: System Response to Torque Pulse Applied to Shaft With Induction Motor Replaced By Equivalent Resistance and Inductance

8.5 Efficiency Calculations

The motors driving a gyro wheel perform no useful work at sync. Their only function is to maintain gyro speed by overcoming windage and bearing friction. Any losses other than these two are therefore considered to be a reduction in motor efficiency and an increase in thermal load on the float. These losses include magnetic drag of the motors, resistive losses in the windings, core losses, and losses due to harmonics of the input waveform. The harmonics can cause negative torques that must be overcome. They also contribute to resistive losses.

It is desired to keep these losses low and constant. This limits thermal drift of the gyro and helps to maintain a constant current requirement into the motor.

In the actual test system used in the project, the PM resistance was approximately 9.0Ω per phase and the induction motor synchronous resistance was 5.2Ω/phase. The input currents at a sync speed of 100 Hz were approximately .2 amperes per phase. The bearing and windage friction and magnetic drag created a torque requirement of 50,000 dyne·cm at sync. Neglecting harmonic and core losses (which can be made negligibly small with good motor and power stage design) the efficiency of the system was

$$\eta = \frac{T\,\omega_s}{T\omega_s + 2(I^2R)} \qquad 8.8$$

$$= \frac{3.14 \text{ watts}}{3.14 + 1.136} = .734 \qquad 8.9$$

If one were to use this system with gas bearings whose damping friction could conceivably be 50,000 dyne cm at a speed of 30,000 rpm, the input current requirement would be the same as for the test systems. The efficiency would then be

$$\eta = \frac{50{,}000 \text{ dyne cm} \times 10^{-7} \frac{\text{nt.m}}{\text{dyne cm}} \cdot 2\pi \cdot 500 \text{ Hz}}{2(.2^2 \cdot .14 \cdot 2) + (50000 \times 10^{-7} \cdot 2\pi \cdot 500)}$$

$$= .933 \qquad 8.10$$

Once again this does not take into account stray losses, core losses, or harmonic losses. The actual value will therefore be less than this.

For comparison's sake the open loop system run at 100 Hz is operating at an efficiency of

$$\eta = \frac{3.14}{3.14 + 2\,(.26^2 \cdot .14 \cdot 2)} = .62 \qquad 8.11$$

Hysteresis synchronous motor efficiency when run at gyro speeds, on the other hand, is approximately 0.30. The improvement provided by the new systems is obvious.

8.6 Addition of Transformers

The transformers used were slightly too small. The small wire size required therefore had a higher resistance than would normally be encountered in a gyro system. Its total resistance per phase including the secondary winding was 38Ω. This considerably reduced system efficiency (motor and transformers) on the test stand to about 40%. At normal gyro velocities and with better transformers, this is expected to improve to about 80%.

As far as performance is concerned, quantitative data were not recorded with the interface in place. It was apparent, though, that the system's response was degraded somewhat. Since the back EMF was no longer dominant over the resistive drop the sensitivity of the system to parameter variations showed a marked increase. Once again, with better transformers and higher back EMF's due to higher speeds this problems should be virtually eliminated.

The main performance differences appeared primarily in the system's susceptibility to noise. Heavier filtering on the back EMF recovery stages was required to eliminate the high frequency interference. Also, a low frequency additive oscillation was introduced into the back EMF signal when the model for the circuit resistances and inductances was slightly off. It was necessary to add a

high pass filter to the back EMF stages to attenuate this.

Starting the system was no problem. The 100 Hz start signal did not adversely affect the interface. Run-up took longer since slightly less current was available due to the transfer losses in the transformers. The system response to transients was slightly more underdamped. One or two more oscillations were apparent before the steady state value was re-attained. This could probably be rectified with a change in the speed loop compensation network.

In summary, the transformer interface posed no insurmountable problems to the successful operation of the gyro power drive. Synchronous lock was reached and maintained over a variety of operating conditions.

Chapter 9

Conclusions and Recommendations

9.1 Conclusion

As stated in the original proposal, the purpose of this project was to evaluate the feasibility of the series motor combination for future gyro applications. Within the limited scope of the time and equipment available it is believed that this end was accomplished.

The two motor systems exhibited several problems when operated in an open loop configuration. It had difficulties in locking into sync. The run up from start was undependable. The transient hunting at sync was unacceptably underdamped. The requirement for a sensor to detect loss of synchronous lock further complicated the gyro float.

The closed loop back EMF series motor system, on the other hand, was shown to have many operational advantages over both the open loop system and the hysteresis synchronous motor system. It was more efficient, provided a faster and more reliable run-up, exhibited a much better damped transient response (little hunting), and always required the same current input for the desired torque output. The system overcomes virtually all of the faults of the older gyro drives. Furthermore, although the new configuration introduces its own inherent

problems, e.g. starting, it has been shown that they can be overcome with little loss in performance.

The closed loop system exhibits attributes similar to Fulton's feasibility PM motor system with several extra capabilities. The power drive systems,since it can now be a switching stage,can be made more efficient then the quasi-linear stage employed previously. The system can also be run quite effectively through a transformer interface which heretofore presented severe starting limitations. The induction motor, since it provides some damping at sync, actually gives the system a better transient response.

The transformer interface was not thoroughly tested. Yet, enough observations were performed to show that the entire system could operate through the interface with little degradation in performance.

Based upon the results of the tests performed in this project it appears that the back EMF controlled series motor combination drive system is a viable alternative to the present hysteresis synchronous drives. It would reduce thermal drift instabilities, hunting instabilities, and would simplify the starting and stopping procedures. If the mechanical problems associated with a 2 motor drive

(or a single,dual function rotor) can be overcome, the system could significantly improve inertial guidance systems.

9.2 Recommendations for Future Study

The scope of the project was limited due to the time and equipment that was available. To further assess the system's capabilities and limitations it is believed that the following tests would be appropriate.

1. Run the device in an actual gyro gas bearing with an inertial load similar to that of an actual gyro. This would enable one to use speeds of 24,000 to 45,000 rpm. The transient response and long-term stability would then closely match those of an actual gyro.

2. Investigate the possibility of placing the permanent magnet on the same structure as the induction cage. It is believed the electrical and torque characteristics of this configuration would be similar to that of the series motor system. The space required would be almost half that of the 2 motor design which would make it similar in size to present systems. It is not known if the mechanical instabilities of such an inhomogeneous rotor would cause significant problems.

3. Investigate the mechanical, torque, and electrical properties of both the hollow core and air gap rotary transformers to assess their applicability to an inertial platform. The air gap device may exert uncompensatible error torques while the hollow core transformers make the float inaccessible for general maintenance.

REFERENCES

1. Wrigley, Walter and Walter M. Hollister and William G. Denhard, Gyroscope Theory, Design, and Instrumentation, Cambridge, MA, The M.I.T. Press, 1969.

2. Savet, Paul H., Gyroscopes: Theory and Design; with Applications to Instrumentation, Guidance, and Control, New York, McGraw-Hill Book Company, 1961.

3. Cochin, Ira, Analysis and Design of the Gyroscope for Inertial Guidance, New York, John Wiley & Sons, 1963.

4. Frazier, Richard H., Philip J. Gilinson, Jr., and George Oberbeck, Magnetic and Electric Suspensions, Cambridge, MA, The M.I.T. Press, 1974.

5. Sher, Lawrence, "Gyro Torque Due to Magnetic Attraction Between Flex Leads," Massachusetts Institute of Technology Instrumentation Lab Report #1706, CAmbridge, MS, 1965.

6. Fulton, Donald, "Development of Back EMF Control Electronics for a PM Gyro Wheel." The Charles Stark Draper Laboratory, Report #R-980, Cambridge, MA, 1976.

7. Musoff, Howard, "A Method for Electrostatic Transfer of Wheel Motor Power through Gyroscope Fluid," Massachusetts Institute of Technology Instrumentation Lab Report #E-1753, Cambridge, MA, 1965.

8. _____ "SFIR-7 Final Progress Report," The Charles Stark Draper Laboratory Report #R-779 (confidential), Cambridge, MA, 1973.

9. Gibson, Randall, "Rotary Transformer Design," Massachusetts Institute of Technology Instrumentation Lab Report #E-1055, Cambridge, MA, 1961.

10. Fitzgerald, A.E., Charles Kingsley, Jr., and Alexander Kusko, Electric Machinery, 3rd edition, The Processes, Devices, and Systems of Electromechanical Energy Conversion, New York, McGraw-Hill Book Company, 1971.

11. Fulton, Donald, "Low Slip Induction Motor Equations as a Function of Air Gap," Intro-Lab Memorandum #77-15G-300, The Charles Stark Draper Laboratory, April 13, 1977.

12. Grebene, Alan B., "The Monolithic Phase-Locked Loop - A versatile Building Block," IEEE Spectrum, March, 1971.

13. Gardner, Floyd M., Phaselock Techniques, New York, John Wiley & Sons, Inc., 1966.

14. _____ "Phase Locked Loop Applications," Signetics - Digital, Linear, MOS - Applications, Signetics Corporation, 1974.

BIBLIOGRAPHY

Abbondanti, Alberto and Michael B. Brennen, "Variable Speed Induction Motor Drives Use Electronic Slip Calculator Based on Motor Voltages and Currents," IEEE trans on Ind Appl., vol IA-11, No. 5, September/October 1975.

Binns, K.J., "Some Aspects of the Development and Design of a High Performance PM Synchronous Motor," Proceedings of the IEE, 1971.

Cahill, D.P.M., and B. Adkins, "The Permanent-Magnet Synchronous Motor," The Proceedings of the IEE, vol. 109, Part A, No. 48, 1962.

_____ Conference on Small Electric Machines, London, Power Division of the Institution of Electrical Engineers, 1976.

Gilinson, P.J.,Jr., "Hunting in Polyphase Synchronous Hysteresis Motors," Report C-4130, The Charles Stark Draper Laboratory, Inc., Cambridge, MA, September, 1974.

Hayt, William H., Engineering Electromagnetics, New York, McGraw-Hill Book Company, 1974.

Jordan, Howard E., "Analysis of Induction Machines in Dynamic Systems," IEEE Trans on Power Apparatus and Systems, vol PAS-84, No. 11, Nov 1965.

Ogata, Katsuhito, Modern Control Engineering, New Jersey, Prentice-Hall, Inc., 1970.

Say, M.G., Alternating Current Machines, New York, John Wiley & Sons, 1976.

Veinott, Cyril G., Fractional-and Subfractional-Horsepower Electric Motors, New York, McGraw-Hill Book Company, 1970.

Woodson, Herbert H., and James R. Melcher, Electromechanical Dynamics, Part I: Discrete Systems, New York, John Wiley & Sons, 1968.

APPENDIX A

PERMANENT MAGNET MOTOR

A.1 PM Motor Parameters and Circuit Model

The permanent magnet motor utilized on the test stand was a 2-phase, 8-pole machine. The rotor which surrounded the stator was composed of an alnico ring magnetized for 8 poles. The two phase stator windings were wound with #32 wire which enabled the device to withstand the high starting currents without overheating.

The back voltage of the motor versus rotor speed for phase B appears in figure A1. It is linear, as expected, and has a proportionality constant given by

$$V_{back}=0.027\ \omega \quad \text{volts}$$

where ω is the rotational velocity in radians per second. At a 90^{o} torque angle, the motor delivers 270,000 dyne·cm of torque per ampere under balanced operation.

The resistance and inductance of the system had to be determined in order to correctly sense the back EMF during normal operation. These parameters were found to be

$$R= 9\ \Omega/\text{phase} \qquad L= 1.1\ \text{mH/phase}.$$

The entire model for one phase of the motor is shown in figure A2.

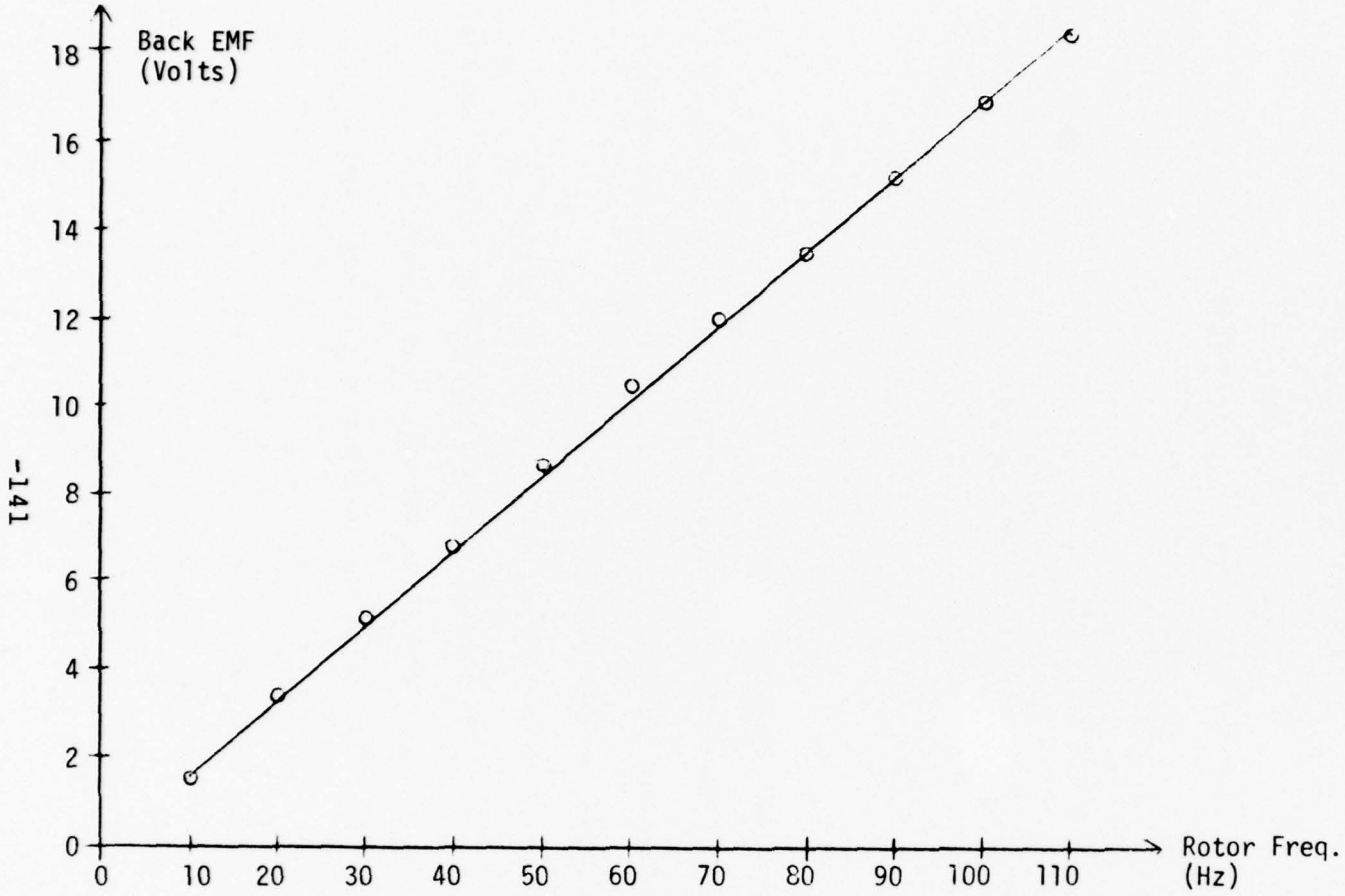

FIGURE A1: PM Motor Generated Back EMF (Phase B)

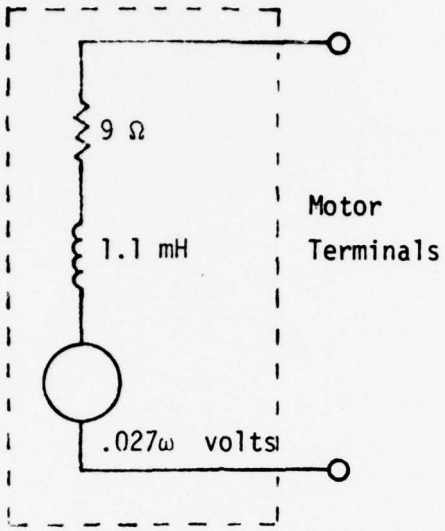

FIGURE A2: PM Motor Equivalent Circuit Model

A.2 PM Motor Torque

The PM motor's torque equations can be developed with reference to the simplified 2 pole, 2 phase smooth air gap machine pictured in Figure A3.

The following idealizations are assumed:

1. The leakage fluxes caused by slot, toothtip, and end turn leakage are negligible.
2. Space harmonics in the air gap field are negligible.
3. The magnetic fields in the air gap are sinusoidal about the circumference.
4. The tangential component of the magnetic field in the air gap is negligible when compared to the radial component.

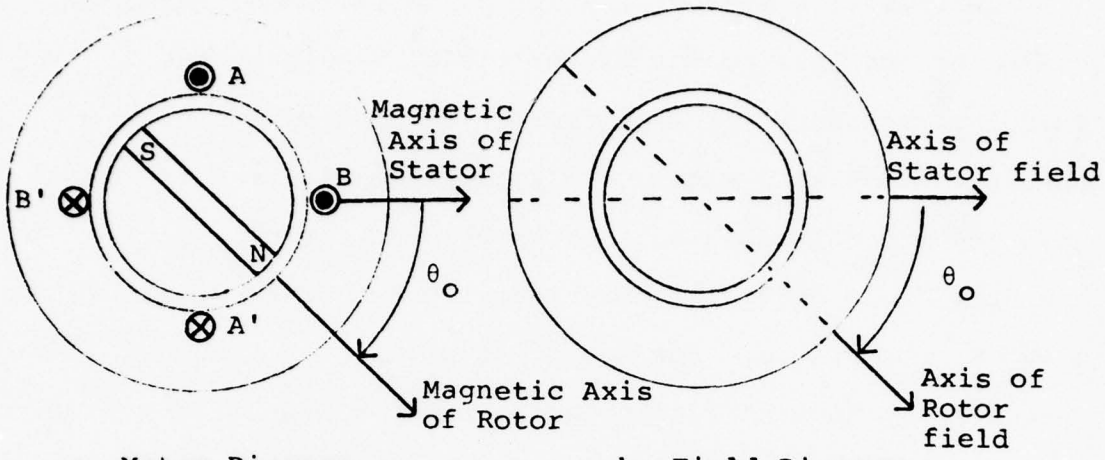

a. Motor Diagram b. Field Diagram

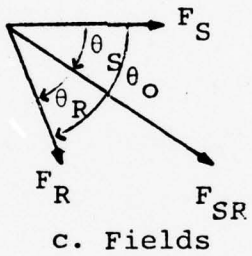

c. Fields

FIGURE A3: Simplified 2-Pole, 2-Phase PM Motor

5. The radial gap length g (the clearance between the rotor and stator) is small when compared to the radius of the stator or rotor.

The hard permanent magnet in the rotor and the currents in the stator create magnetic flux in the air gap separating the two. The rotor flux is in space phase with the PM rotor and its peaks occur at a given location along the periphery whenever a magnetic pole of the permanent magnet is directly across from that point.

The rotating stator flux field, on the other hand, is caused by the interaction of the fields set up by the 2 phases of current. If $i_a = I_o \cos(\omega t + \Phi)$ and $i_b = I_o \sin(\omega t + \Phi)$, then the field will rotate clockwise (see Figure A3)at a rate given by ω electrical radians per second. At t=0, and if $\Phi = 0^c$, the field axis will coincide with the stator field axis drawn in the Figure. For $\Phi = 90^o$ it will point straight down (2 pole machine). Therefore, the position of the stator field can be controlled by controlling the phase, Φ, of the stator currents.

The mutual flux caused by the rotor magnet and stator currents creates magnetic poles on the two axes as shown in Figure A3-b. Torque is produced by the interaction of these fields as they attempt to align themselves.

Using the preceding idealizations as a basis, the total air gap field, i.e. the vector sum of stator and rotor fields, is a radial field, $\vec{H}$ or $\vec{B}$, whose intensity varies with angle around the periphery of the rotor. The line integral of $\vec{H}$ (magnetic field intensity) across the gap reduces simply to $\vec{H} \cdot g$ and the resultant mmf of the system is therefore,

$$F_t = H \cdot g \qquad \text{A.1}$$

where H and hence F_t is a function of position about the perimeter of the air gap.

The mmf waves of the stator and rotor are spatial sine waves. They can be represented by the space vectors F_s and F_r as in Figure A3-c. The angle θ_o, measured in electrical degrees, is the phase angle between the mmf waves' respective magnetic axes. The resultant wave F_t is therefore also a sine wave with a peak value given by

$$F_t = (F_s^2 + F_r^2 - 2F_sF_r\cos\theta_o)^{1/2} \qquad A.2$$

The peak magnetic field intensity H_{peak} due to this wave is

$$H_{peak} = \frac{F_t}{g} \qquad A.3$$

The coenergy density at a point in the air gap where the magnetic field intensity is H is

$$W' = \frac{\mu_o}{2} H^2 \qquad A.4$$

The coenergy density averaged over the volume of the air gap is

$$W' = \frac{\mu_o}{2} \text{ (average value of } H^2) = \frac{\mu_o}{2} \frac{H^2_{peak}}{2} = \frac{\mu_o}{4} \frac{F_t^2}{g^2} \qquad A.5$$

The total coenergy therefore is,

$$W_o' = \frac{\mu_o \pi D \ell}{4g} F_t = \frac{\mu_o \pi D \ell}{4G} (F_s^2 + F_r^2 - 2F_sF_r\cos\theta_o) \qquad A.6$$

where D is the average diameter at the air gap, ℓ is its axial length, and g is the air gap clearance.

The electromagnetic torque produced by the interaction of the fields is then

$$T = \frac{\partial w_o'}{\partial \theta_o} = \frac{\mu_o \pi \ell}{2g} F_s F_r \sin \theta_o \qquad A.7$$

for a 2 pole machine. For a P - pole machine, the torque becomes

$$T = -\frac{P}{2}\frac{\mu_o}{2}\frac{\pi D \ell}{g} F_s F_r \sin \theta_o \qquad A.8$$

Torque is thus seen to be proportional to the peak value of stator and rotor mmf waves and the sine of the electrical space phase angle θ_o between them. Equal and opposite torques are exerted on stator and rotor.

The preceding equation can be rewritten in a more useable form by rewriting the mmf quantities in terms of stator current amplitude and rotor magnet strength. For a full pole pitch stator winding distributed in several slots, the fundamental mmf component can be written as

$$F_{s_{peak}} = \frac{4}{\pi} K_w \frac{N_{ph}}{p} I_a \qquad A.9$$

where K_w is a winding factor, N_{ph} is the effective turns per phase on the stator, P is the number of poles, and I_a is the peak value of the input current for balanced operation.

The rotor mmf can be written in terms of the permanent magnet's strength (H_r) as

$$F_{r_{peak}} = H_{r_{peak}} g \qquad \text{A.10}$$

Upon substitution into the torque equation one obtains

$$T = -\mu_o D \ell k_w I_a H_{r_{peak}} \sin \Theta_o$$

$$= K I_a H_{r_{peak}} \sin \Theta_o \qquad \text{A.11}$$

The PM motor torque is thus proportional to the stator current, the strength of the permanent magnet in the rotor and the phase angle between the stator and rotor fluxes.

APPENDIX B

INDUCTION MOTOR - TORQUE SLIP CURVES

The induction motor used was a small 2-phase, 8-pole machine originally built for a pumping system in an inertial platform. Its steady-state equivalent circuit is shown in figure B1. Core loss is omitted.

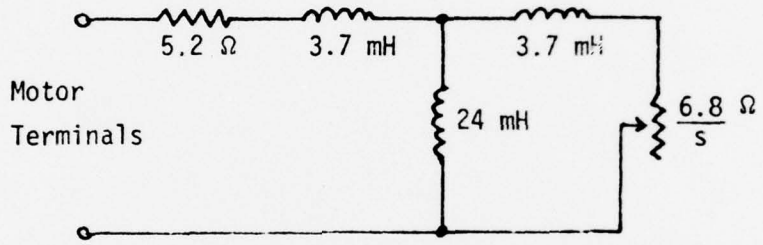

FIGURE B1: Steady-State Induction Motor Single Phase Equivalent Circuit Model

The computed torque-slip curves based upon the equivalent circuit along with the actually measured torque are plotted in figure B2 for both a constant voltage source and a constant current source.

At synchronous speeds, each phase of the induction motor can be modelled as a resistor and inductor in series with a small noise term. The parameters were found to be

$R_{syn} = 5.2\Omega$ $\qquad$ $L_{syn} \triangleq 28$ mH

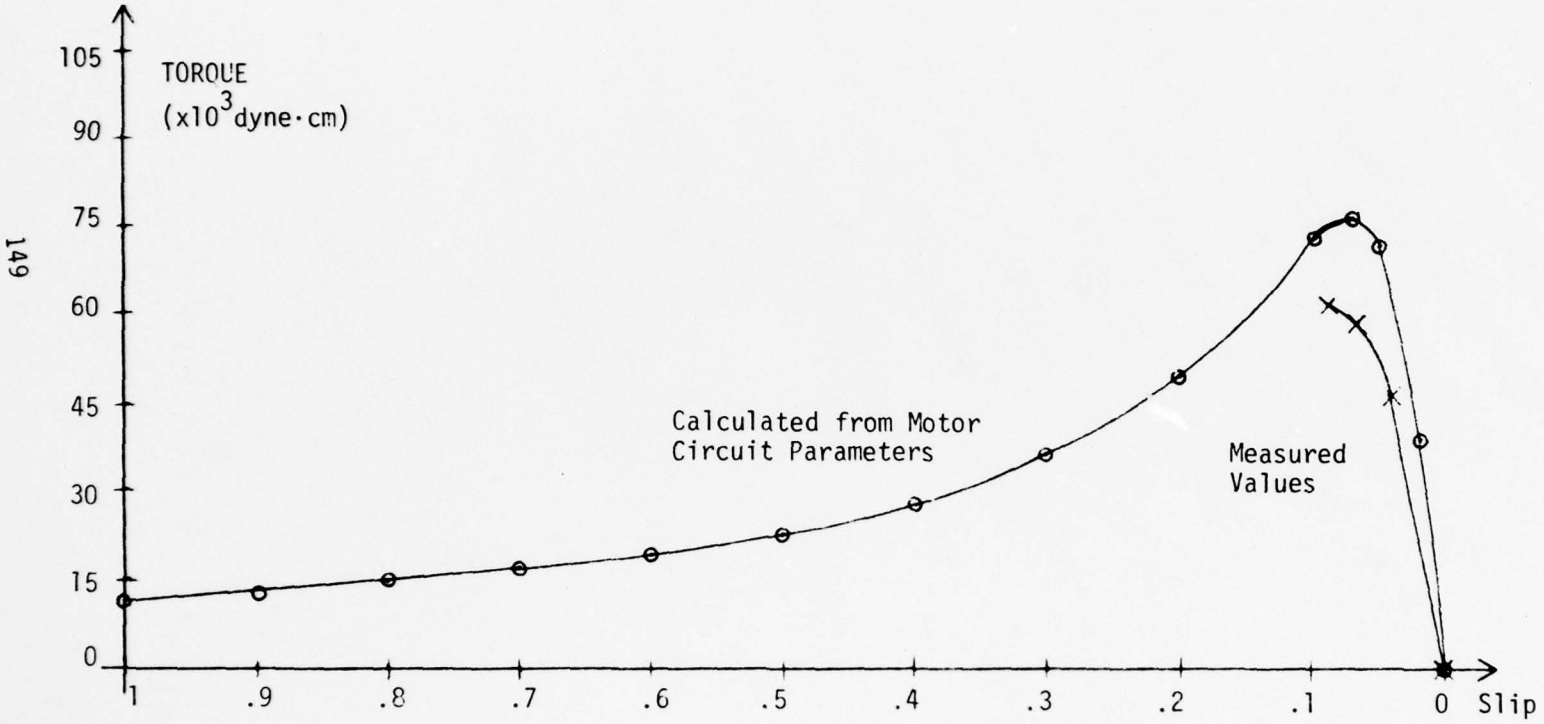

FIGURE B2-b: Torque-Slip Curves for Induction Motor with A Constant Current Source ($.3A_{rms}$)

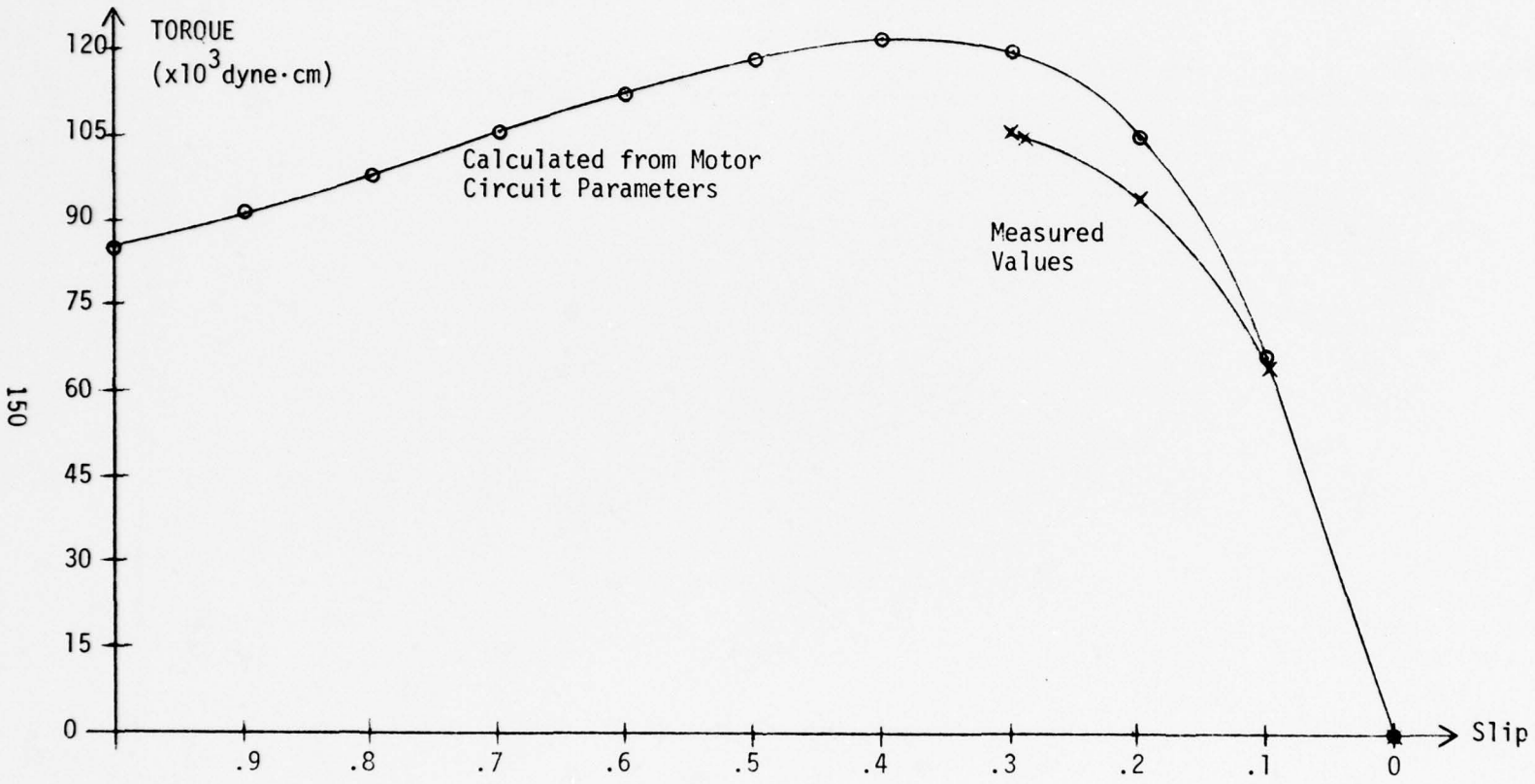

FIGURE B2-a: Torque-Slip Curves for Induction Motor With A Constant Voltage Source of 15 V_{rms}

Appendix C

Circuit Implementation

The following five prints are the control, power, and sensing electronics that were designed, built, and tested with the 2 motor gyro drive system.

Figure C1 is the circuit that generates the two 100 Hz, quadrature sine waves for starting the systems.

Figures C2 and C3 are the circuits used for obtaining a signal proportional to the rotor velocity.

Figure C4 is the detailed implementation of the back EMF sensor and control electronics used for driving the 2 motor system.

Figure C5 depicts the pulse-ratio modulation power stage.

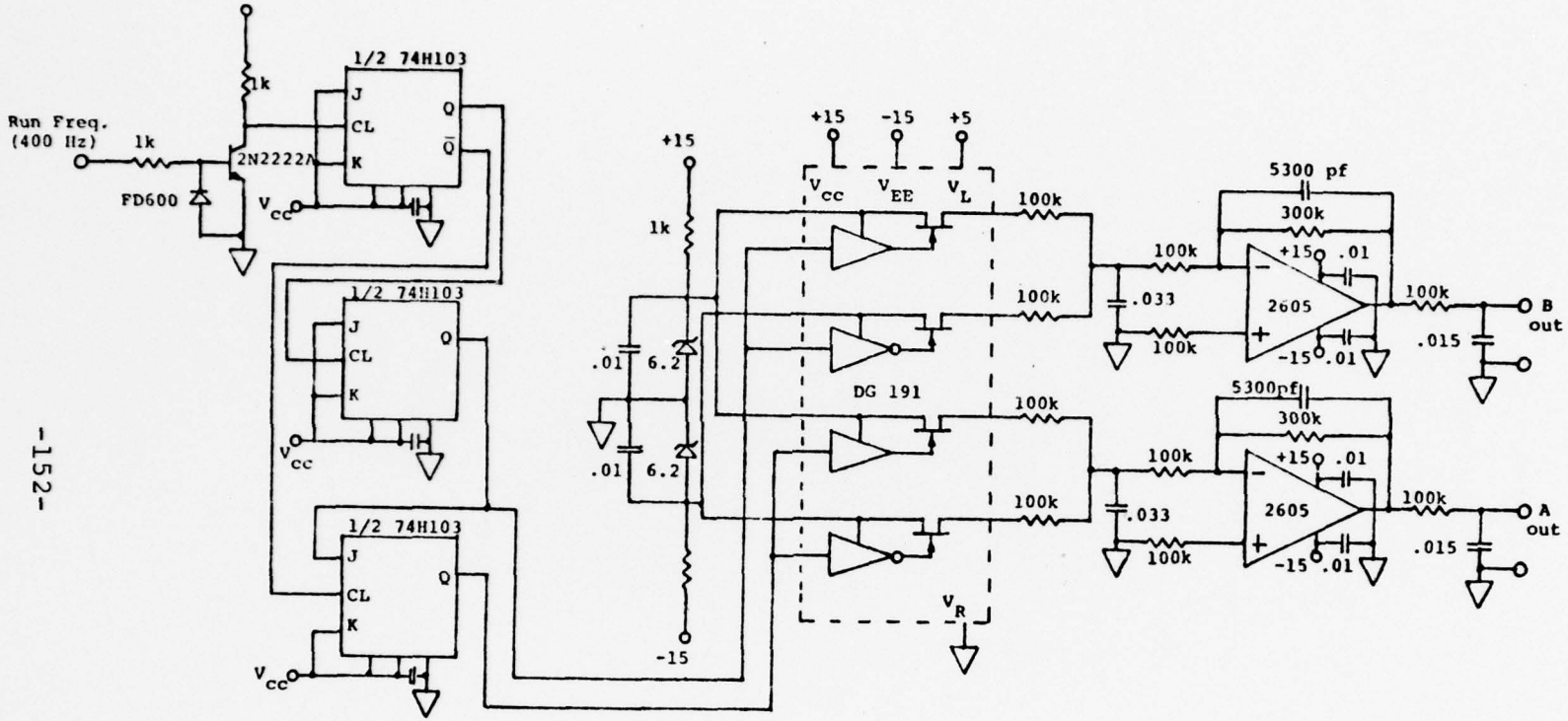

FIGURE C1: Motor Starting Circuit

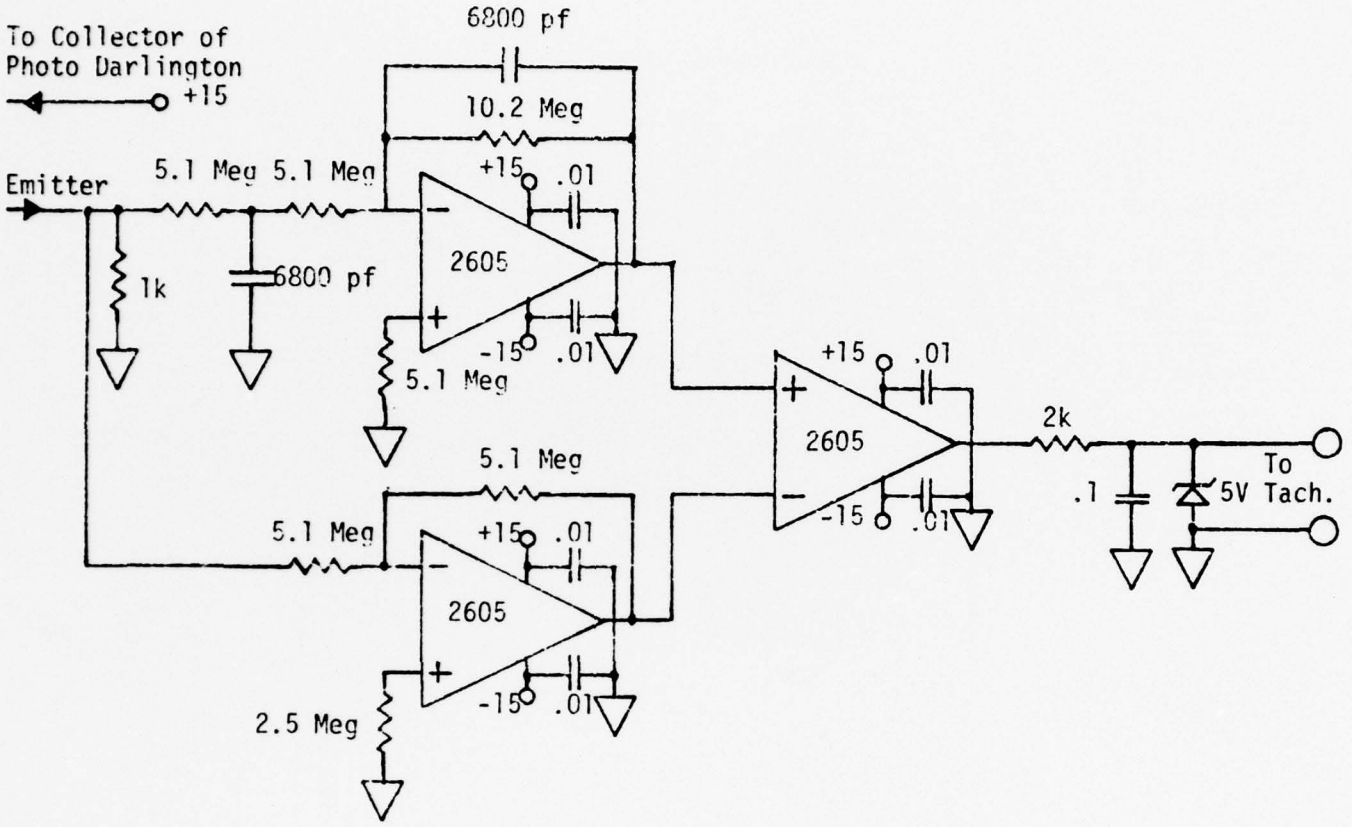

FIGURE C2: Two Motor System Speed/Position Sensor Circuit

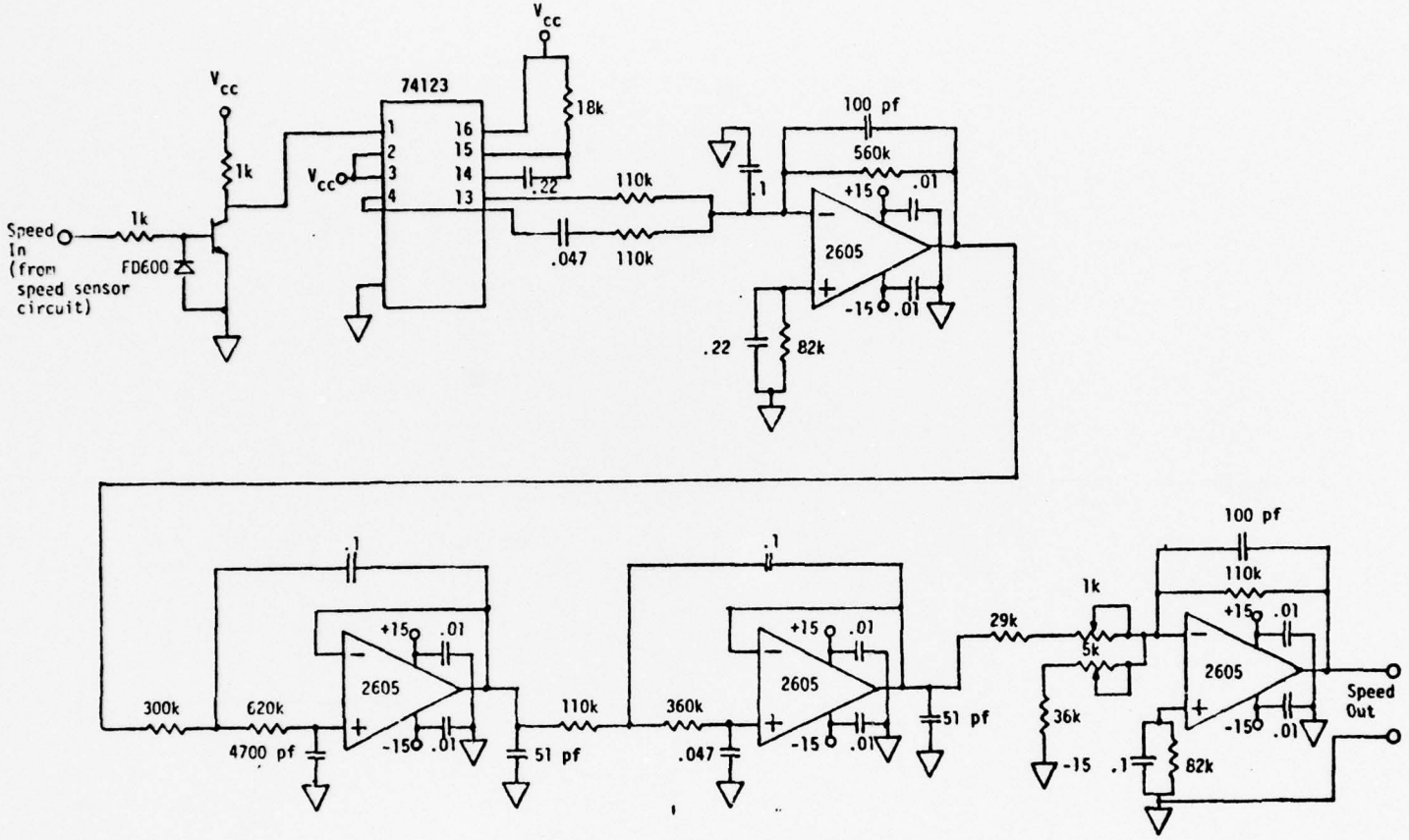

FIGURE C3: Tachometer/Converter Circuit

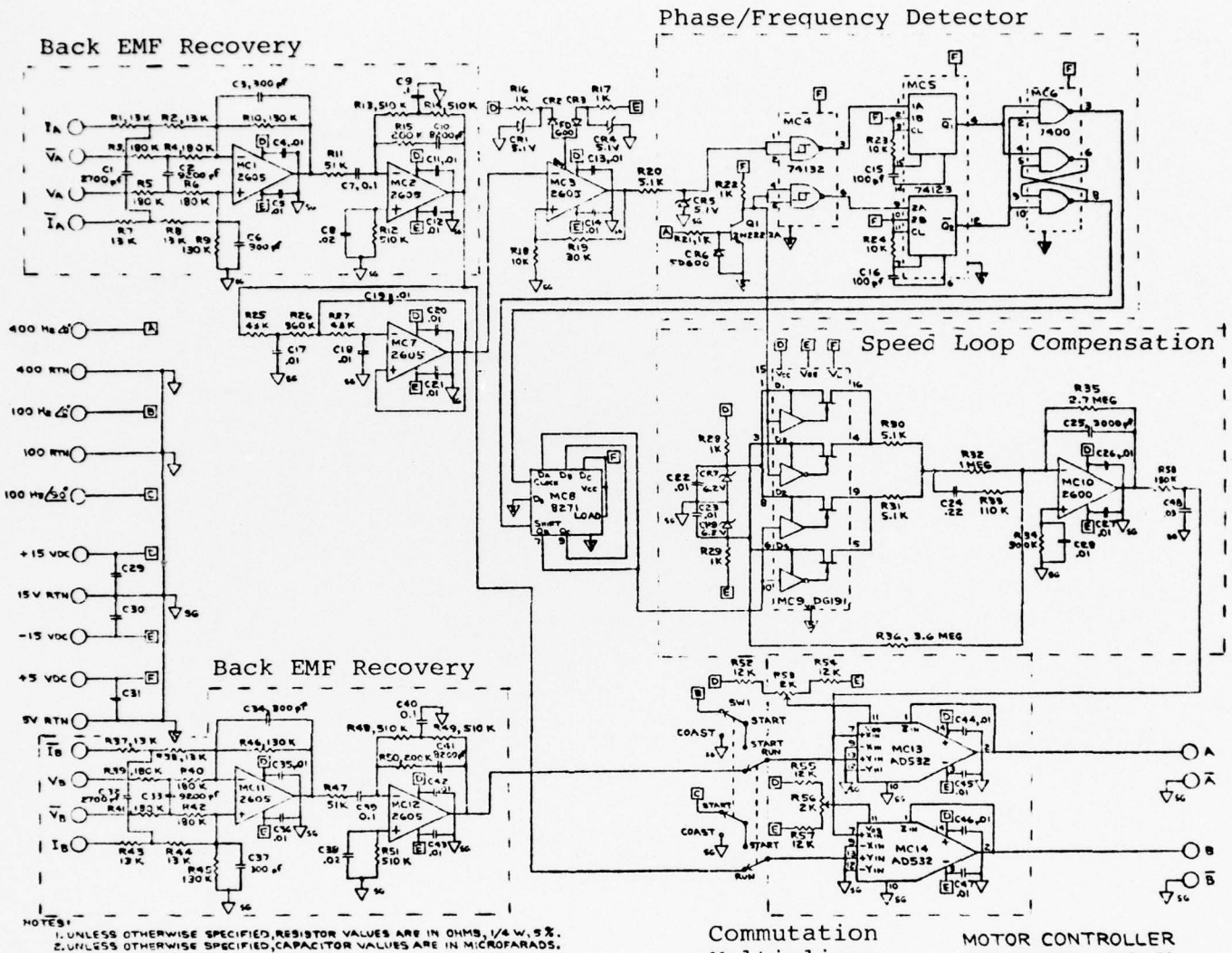
Back EMF Recovery
Phase/Frequency Detector
Speed Loop Compensation
Back EMF Recovery
400 Hz
400 RTN
100 Hz
100 RTN
100 Hz
+15 VDC
15 V RTN
-15 VDC
+5 VDC
5V RTN
MC1 2605
MC2 2609
MC3 2603
MC4
MC5
MC6
7400
74132
74123
MC7 2605
MC8 8271 LOAD
MC9 DG191
MC10 2600
MC11 2605
MC12 2605
MC13 AD532
MC14 AD532
START
START RUN
COAST
RUN
SW1
NOTES:
1. UNLESS OTHERWISE SPECIFIED, RESISTOR VALUES ARE IN OHMS, 1/4 W, 5%.
2. UNLESS OTHERWISE SPECIFIED, CAPACITOR VALUES ARE IN MICROFARADS.
Commutation Multipliers
MOTOR CONTROLLER
MARC RICHARD 21 Jul 78
SK MR72178

FIGURE C4

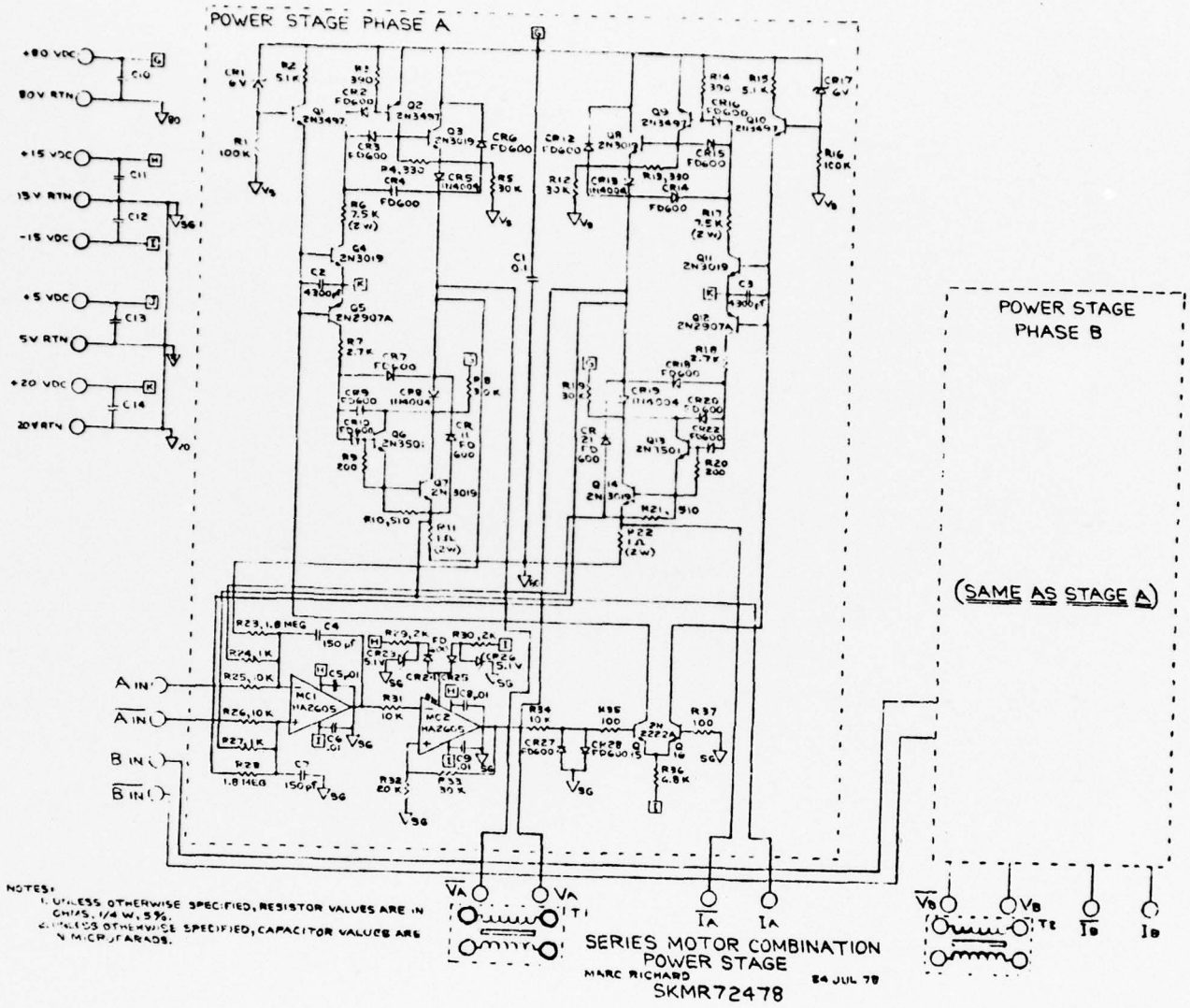

NOTES:
1. UNLESS OTHERWISE SPECIFIED, RESISTOR VALUES ARE IN OHMS, 1/4 W, 5%.
2. UNLESS OTHERWISE SPECIFIED, CAPACITOR VALUES ARE IN MICROFARADS.

FIGURE C5

APPENDIX D

TRANSFORMER INTERFACE

The transformers used were tape wound circular cores made of 2 mil square orthonol. The effective core cross sectional area was 0.686 cm^2. The case window area was 4.39 cm^2 (.865 x 10^6 circular mils).

These 1 to 1 transformers had 1000 turns on each winding of #30 wire.

The transformer size was marginal. In an actual system the interface transformers should be somewhat larger in core area to overcome the problem of small wire size and possible overheating.

Appendix E

Phase Locked Loop Analogy for the Acquisition of Synchronism in the Two Motor System

E.1 Phase Locked Loop[12,13,14]

A phase locked loop is a frequency feedback system comprised of a phase comparator, low pass filter (LPF), and an error amplifier in the forward path and a VCO in the feedback path (see Figure E1).

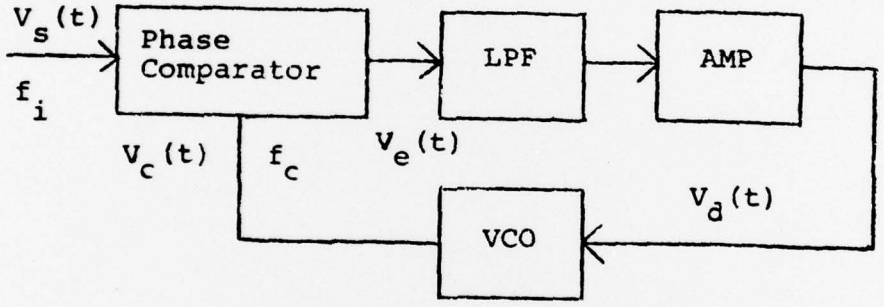

FIGURE E1: Phase Locked Loop Block Diagram

The phase comparator is in actuality a multiplier circuit that mixes the input signal with the VCO signal. This mix produces seem and difference frequencies $f_i \pm f_o$. When the loop is in lock, i.e. $f_o = f_i$, the VCO duplicates the input frequency so that the difference frequency component is zero, while the phase difference has a DC component. The low pass filter removes the sum frequency component but passes the DC value.

With no input signal, $V_d = 0$ and the VCO operates at a set frequency f_o known as the free running frequency. With an input signal, the phase comparator compares the phase and frequency of the input with the VCO frequency and generates an error voltage $V_e(t)$ that is related to both the phase and frequency difference between the two signals. V_e is then filtered, amplified, and applied to the control terminal of the VCO. V_d forces the VCO frequency to vary in a direction that reduces the frequency difference between f_o and f_i.

If f_i is sufficiently close to f_o, the difference frequency component out of the comparator will pass relatively unattenuated through the filter and eventually the VCO will synchronize or lock with the incoming signal. Once locked, there is only a finite phase difference θ_o necessary to generate V_d.

E.2 Capture Process

With an input signal, the phase comparator mixes the input and VCO signals to produce the sum and difference components already mentioned. If the difference component falls outside the band edge of the low pass filter than it is removed and no signal is transmitted to the VCO. As f_i approaches f_o, the frequency $\Delta f = f_i - f_o$ approaches the band edge of the LPF. Some of it is then transmitted to the VCO which tends

to drive the VCO towards the frequency of the input signal which in turn decreases Δf which allows more information to be passed.

A second way to describe this process is as follows. Since frequency is the time derivative of phase, the frequency and phase errors in the loop can be related as

$$2\pi\Delta f = \frac{d\phi_o}{dt} \qquad \text{E.1}$$

where Δf is the instantaneous frequency separation between f_o and f_i. If the feedback loop of the PLL were opened, then for a given f_i and f_o the phase comparator output will be a sinusoidal beat note of frequency $f = \Delta f$. If Δf is small enough, the LPF will not attenuate it. The beatnote then would modulate the VCO frequency. If the loop were then closed, the modulated VCO frequency would change the phase/frequency relation between f_i and f_o and therefore Δf would become a function of time. If during the modulations process the VCO frequency moves closer to f_i, which decreases Δf, $d\phi/dt$ would decrease and the output of the phase comparator becomes a slowly varying function of time. If the VCO is modulated away, $d\phi_o/dt$ increases and V_e becomes a rapidly varying function of time. Note that since the VCO converts a voltage to a frequency and frequency is the derivative of phase, the VCO acts as an integrator in the feedback path.

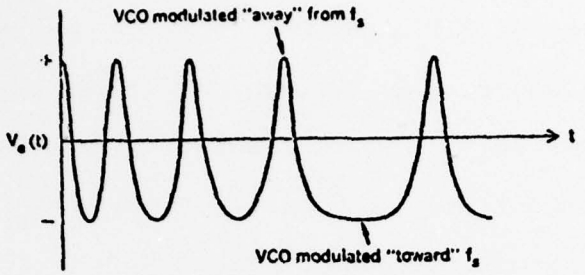

a. Expanded View of Aperiodic Cusps During Capture

b. Entire Capture Process

FIGURE E2: Phase Detector Output Waveform As PLL Acquires Lock

The V_e beat note will then no longer be sinusoidal. It will be a set of aperiodic cusps. Due to its asymmetry, the waveform will have a finite DC component. This component will tend to push f_o to f_i. When in lock, $\Delta f = 0$ and only a steady-state dc error voltage remains (see Figure E2).

The system will lock whenever the input frequency falls within the capture range of the system. By definition the capture range is the frequency centered about the VCO free running frequency over which the loop can acquire lock with the input signal. It depends primarily upon the band edge of the LPF together with the closed loop gain of the system.

The mathematics of PLL's is very complex and necessarily nonlinear. Hence, expressions predicting capture range can be derived only for the simplest systems which employ either no LPF or only a first order system. Most equations predicting capture range are therefore empirical approximations.